2016

Ligand Engineering For Advanced Functional Composite Materials

Michael H. Bell
University of South Carolina

Recommended Citation
Bell, M. H.(2016). *Ligand Engineering For Advanced Functional Composite Materials.* (Doctoral dissertation). Retrieved from https://scholarcommons.sc.edu/etd/3818

LIGAND ENGINEERING FOR ADVANCED FUNCTIONAL COMPOSITE MATERIALS

by

Michael H. Bell

Bachelor of Science
Stockton University, 2009

Submitted in Partial Fulfillment of the Requirements

For the Degree of Doctor of Philosophy in

Chemistry

College of Arts and Sciences

University of South Carolina

2016

Accepted by:

Brian Benicewicz, Major Professor

Ken Shimizu, Committee Member

Hans-Conrad zur Loye, Committee Member

Harry Ploehn, Committee Member

Lacy Ford, Senior Vice Provost and Dean of Graduate Studies

DEDICATION

In loving memory of my sister, Cathleen L. Bell.

ACKNOWLEDGEMENTS

First and foremost, I would like to thank my research advisor, Dr. Brian Benicewicz for the opportunity to work in his research group and the constant support he has provided. None of this would be possible without his expertise and guidance. I would like to thank my doctorial committee members, Dr. Ken Shimizu, Dr. Hans-Conrad zur Loye, and Dr. Harry Ploehn for their contributions and encouragement. Thank you to Dr. MVS Chandrashekar for attending my defense as an interim committee member.

A tremendous thank you is owed to my collaborators at Rensselaer Polytechnic Institute. Dr. Linda Schadler, Timothy Krentz, Yanhui Huang, and Suvi Virtanen of the Schadler group have been instrumental in completing the work presented herein. Thank you to Ke Wu and Dr. Curt Breneman of the Beneman group for their contributions.

The support and environment I have experienced within the Benicewicz group has been unrivaled and I must express my deepest appreciation to group members both past and present for the culture they created. I would like to give a special thank you to Tony Neely for all of his help along the way. He has constantly found the time to discuss research and help me in any way possible even after his departure.

Finally, I would like to my family for their unwavering support through all my endeavors that ultimately lead me here.

ABSTRACT

The surface modification of solid inorganic substrates for thermodynamic compatibility with organic polymer media has become an important area of study for the development of advanced functional composite materials. Polymer ligands covalently bound to the substrate surface have been an effective means to achieve said compatibility. Current investigations focus on multifunctional ligand engineering where multiple chemically distinct species, each with specific functionality, can be implemented on the filler surface simultaneously. A combination of matrix compatible polymer brushes and conjugated charge trapping moieties attached to filler surfaces are investigated for enhancements in dielectric properties. Presented herein are the synthesis and characterization of multifunctional ligand grafted nanoparticles as well as the properties afforded by them.

Click chemistry has proven to be a mild and efficient strategy for the functionalization of silica surfaces. Presented is a one pot synthesis using click chemistry for simultaneous attachment of two chemically distinct species. RAFT polymerization was used to synthesize PGMA polymer chains for compatibility with an epoxy resin. Short conjugated species (terthiophene or ferrocene) were used to add charge trapping functionality. The ligands were synthesized to contain alkyne terminal groups while the silica substrate was modified to contain azide functionality. Assembly of the bimodal functionalized nanoparticles was successful using the Huisgen cycloaddition click reaction. Analysis of the resultant composites showed improvements in dielectric breakdown

strength over neat epoxy, and epoxy filled with unmodified and monomodal PGMA modified silica.

With the efficacy of multifunctional grafted silica established, further investigation was then performed into the parameters that govern dielectric breakdown in composites. Using a grafting-from methodology and sequential addition of ligands, multiple graft densities of PGMA chains were attached to silica ultimately achieving multiple states of filler dispersion. The effect of dispersion was explored for both bimodal and monomodal surface modified nanoparticles on dielectric breakdown strength. A diminishing return was observed for improvements in DBS with increasing dispersion. The effect of short ligand chemistry was also explored at well-dispersed states. Excellent correlation was observed for calculated values of ionization energy + electron affinity (IE+EA) of short conjugated species and experimentally obtained DBS of the composite. Concentration of conjugated ligand groups present at the filler surface was also explored by implementing bimodal brush grafted nanoparticles.

Focus was then shifted to the modification of metal oxide nanoparticles. Ligands were designed to contain phosphate or phosphonic acid moieties for robust covalent attachment. Grafting-to strategies were again used for surface functionalization. A bimodal population of PDMS chains was used to induce compatibility of 5 nm TiO_2 nanoparticles with a silicone matrix. Two species of anthracene ligands were synthesized both containing phosphonic acid moieties for surface attachment. The anthracene ligands differed in substitution at the 10 position to study the effect of adding an electron withdrawing group on composite dielectric breakdown strength. A novel phosphate containing RAFT agent

also was synthesized in an attempt to perform surface initiated RAFT polymerization on the surface of ZrO_2 nanoparticles.

Finally, surface modification of silica microparticles for enhanced fracking proppants was explored. An activated free radical azo initiator was synthesized and subsequently attached to the silica particle. Free radical polymerization was then used to polymerize acrylamide from the particles surface. The particles were studied for their ability to remain suspended in aqueous solution. It was found that surface modified particles had the ability to remain suspended longer in aqueous solutions than unmodified particles. Correlation was observed between the wt% of polymer present on the particle surface and suspension time of the particles.

TABLE OF CONTENTS

DEDICATION iii

ACKNOWLEDGEMENTS iv

ABSTRACT v

LIST OF TABLES xi

LIST OF FIGURES xii

LIST OF ABBREVIATIONS xv

CHAPTER 1 INTRODUCTION 1

  1.1 NANOCOMPOSITES 2

  1.2 COMPOSITE FILLERS 6

  1.3 GRAFTING METHODS 7

  1.4 CONTROLLED RADICAL POLYMERIZATION METHODS 9

  1.5 NANOCOMPOSITES VIA RAFT POLYMERIZATION 14

  1.6 DIELECTRIC NANOCOMPOSITES 16

  1.7 DISSERTATION OUTLINE 19

  1.8 REFERENCES 22

CHAPTER 2 ONE POT GRAFTING-TO SYNTHESIS OF BIMODAL FUNCTIONALIZED SILICA FOR DIELECTRIC NANOCOMPOSITES 31

  2.1 ABSTRACT 32

  2.2 INTRODUCTION 32

  2.3 EXPERIMENTAL SECTION 34

2.4 RESULTS AND DISCUSSION 40

2.5 CONCLUSION 49

2.6 ACKNOWLEDGEMENTS 50

2.7 REFERENCES..50

CHAPTER 3 PREPARATION AND INVESTIGATION OF BIMODAL FILLERS FOR ENHANCED NANODIELECTRICS..54

3.1 ABSTRACT..55

3.2 INTRODUCTION..55

3.3 EXPERIMENTAL SECTION..61

3.4 RESULTS AND DISCUSSION 69

3.5 CONCLUSION 87

3.6 ACKNOWLEDGEMENTS 88

3.7 REFERENCES..88

CHAPTER 4 SURFACE MODIFIED METAL OXIDE NANOPARTICLES FOR IMPROVED DIELECTRIC COMPOSITES 93

4.1 ABSTRACT..94

4.2 INTRODUCTION..95

4.3 EXPERIMENTAL SECTION..97

4.4 RESULTS AND DISCUSSION 106

4.5 CONCLUSIONS 116

4.6 ACKNOWLEDGEMENTS 117

4.7 REFERENCES..117

CHAPTER 5 SURFACE INITIATED AQUEOUS FREE RADICAL POLYMERIZATION FOR FRACKING ADDITIVES WITH ENHANCED SUSPENSION 120

5.1 ABSTRACT..121

5.2 INTRODUCTION 121
5.3 EXPERIMENTAL 124
5.4 RESULTS AND DISCUSSION 126
5.5 CONCLUSION 134
5.6 ACKNOWLEDGEMENT 134
5.7 REFERENCES...135
CHAPTER 6 CONCLUSION AND OUTLOOK...137
BIBLIOGRAPHY 143

LIST OF TABLES

Table 2.1 Free space length (L_f) and dielectric breakdown strength of synthesized composites.....45

Table 3.1 Synthetic characteristics of monomodal (MM) and bimodal (BM) grafted nanoparticles 74

Table 3.2 L_f and Weibull scale (and 95% confidence interval CI) and shape parameters, along with percent change of DBS for synthesized monomodal (MM) and bimodal (BM) composites.....75

Table 3.3 Calculated ionization energy (IE) and electron affinity (EA) for the synthesized conjugated electroactive ligands. Calculations obtained by quantum computation 80

Table 3.4 Graft density (σ) and molecular weights of PGMA-PTTEMA bimodal brush grafted SiO_2 and PTTEMA monomodal brush grafted SiO_2 85

Table 3.5 Observed free space length and % change in dielectric breakdown strength for PGMA-PTTEMA bimodal brush grafted SiO_2 and PTTEMA grafted SiO_2 87

Table 4.1 AC dielectric breakdown values for TiO_2 nanoparticles in commercial Sylgard 184 silicone (wt% values represent TiO2 in the final casted sample) 112

Table 5.1 Feed ratio of monomer to initiator and percent weight loss for the Syloid samples synthesized in this study 129

LIST OF FIGURES

Figure 1.1 Experimentally obtained morphology diagram representing polystyrene grafted silica nanoparticles in polystyrene..........3

Figure 1.2 Evolution of surface modification on nanoparticles..........5

Figure 1.3 Grating methods for ligand attachment to metal oxide substrates 7

Figure 1.4 Various methods for grafting polymer chains to a substrate surface: A) physisorbtion, B) grafting-to, and C) grafting-from methods..........9

Figure 1.5 Reversible deactivation by coupling (NMP mechanism)..........11

Figure 1.6 Reversible deactivation with transfer to a metal complex (ATRP mechanism)..........12

Figure 1.7 Mechanism of RAFT polymerization..........13

Figure 1.8 Synthesis and attachment of activated RAFT agent to SiO_2 nanoparticle 15
Figure 1.9 Optical microscopy image of tree formed as a result of avalanche breakdown in epoxy resin..........17

Figure 2.1 Synthesis of the bimodal grafted nanoparticles used in this study..........34

Figure 2.2 Comparison of FT-IR spectra for azide grafted silica and bimodal PGMA-terthiophene grafted silica. Note the disappearance of the azide peak at 2100 cm^{-1} and appearance of carbonyl peak at 1700 cm^{-1}..........43

Figure 2.3 TEM micrographs of synthesized composites: a) 1 wt% bare silica in epoxy b) 2 wt% monomodal PGMA grafted silica in epoxy c) 2 wt% bimodal grafted PGMA-terthiophene silica in epoxy d) 2 wt% bimodal PGMA-ferrocene silica in epoxy 45

Figure 2.4 (top) Real permittivity measurements and (bottom) imaginary component of permittivity (loss) as a function of frequency for the synthesized composites..........48

Figure 3.1 Activated short ligands synthesized a) activated thiopheneacetic acid b) activated 9-anthraceneacetic acid c) activated terthiopheneethoxy oxobutanoic acid.......71

Figure 3.2 UV-vis spectrum of anthracene coated silica nanoparticles (left) and silica particles containing both anthracene and CPDB (right) 73

Figure 3.3 UV-vis spectra for a) terthiophene grafted silica b) terthiophene + CPDB grafted Silica and c) TGA analysis of both terthiophene and terthiophene + CPDB grafted particles 74

Figure 3.4 TEM micrographs of monomodal PGMA grafted silica at various states of dispersion 77

Figure 3.5 TEM micrographs of bimodal PGMA-anthracene grafted silica at various states of dispersion. 77

Figure 3.6 TEM micrographs of bimodal PGMA-thiophene grafted silica at non and well dispersed sates..78

Figure 3.7 TEM micrographs of bimodal PGMA-terthiophene grafted silica at non and well dispersed sates...78

Figure 3.8 Plot of PGMA grafted chain density vs free space length (L_f) for the synthesized monomodal and bimodal composites 78

Figure 3.9 Plot of percent change in dielectric breakdown strength vs free space length (L_f) of the synthesized composites..79

Figure 3.10 Plot of calculated ionization energy + electron affinity of the synthesized electroactive short ligands vs experimentally obtained values for the correlating nanocomposites...82

Figure 3.11 (a) TGA traces and (b) GPC chromatograms for PGMA-PTTEMA bimodal grafted SiO_2 after each polymerization step 85

Figure 3.12 TEM micrographs for (left) PGMA-PTTEMA bimodal brush grafted SiO_2 and (right) PTTEMA monomodal grafted SiO_2...86

Figure 4.1 ^1H NMR of comparison of 9-anthracenemethanol and 9-anthracenemethylbromide...107

Figure 4.2 ^1H NMR comparison of 9-anthracenemethanol and 10-bromo-9-anthracenemethylbromide...108

Figure 4.3 TEM micrographs of a) bare TiO_2 b) TiO_2 grafted with bimodal PDMS brushes and c) TiO_2 grafted with bimodal PDMS brushes and anthracene phosphonic acid. All samples contain 2 wt% TiO_2 in Sylgard 184 110

Figure 4.4 Weibull probability plot for silicone composite samples with varied interfacial chemistry..111

Figure 4.5 ^{1}H NMR spectra for CDSS-OH and CDSS-phosphate 114

Figure 4.6 MMA conversion with time for SI RAFT polymerization from 4 nm ZrO_2 using phosphate RAFT agent...115

Figure 4.7 Theoretical and experimental MMA molecular weight with monomer conversion for SI RAFT polymerization from 4 nm ZrO_2 using phosphate RAFT agent...115

Figure 5.1 FT-IR spectra comparison of ACVA and activated ACVA (AACVA).........127

Figure 5.2 IR spectra of the synthesized surface modified Syloid particles....................130

Figure 5.3 TGA traces showing weight loss for the grafted Syloid samples...................131

Figure 5.4 Suspensions of Syloid-244 in water from left to right: PAM grafted Syloid + free PAM, PAM grafted Syloid, bare Syloid + free PAM, and bare Syloid....................132

Figure 5.5 Transmittance of aqueous Syloid solutions over 100 hours...........................132

Figure 5.6 Grafted PAM and PAM free chains generated during polymerization reaction..133

LIST OF ABBREVIATIONS

ACVA	4,4′-Azobis(4-cyanovaleric acid)
AACVA	Activated 4,4′-Azobis(4-cyanovaleric acid)
AIBN	Azobisisobutyronitrile
ATRP	Atom transfer radical polymerization
BM	Bimodal
CDSS	4-Cyano-4-(dodecylsulfanylthiocarbonyl)sulfanylpentanoic acid
CPDB	4-cyanopentanoic acid dithiobenzoate
CNT	Carbon nano tubes
CRP	Controlled radical polymerization
CTA	Chain transfer agent
DBS	Dielectric breakdown strength
DCC	N,N'-Dicyclohexylcarbodiimide
DCM	Dichloromethane
DMAP	4-Dimethylaminopyridine
DMF	N,N-dimethylformamide
DMSO	Dimethylsulfoxide
EA	Electron affinity
FT-IR	Fourier transform infrared spectroscopy
GMA	Glycidyl methacrylate
GPC	Gel permeation chromatography
HF	Hydrofluoric acid

HOMO	Highest occupied molecular orbital
HRMS	High resolution mass spectroscopy
IE	Ionization Energy
LED	Light emitting diode
LUMO	Lowest unoccupied molecular orbital
NHS	N-hydroxysuccinimide
NMP	Nitroxide mediated polymerization
NMR	Nuclear Magnetic Resonance
NP	Nanoparticle
MM	Monomodal
MMA	Methylmethacrylate
PAM	Poly(acrylamide)
PDMS	Poly(dimethylsiloxane)
PGMA	Pol(glycidylmethacrylate)
PMAA	Poly(methacrylic aid)
PMDETA	N,N,N′,N″,N″-pentamethyldiethylenetriamine
PMMA	Poly(methylmethacrylate)
PTTEMA	Poly(terthiopheneethylmethacrylate)
RAFT	Reversible addition-fragmentation chain transfer
RPM	Rotations per minute
TEM	Transmission electron microscopy
TEMPO	(2,2,6,6-tetramethylpiperidin-1-yl)oxidanyl
THF	Tetrahydrofuran
TGA	Thermogravimetric Analysis
TMSBr	Bromotrimethylsilane

SI	Surface initiated
UV-vis	Ultraviolet visible spectroscopy

CHAPTER 1

INTRODUCTION

1.1 Nanocomposites

Polymer nanocomposites (PNCs), or hybrid materials consisting of organic polymer and inorganic nano-sized fillers, are well established for their superior performance in optical, electrical, and thermomechanical properties.[1–6] The property enhancements attained when incorporating nano-sized (<100nm) fillers are not seen or even reversed with micron and larger sized fillers.[2,7] The large interfacial region present when considering nanocomposites is advantageous in that it brings forth the property enhancements not seen with larger scale fillers. The large interface can also be disadvantageous as it increases the unfavorable enthalpic interaction of a hydrophobic organic polymer matrix with a hydrophilic inorganic filler. Because of this large enthalpic penalty, nanoparticles introduced into a polymer tend to aggregate and self-associate rather than disperse evenly. Aggregated nano-fillers resemble their micron sized counterparts and do not bring forth the desired property enhancements. To increase filler-polymer compatibility, it is commonplace to attach organic molecules to the filler surface. Ligands ranging from small molecule organics to polymer chains have been employed to aide in filler dispersion with varying success.

Matrix compatible polymeric ligands attached to the filler surface, commonly referred to as polymer brushes, have shown great success in promoting filler-matrix compatibility and are now commonplace in the literature.[8–10] The parameters that govern matrix compatibility and filler dispersion have been investigated by Kumar et al.[11] It was found that dispersion was influenced by the long and short range enthalpic interactions of the nanoparticles and the entropic displacement of polymer chains on the nanoparticle surface. Tuning the variables responsible for controlling these interactions, (polymer graft density (σ) and chain length (N)) can realize a variety of self-assembled anisotropic structures or uniformly dispersed particles. Figure 1.1 shows the experimentally obtained filler morphologies obtained by Kumar et al. Evenly dispersed particles were obtained with sufficient polymer coverage. Numerous polymer chemistries have been achieved on filler surfaces though the majority of polymeric species tend to be derived from chain growth monomers.[10]

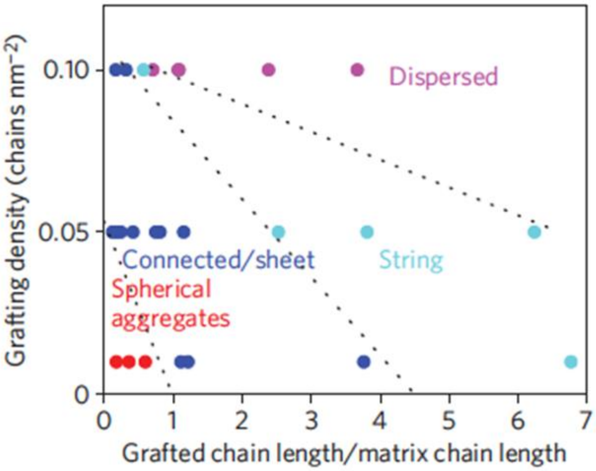

Figure 1.1: Experimentally obtained morphology diagram representing polystyrene grafted silica nanoparticles in polystyrene.[11]

Bimodal brush grafted nanoparticles are nanoparticles containing two populations of polymer brushes attached to the surface, one long, and one short population. By adding two separate populations of polymer chains to the filler surface, enthalpic and entropic contributions were overcome independently resulting in well dispersed composites over a larger range of polymer chain graft density and length.[12] The long chain population entangles with the matrix and a short dense population screens particle core-core attraction. Realization of the bimodal polymer grafted structure has been achieved in a variety of ways. Benicewicz et al. presented a sequential surface initiated RAFT polymerization for the synthesis of bimodal styrene brushes on silica nanoparticles.[13] Matyjaszewski et al. presented surface initiated polymerization using ATRP for the synthesis of bimodal styrene brushes on silica.[14] Schadler et al. has presented bimodal PDMS brushes grafted onto metal oxide nanoparticles.[15,16] With effective synthetic methodology established bimodal brush systems have been explored for various thermomechanical, electrical, and optical enhancements.[12,15,17]

Mixed brush grafted nanoparticles, where two distinct chemical populations of polymer brushes are attached to a substrate surface have been synthesized previously with a focus on environmental responsiveness to a solvent.[18–22] Benicewicz et al. successfully implemented silica nanoparticles consisting of polystyrene short brushes and poly(methylmethacrylate) (PMMA) long brushes into a PMMA matrix.[6,13] The nanoparticles were well dispersed and demonstrated that only the long chain population needed to be compatible with the polymer matrix and even immiscible polymers can effectively screen enthalpic interactions of the matrix and filler. The finding opened the door for the possibility of highly functional mixed bimodal brushes where the short population can impart additional functionality (optical, electrical, responsive etc.) without being compatible with the bulk polymer matrix. With appropriate ligand engineering advanced multifunctional nanoparticles based on bimodal architecture can be realized.

Nanoparticles containing more than one chemical functionality on the surface are emerging as powerful tools for tailoring nanocomposite properties. Along with polymer brushes, additional ligands can be added to the filler surface with goal of adding functionality to the composite beyond what the intrinsic properties of the filler can offer. Thus far, multifunctional nanoparticles have been designed for enhancements in optical, biological, and dielectric properties. Schadler et al. has investigated multifunctional grafted ZrO_2 nanoparticles for color converting LED encapsulants. High refractive index ZrO_2 nanoparticles were made compatible with a silicone matrix using bimodal polydimethylsiloxane (PDMS) brushes while an organic phosphor was also attached to the particle surface allowing for simultaneous particle dispersion and light color conversion.[23] Benicewicz et al. investigated dye labeled polymethylacrylic acid (PMAA) grafted nanoparticles where PMAA polymers can bind to biomolecules and a fluorescent dye can be used to track particle movements in biological enviroments.[24] This thesis will discuss in detail the advancements made in dielectric applications using multifunctional nanoparticles.[25–27] Realization of the property enhancements attainable through multifunctional ligand engineering is reliant upon synthetic methodology capable of creating the highly decorated particles. Figure 1.2 highlights some of the advances in surface modified nanoparticles.

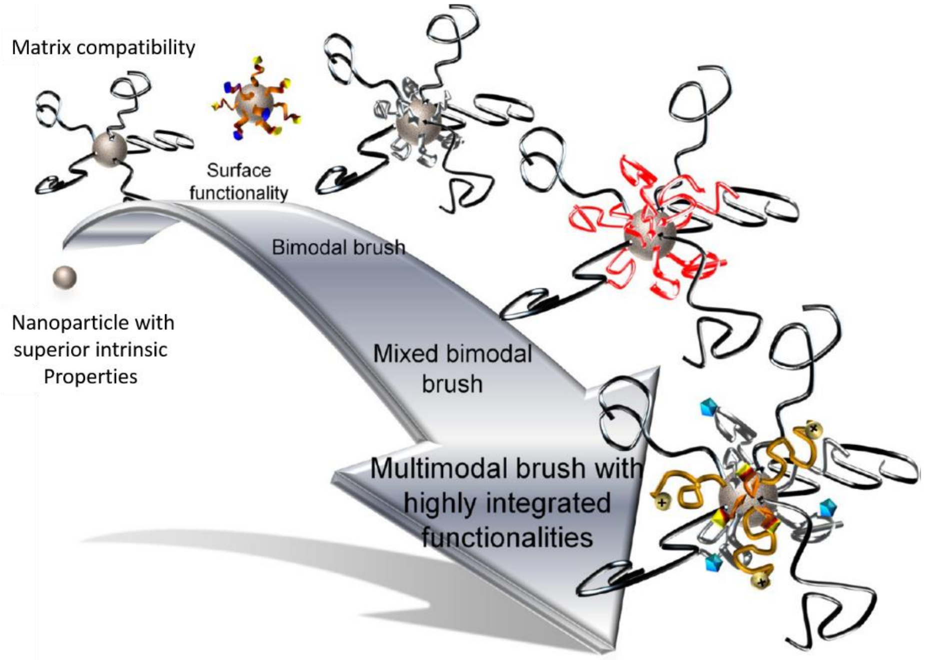

Figure 1.2: Evolution surface modification on grafted nanoparticles.[28]

1.2 Composite Fillers

Silica

Silica nanoparticles are versatile solid supports that are widely available and moderately priced. Reported silica substrates include glass, fumed, and colloidal silica. Surface modification employs organosilane coupling reagents that work by small molecule condensation at the substrate surface to form Si-O-Si bonds. The reaction is reliant on the presence of hydroxyl groups present at the silica surface. The term coupling reagent is used because they will generally include additional functional groups for subsequent surface reactions. Chlorosilane, alkoxysilane, and allylsilane functionalities have been used to treat silica surfaces.[26,29–32] Organosilane coupling reagents are widely available commercially, making the modification of silica an attractive process for composite synthesis.

Metal Oxides

Several metal oxide fillers exist each with unique properties that can be imparted into polymer nanocomposites. Popular oxides include but are not limited to cobalt, iron, titanium, zirconium, aluminum, indium, and tin. Modification of the metal oxide surface has been performed using amine, ammonium, carboxylic acid, silane, phosphate, phosphonate, and phosphonic acid moieties.[33–43] Long chain aliphatic carboxylic acids are used in the synthesis of metal oxide nanoparticles that act as stabilizers to prevent oxidation and allow for suspension in organic solvents. Carboxylic acids do not form covalent linkages with metal oxides therefore ligand exchange can be readily performed with supplementary carboxylic acids or other compatible moieties. Organosilane reagents covalently bond to metal oxides however, there is competition for surface modification with homocondensation of the silanes.[44] Organophosphorus reagents are attractive as they do not homocondense and provide a robust linkage through the homolytically stable M-O-P bond. The M-O-Si bond formed with silane coupling is hydrolyzed easily in acidic, basic or nucleophilic catalysts.[45] Phosphorus derived linkers offer a more robust linkage but commercial availability is limited compared to organosilane coupling reagents. Figure 1.3 highlights functional groups used to metal oxide grafting.

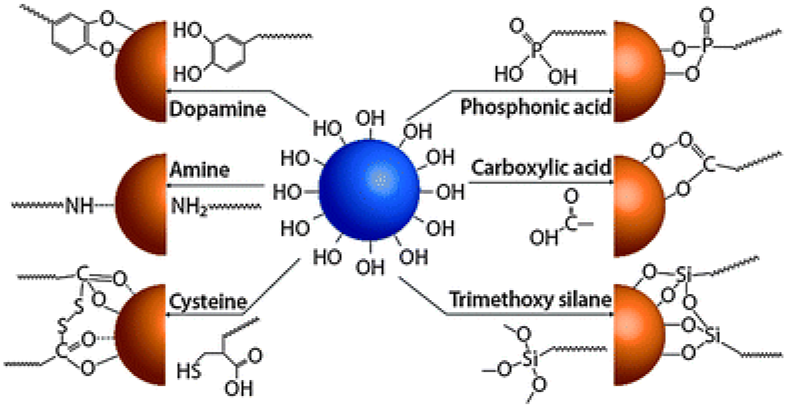

Figure 1.3: Grafting methods for ligand attachment to metal oxide substrates.[46]

1.3 Grafting Methods

Covalent attachment of polymer chain ends to a substrate can be achieved by utilizing one of two synthetic strategies: grafting-to or grafting-from. The grafting-to method uses a reactive polymer chain end to attach to a chemically compatible moiety on the substrate surface. The modular approach of grafting-to is advantageous for industrial applications. The limitation of the grafting-to method lies within steric constraints of attaching polymer chains to a substrate surface. Once an initial population of polymer is established on the surface it becomes increasingly difficult for new polymers to diffuse to the surface and attach. Limited polymer graft densities are able to be achieved using the grafting-to method therefore it has a limited scope of applications where high density brushes are required.

Grafting-from uses an initiator or chain transfer agent (CTA) covalently attached to a substrate surface to grow polymer chains outward from the surface. The steric constraint associated with grafting-to is alleviated by grafting a small molecule initiator or CTA to the substrate surface. Monomer can effectively diffuse to the surface and propagating chain ends. Using the grafting-from approach a full range of polymer graft densities can be achieved allowing for various polymer brush heights and morphologies at the substrate surface. The morphology of attached polymers at varying graft density was explored further by Kumar et al.[47]

Not mentioned above are non-covalent means for polymer association with a substrate surface. Physisorbtion refers to polymers associated with a substrate through non covalent interaction. Physisorption is worth noting because it is a popular methodology for surface functionalization however this work will focus on the more robust covalent attachment methods mentioned above. All three attachment methods are illustrated in Figure 1.4. Selection of the most appropriate grafting method is determined upon the requirements of the end application where grafted chain density, brush height, chemistry, and process all need to be considered.

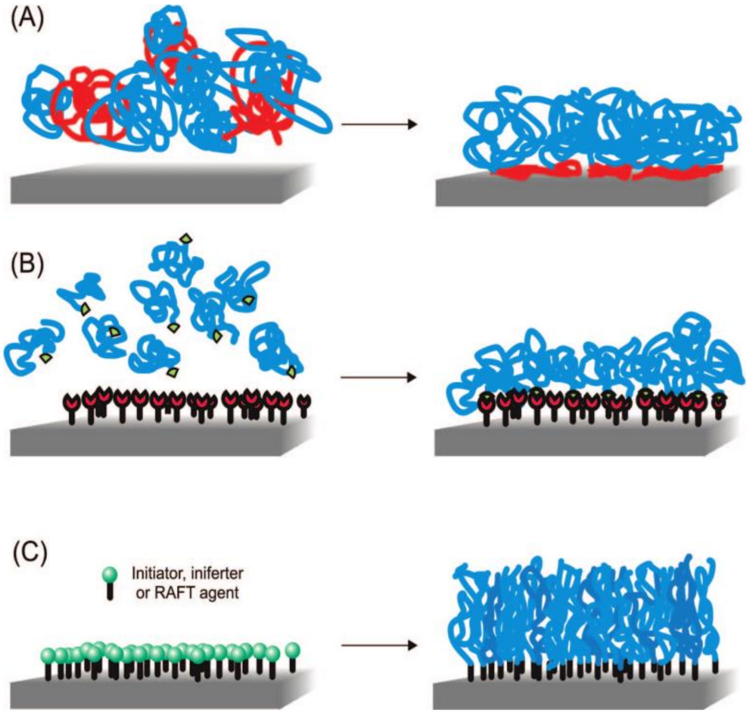

Figure 1.4: Various methods for grafting polymer chains to a substrate surface: A) physisorbtion, B) grafting-to and C) grafting-from methods.[48]

1.4 Controlled Radical Polymerization Methods

Beginning in the 1980's, new controlled polymerization techniques began to emerge that gave living characteristics to free radial polymerization. The development of controlled radical polymerization (CRP) techniques allowed for precise control over polymer molecular weights with narrow polydispersity and the ability to create well defined polymer architectures. CRP techniques began with nitroxide mediated polymerization(NMP)[49] followed by atom transfer radical polymerization (ATRP).[50] Then in 1998 a group from CSIRO in Australia developed reversible addition-fragmentation chain transfer polymerization (RAFT).[51] Living polymerizations that preceded CRP included cationic, anionic and ring opening polymerization. Control over the radical process was desired as it can be performed under relatively mild conditions, is more tolerant of functional groups, and was already largely utilized by industry for the majority of manufactured polymers.

To understand living radial polymerization, one must first consider conventional radical polymerization processes. In traditional free radical polymerization, radicals are generated by, most commonly, the thermal or photo decomposition of an initiator species. Upon initiation, polymers are produced by a propagating chain reaction where monomer is sequentially added to the growing chain end. The rate of termination is much higher than the rate of initiation therefore, high molecular weight polymers are formed early in the reaction and terminated quickly. Conversion will be low early in the reaction but will continue to increase as the initiator decomposes. The propagating species can undergo a variety of termination reactions including, chain combination, disproportionation, and chain transfer. The resultant polymers are ill defined without control over molecular weight and architecture.[52]

For an ideal living polymerization: all chains will be initiated early in the reaction, grow at the same rate, and lack termination reactions. For this to be possible, termination reactions need to be suppressed. This can be achieved through reversible deactivation or reversible chain transfer. Under these conditions the molecular weight can grow linearly with narrow molecular weight distributions. Because the reaction is not terminated, polymerization can be reinitiated after completion allowing for advanced polymer architectures such as blocks, star, dendrimers, and networks.[46,53,54]

NMP

Nitroxide mediated polymerization (NMP) uses a reversible deactivation by coupling mechanism consisting of an alkoxyamine species to control the kinetics of polymerization.[55] The active (propagating) species is formed via dissociation of a nitroxide radical. The equilibrium between dormant and active species favors the dormant species limiting the number of active radical species present during the reaction. This limits the possibility of termination reactions at the propagating chain end.[56–59] Figure 1.5 shows the mechanism of monomer addition for NMP.

Numerous alkoxyamine derivatives have been synthesized and successfully employed in mediating NMP though 2,2,6,6-tetramthylpiperidnyloxy (TEMPO) is the most ubiquitous.[60] NMP has achieved the most success polymerizing styrenic monomers however, acrylic and methacrylic monomers have been have been successfully polymerized by NMP as of late.[61–64] NMP derived polymers have been attached to a variety of substrates using both the grafting-to and grafting-from approach. Substrates have included colloidal silica, fumed silica, CdSe quantum dots, carbon nanotubes (CNT's), metal oxides, and clays.[65–71] The reaction temperatures to achieve activation of the nitroxide radical is high, further limiting the selection of monomers containing thermally sensitive functional groups.

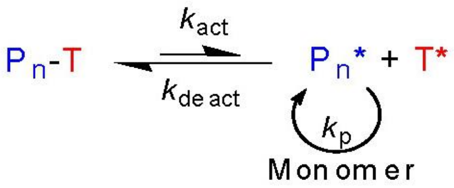

Figure 1.5: Reversible deactivation by coupling (NMP mechanism).

ATRP

Atom transfer radical polymerization or ATRP was first reported by Matyjaszewski et al. in 1995.[50] The process uses a reversible deactivation of an alkyl halide initiator with transfer to a metal complex to control free radical polymerization.[72] The halide is homolytically transferred to the metal-ligand complex, allowing for monomer addition before the equilibrium shifts back to the dormant species where the chain end is restored to the alkyl halide species. The reversible deactivation mechanism is found in Figure 1.6. Uniform growth is accomplished with fast initiation and rapid reversible deactivation.

ATRP has quickly become the most popular method of controlled radical polymerization because it is compatible with a wide range of monomers and reaction conditions. The utility of ATRP has resulted in numerous reports being published combining ATRP polymers with inorganic substrates.[48,73–80] The removal of the metal catalyst from a polymeric or hybrid composite system can be problematic limiting its application in some functional materials.

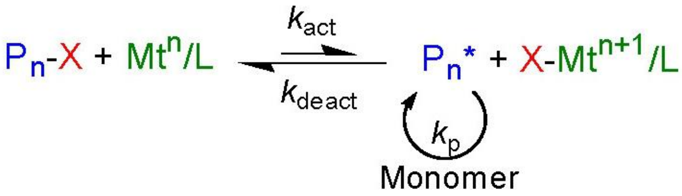

Figure 1.6: Reversible deactivation with transfer to a metal complex (ATRP mechanism)

RAFT

Reversible addition fragmentation chain-transfer or RAFT polymerization was developed in the late 1990’s by a group of Australian scientists at CSIRO. Unlike NMP and ATRP, RAFT uses a reversible chain transfer mechanism to achieve living polymerization kinetics. Control over polymerization is derived from the RAFT chain transfer agent or CTA. The RAFT CTA consists of either a dithioester or trithiocarbonate functional group. The mechanism of polymerization is shown in Figure1.7. It is important to note: RAFT CTAs are consumed early in the reaction to ensure that all chains are initiated before propagation. The ratio of RAFT agent to initiator is kept high to limit the number of active species and lessen the probability of termination between active radical species. There is a rapid rate of exchange between radical active and dormant chains.

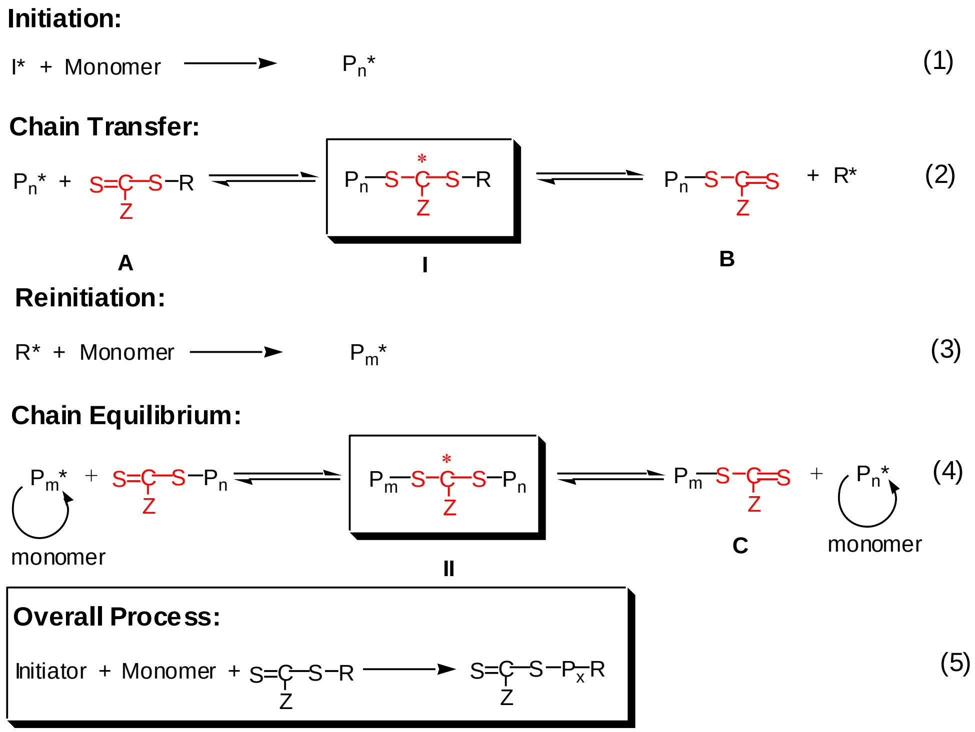

Figure 1.7: Mechanism of RAFT polymerization.

The Z and R groups of the RAFT agent are responsible for controlling the rate of addition of the propagating radical species to the CTA. The Z group determines reactivity by its ability to stabilize an adjacent radical center. The R group should be a good homolytic leaving group with respect to Pn* and be able to reinitiate polymerization. Several RAFT CTAs have been synthesized for appropriate compatibility with various monomer classes.[81]

RAFT use in the literature has grown exponentially as a result of its versatility and avoidance of metal catalysts that can contaminate final products. A wide variety of monomers have been successfully polymerized using the technique including styrenics, acrylates, methacrylates, acrylamides, methacrylamides, and dienes. The process is tolerant to a large number of functional groups and reactions conditions including bulk, solution, emulsion and suspension.[82–84] Reaction temperature required for polymerization is the same as conventional free radical polymerization processes however the RAFT process is tolerant to higher temperatures as well.

1.5 Nanocomposites via RAFT Polymerization

Polymers derived using RAFT polymerization have been used for all three methods of nanoparticle surface modification, grafting-to, grafting-from and physisorbtion. RAFT CTAs produce thiocarbonyl polymer end groups that can be reduced to thiols with $NaBH_4$.[85] Both thiol and thiocarbonyl end groups are known to bind to gold nanoparticles making the combination of RAFT and gold substrates attractive for sensing, nanomedicine, and catalytic applications.[86–94] Alternative chain end chemistry can be implemented pre or post polymerization for compatibility with silica and metal oxide surfaces.[32] Metal oxide nanoparticles have been modified using RAFT polymers by incorporating organophosphorus moieties into RAFT polymer end groups and subsequently grafting to metal oxide surfaces.[34,95] Brittain et al. developed a method for using click chemistry to functionalize silica nanoparticles where alkyne terminated polyacrylamide chains were clicked to azide surface functionalized silica nanoparticles.[32] Block copolymers where one block contains silane side chains have been also been used for grafting to silica substrates. The blocks consisted of poly(N-isopropylacrylamide)-b-poly(γ-methacryloxypropyltrimethoxysilane) and were subsequently bound to the silica substrate though the silane containing block.[96]

Surface initiated RAFT polymerization uses a RAFT CTA bound to a substrate surface. The grafting-from approach allows for multiple polymer graft densities therefore multiple interesting brush morphologies.[47] Benicewicz et al. first developed a silane containing RAFT agent for direct attachment to silica surfaces.[97] Purification by column chromatography was difficult as the silane groups present in the RAFT agent tended to bind to the column substrate resulting in low yields. A method was later developed that sequentially added an aminosilane coupling reagent followed by an activated RAFT agent.[98] Figure 1.8 demonstrates nanoparticle functionalization using an activated RAFT agent. Activated RAFT agents contain a modified carboxylic acid that possess excellent leaving group chemistry. 2-Mecatothiazoline and N-hydroxysuccinimide (NHS) esters are commonly employed. The process proved to be a versatile method for surface modification of silica nanoparticles with effective graft densities of 0.01 – 0.7 ch/nm^2 being achieved. The versatility of RAFT has allowed for nanocomposites to be synthesized for several applications including hybrid materials, thermosresponsive, optical, electrical, self-healing, bio, and drug delivery.[46]

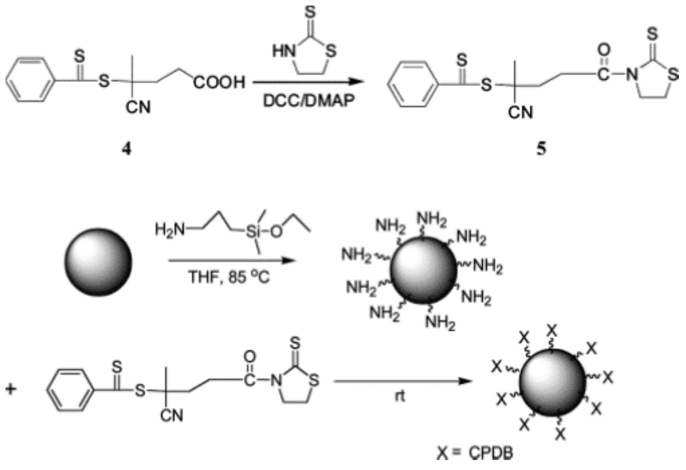

Figure 1.8: Synthesis and attachment of activated RAFT agent to SiO$_2$ nanoparticle.[98]

1.6 Dielectric Nanocomposites

With the progression of the microelectronics industry, devices have become increasingly smaller, a trend that will continue for the foreseeable future according to Moore’s law. Because of this trend, superior insulating materials or dielectrics are in demand to meet the critical requirements of the electronics industry. A goal for the industry is to find materials that meet electrical, thermal, and mechanical requirements. A material’s electrical insulating properties are essential in determining device performance and lifetime. Dielectric breakdown strength characterizes the materials electrical insulating properties or ability to resist dielectric breakdown caused by an applied electric field.

Dielectric breakdown is the point at which a material experiences catastrophic failure under an applied external electric field thereby going from an insulator to a conductor. There are three mechanisms of failure to consider when examining dielectric breakdown in polymers; intrinsic, thermal, and avalanche. Intrinsic breakdown describes the inherent electrical strength of a material and is independent of external conditions. This occurs when sufficient energy required to move electrons form the valence band to the conducting band is applied. Intrinsic breakdown is rarely observed in real world conditions as polymers and composites often contain defects and impurities that can cause alternative breakdown mechanisms before reaching the intrinsic breakdown field. Thermal breakdown occurs due to thermal conduction arising from polarization in the material. Avalanche breakdown occurs when free or “hot” electrons of sufficient energy collide with bound electrons in the material. The collisions result in the liberation of bound electrons, causing the rapid multiplication of hot electrons or an “avalanche”, ultimately resulting in a conducting pathway along the mean free path in the material.[99–101] Avalanche breakdown is thought to be one of the most common mechanisms of dielectric breakdown in polymers. Figure 1.9 shows an image of avalanche breakdown in epoxy resin.

Figure 1.9: Optical microscopy image of tree formed as a result of avalanche breakdown in epoxy resin.

Polymers have become attractive dielectric materials because of their low cost, processability, and high dielectric breakdown strength relative to traditional inorganics. There are several polymers available to the electronics industry that offer a variety desired properties. Reports have shown that incorporation of nano sized fillers can increase the dielectric breakdown strength of polymeric materials. The hybrid materials are called dielectric nanocomposites or nanodielectrics. The large interface of the nano filler allows for enhancements in dielectric breakdown strength at loadings on the order of 1-5%.[102–106] The exact mechanism for the dielectric breakdown enhancements is elusive but it is widely accepted that the filler-matrix interface offers a charge trapping layer that can trap migrating charge alleviating percolation across the matrix.[107–111] Regular distribution of the nano fillers throughout the matrix is thought to disrupt the continuity of migrating charge through a torturous pathway.

The literature presents several investigations into the effects of adding nano sized fillers to polymers on dielectric breakdown strength. One of the factors largely attributed to variations of dielectric breakdown strength is dispersion of the filler.[112–115] Since the interface is believed to be largely responsible for breakdown enhancements, preservation of the interface is crucial. Modifications to dielectric filler surfaces with organic ligands have been made with the intention to reduce variations in surface energy of the two components. Perry et al. presented phosphonic acid modified $BaTiO_3$ nanoparticles in polycarbonate where the surface groups added were believed to reduce the incompatibility of the filler and matrix.[116] The resultant increase in breakdown strength was attributed to increases in filler dispersion. Gao et al. demonstrated that silica nanoparticles modified with a methacrylic silane coupling agent were better dispersed in epoxy resin and showed improvements in breakdown strength.[112]

Chemistry added to the filler surface has also shown to alter dielectric breakdown strength by altering the electronic nature of the filler. It is difficult to distinguish the nature of breakdown strength improvements where added ligands both alter interfacial chemistry and improve dispersion however, a few examples have demonstrated a clear contribution of surface chemistry. Schadler et al. modified TiO_2 nanoparticles with N-(2-aminoethyl) 3-aminopropyl-trimethoxysilane (AEAPS), a silane coupling agent.[108] When introduced into LDPE, the particles were agglomerated compared to untreated particles however showed increases in dielectric breakdown strength. Because dispersion was decreased upon surface modification, the improvements in breakdown strength were attributed to the polar nature of the surface groups. Schuman et al. introduced TiO_2 surface modified with aromatic phosphonic acids in epoxy resin. Correlation was observed between the nature of aromatic substitution and composite breakdown strength following Hammett parameters where strong electron withdrawing groups enhanced dielectric breakdown strength.

1.7 Dissertation Outline

This dissertation focuses on the design, synthesis, and characterization of applied polymer composite materials as well as the property enhancements afforded by them. Multifunctional ligand engineering was used to design ligands for nanoparticle attachment that impart functionality for environmental compatibility as well as property enhancements beyond what is inherent of the filler. Modifications on both silica and metal oxide surfaces were performed using various synthetic strategies. The synthesized composites were then used to investigate the multifunctional particles' contribution to dielectric properties.

In Chapter 2, a modular one pot grafting-to synthetic methodology based on click chemistry is presented to construct silica nanoparticles containing two distinct chemical populations. The multifunctional ligand grafted particles were then incorporated into an epoxy resin with the goal of investigating variations in dielectric properties. A long population of alkyne terminated poly(glycidylmethacrylate) (PGMA) was synthesized via RAFT polymerization to impart filler compatibility with the epoxy matrix. Ferrocene and terthiophene were selected as electroactive short ligands and synthesized to contain click functionality. The short and long ligands were simultaneously attached to azide coated 15 nm silica nanoparticles. The interface was designed to enhance dielectric properties by simultaneously promoting filler dispersion with polymer chains and charge trapping with the electroactive short ligands. It was found that by using the one pot click methodology, diffusion of the two distinct ligand populations was successful to the particle surface. The multifunctional ligand approach proved successful in improving the dielectric breakdown strength of the composite compared to neat epoxy and silica filled epoxies.

Chapter 3 expounds on the initial finding of Chapter 2 and answers questions left at the conclusion of the work. What is the effect of dispersion on the multifunctional system? What is the effect of the electroactive ligands independent of dispersion? Can predictions be made for composite performance based on surface chemistry? A synthetic methodology that sequentially implements ligands to the particle surface was presented. The synthetic strategy presented offers a way to precisely control the dispersion of silica nanoparticles in an epoxy resin by modifying the quantity of polymer chains attached to the surface, as well as, incorporate electroactive functionality at the interface. The multiple states of dispersion achieved in this work have not been seen in previous studies investigating dielectric breakdown strength of epoxy composites. The demonstrated control over filler dispersion also presented the opportunity to study varied chemistry covalently bound to the filler surface in well dispersed states. The trends observed for the varied chemistry at the filler interface proved useful in developing a metric that could further predict improvements of composite electrical strength based on surface chemistry.

Chapter 4 deals with the modification of metal oxide nanoparticles, specifically TiO_2 and ZrO_2 with the focus of again improving dielectric breakdown strength. Functional anthracene ligands containing phosphonic acids were synthesized for attachment to 5 nm TiO_2 nanoparticles. Two anthracene phosphonic acid species were synthesized differing in electronic substitution. TiO_2 nanoparticles were decorated with a bimodal population of PDMS chains for compatibility with a commercial silicone matrix. Comparisons of dielectric breakdown strength were then made between TiO_2 nanoparticles varying in surface modification. A novel RAFT agent was also proposed that would allow for surface initiated RAFT polymerization from the surface of metal oxide fillers. The implication being, the same level of graft density control seen with silica substrates could now be realized with metal oxides. The RAFT agent contained a phosphate moiety and was synthesized in two synthetic steps. The RAFT agent was successfully attached to 4 nm ZrO_2 nanoparticles. Investigation into the kinetics of SI polymerization using the RAFT agent showed that the reagent was not successful in controlling the living kinetics of MMA.

Finally, Chapter 5 deviates from the goal of improving dielectric properties and moves to improving the suspension of industrial fracking proppants. Current industrial formulations use sand or metal oxide particulates as proppants for hydrocarbon extraction. The unmodified proppants can quickly settle out of solution and cause clogs in modern drilling operations. Presented in Chapter 5, is an aqueous surface initiated free radical polymerization used to polymerize polyacrylamide from the surface of 5 μm silica particles. A novel activated azo free radical initiator was synthesized for attachment to the surface of the silica particles and subsequent SI free radical polymerization. The suspension time in water of the synthesized polymer grafted particles was then monitored using transmittance measurements. The polymer grafted samples had longer suspension times compared to ungrafted polymer samples in water. Correlation was also observed for the weight percent of polymer present on the particle surface and the suspension time in water where samples with higher grafted polymer content remained suspended longer.

1.8 References

(1) Schadler, L. S.; Kumar, S. K.; Benicewicz, B. C.; Lewis, S. L.; Harton, S. E. *MRS Bull.* **2007**, *32* (04), 335.

(2) Winey, K. I.; Vaia, R. A. *MRS Bull.* **2007**, *32* (04), 314.

(3) Hule, R. A.; Pochan, D. J. *MRS Bull.* **2007**, *32* (04), 354.

(4) Krishnamoorti, R. *MRS Bull.* **2007**, *32* (04), 341.

(5) Baur, J.; Silverman, E. *MRS Bull.* **2007**, *32* (04), 328.

(6) Li, Y.; Krentz, T. M.; Wang, L.; Benicewicz, B. C.; Schadler, L. S. *ACS Appl. Mater. Interfaces* **2014**, *6* (9), 6005.

(7) Nelson, J. K.; Hu, Y. *J. Phys. D. Appl. Phys.* **2005**, *38* (2), 213.

(8) Sunday, D.; Ilavsky, J.; Green, D. L. *Macromolecules* **2012**, *45* (9), 4007.

(9) Maillard, D.; Kumar, S. K.; Rungta, A.; Benicewicz, B. C.; Prud'Homme, R. E. *Nano Lett.* **2011**, *11* (11), 4569.

(10) Kumar, S. K.; Jouault, N.; Benicewicz, B.; Neely, T. *Macromolecules* **2013**, *46* (9), 3199.

(11) Akcora, P.; Liu, H.; Kumar, S. K.; Moll, J.; Li, Y.; Benicewicz, B. C.; Schadler, L. S.; Acehan, D.; Panagiotopoulos, A. Z.; Pryamitsyn, V.; Ganesan, V.; Ilavsky, J.; Thiyagarajan, P.; Colby, R. H.; Douglas, J. F. *Nat. Mater.* **2009**, *8* (4), 354.

(12) Natarajan, B.; Neely, T.; Rungta, A.; Benicewicz, B. C.; Schadler, L. S. *Macromolecules* **2013**, *46* (12), 4909.

(13) Rungta, A.; Natarajan, B.; Neely, T.; Dukes, D.; Schadler, L. S.; Benicewicz, B. C. *Macromolecules* **2012**, *45* (23), 9303.

(14) Yan, J.; Kristufek, T.; Schmitt, M.; Wang, Z.; Xie, G.; Dang, A.; Hui, C. M.;

Pietrasik, J.; Bockstaller, M. R.; Matyjaszewski, K. *Macromolecules* **2015**, *48* (22), 8208.

(15) Li, Y.; Tao, P.; Viswanath, A.; Benicewicz, B. C.; Schadler, L. S. *Langmuir* **2013**, *29* (4), 1211.

(16) Li, Y.; Wang, L.; Natarajan, B.; Tao, P.; Benicewicz, B. C.; Ullal, C.; Schadler, L. S. *RSC Adv.* **2015**, *5* (19), 14788.

(17) Qiao, Y.; Yin, X.; Wang, L.; Islam, M. S.; Benicewicz, B. C.; Ploehn, H. J.; Tang, C. *Macromolecules* **2015**, *48* (24), 8998.

(18) Sidorenko, A.; Minko, S.; Schenk-Meuser, K.; Duschner, H.; Stamm, M. *Langmuir* **1999**, *15* (24), 8349.

(19) Feng, J.; Haasch, R. T.; Dyer, D. J. *Macromolecules* **2004**, *37* (25), 9525.

(20) Zhao, B.; Zhu, L. *Macromolecules* **2009**, *42* (24), 9369.

(21) Zhao, B. *Polymer (Guildf).* **2003**, *44* (15), 4079.

(22) Zhao, B.; He, T. *Macromolecules* **2003**, *36* (23), 8599.

(23) Li, Y.; Tao, P.; Siegel, R. W.; Schadler, L. S. *MRS Proc.* **2013**, *1547*, 161.

(24) Wang, L.; Benicewicz, B. C. *ACS Macro Lett.* **2013**, *2* (2), 173.

(25) Krentz, T. M.; Huang, Y.; Nelson, J. K.; Schadler, L. S.; Bell, M.; Benicewicz, B. *2014 Annu. Rep. Conf. Electr. Insul. Dielectr. Phenom.* **2014**, 643.

(26) Huang, Y.; Krentz, T. M.; Nelson, J. K.; Schadler, L. S.; Bell, M.; Benicewicz, B. In *2015 IEEE Electrical Insulation Conference (EIC)*; IEEE: Seattle, WA, 2015; pp 325–328.

(27) Virtanen, S.; Krentz, T.; Nelson, J.; Schadler, L.; Bell, M.; Benicewicz, B.; Hillborg, H.; Zhao, S. *IEEE Trans. Dielectr. Electr. Insul.* **2014**, *21* (2), 563.

(28) Li, Y.; Krentz, T. M.; Wang, L.; Benicewicz, B. C.; Schadler, L. S. *ACS Appl. Mater. Interfaces* **2014**, *6* (9), 6005.

(29) Tripp, C. P.; Hair, M. L. *J. Phys. Chem.* **1993**, *97* (21), 5693.

(30) Wang, Y.; Hu, S.; Brittain, W. J. *Macromolecules* **2006**, *39* (17), 5675.

(31) Fadeev, A. Y.; McCarthy, T. J. *Langmuir* **2000**, *16* (18), 7268.

(32) Ranjan, R.; Brittain, W. J. *Macromolecules* **2007**, *40* (17), 6217.

(33) Ata, M. S.; Liu, Y.; Zhitomirsky, I. *RSC Adv.* **2014**, *4* (43), 22716.

(34) Boyer, C.; Bulmus, V.; Priyanto, P.; Teoh, W. Y.; Amal, R.; Davis, T. P. *J. Mater. Chem.* **2009**, *19* (1), 111.

(35) Bulusu, A.; Paniagua, S. A.; Macleod, B. A.; Sigdel, A. K.; Berry, J. J.; Olson, D. C.; Marder, S. R.; Graham, S. *Langmuir* **2013**, *29* (12), 3935.

(36) Dong, H.; Huang, J.; Koepsel, R. R.; Ye, P.; Russell, A. J.; Matyjaszewski, K. *Biomacromolecules* **2011**, *12* (4), 1305.

(37) Hotchkiss, P. J.; Jones, S. C.; Paniagua, S. a; Sharma, A.; Kippelen, B.; Armstrong, N. R.; Marder, S. R. *Acc. Chem. Res.* **2012**, *45* (3), 337.

(38) Koh, S. E.; McDonald, K. D.; Holt, D. H.; Dulcey, C. S.; Chaney, J. a; Pehrsson, P. E. *Langmuir* **2006**, *22* (14), 6249.

(39) Mutin, P. H.; Guerrero, G.; Vioux, A. *J. Mater. Chem.* **2005**, *15* (35-36), 3761.

(40) Neouze, M.-A.; Schubert, U. *Monatshefte für Chemie - Chem. Mon.* **2008**, *139* (3), 183.

(41) Tahir, M. N.; Eberhardt, M.; Theato, P.; Faiß, S.; Janshoff, A.; Gorelik, T.; Kolb, U.; Tremel, W. *Angew. Chemie - Int. Ed.* **2006**, *45* (6), 908.

(42) Thissen, P.; Valtiner, M.; Grundmeier, G. *Langmuir* **2010**, *26* (1), 156.

(43) Ulman, A. *Chem. Rev.* **1996**, *96* (4), 1533.

(44) Silverman, B. M.; Wieghaus, K. A.; Schwartz, J. *Langmuir* **2005**, *21* (1), 225.

(45) Brinker, C. J.; Scherer, G. W. *Sol-Gel Science: The Physics and Chemistry of Sol-Gel Processing*; Academic Press: New York, 3013.

(46) Boyer, C.; Stenzel, M. H.; Davis, T. P. *J. Polym. Sci. Part A Polym. Chem.* **2011**, *49* (3), 551.

(47) Dukes, D.; Li, Y.; Lewis, S.; Benicewicz, B.; Schadler, L.; Kumar, S. K. *Macromolecules* **2010**, *43* (3), 1564.

(48) Barbey, R.; Lavanant, L.; Paripovic, D.; Schuwer, N.; Sugnaux, C.; Tugulu, S.; Klok, H.-A. *Chem. Rev.* **2009**, *109* (Copyright (C) 2012 American Chemical Society (ACS). All Rights Reserved.), 5437.

(49) Solomon, D. H.; Rizzardo, E.; Cacioli, P. Polymerization process and polymers produced thereby. US4581429, April 1986.

(50) Wang, J. S.; Matyjaszewski, K. *J. Am. Chem. Soc.* **1995**, *117* (6), 5614.

(51) Chiefari, J.; Chong, Y. K. B.; Ercole, F.; Krstina, J.; Jeffery, J.; Le, T. P. T.; Mayadunne, R. T. A.; Meijs, G. F.; Moad, C. L.; Moad, G.; Rizzardo, E.; Thang, S. H.; South, C. *Macromolecules* **1998**, *31* (16), 5559.

(52) Odian, G. *Radical Chain Polymerization*, Fourth Ed.; John Wiley & Sons, Inc.: Hoboken, NJ, USA, 2004.

(53) Fukuda, T.; Terauchi, T.; Goto, A.; Tsujii, Y.; Miyamoto, T.; Shimizu, Y. *Macromolecules* **1996**, *29* (8), 3050.

(54) Matyjaszewski, K.; Tsarevsky, N. V. *Nat. Chem.* **2009**, *1* (4), 276.

(55) Greszta, D.; Mardare, D.; Matyjaszewski, K. *Macromolecules* **1994**, *27*, 638.

(56) Catala, J. M.; Bubel, F.; Ouland Hammouch, S. *Macromolecules* **1995**, *28*, 8441.

(57) Georges, M. K.; Veregin, R. P. N.; Kazmaier, P. M.; Hamer, G. K. *Macromolecules* **1993**, *26* (11), 2987.

(58) Moad, G.; Rizzardo, E. *Macromolecules* **1995**, *28*, 8722.

(59) Rizzardo, E.; Serelis, A.; Solomon, D. *Aust. J. Chem.* **1982**, *35* (10), 2013.

(60) Hawker, C. J.; Bosman, A. W.; Harth, E. *Chem. Rev.* **2001**, *101* (12), 3661.

(61) Guillaneuf, Y.; Gigmes, D.; Marque, S. R. A.; Astolfi, P.; Greci, L.; Tordo, P.; Bertin, D. *Macromolecules* **2007**, *40* (9), 3108.

(62) Couvreur, L.; Lefay, C.; Belleney, J.; Charleux, B.; Guerret, O.; Magnet, S. *Macromolecules* **2003**, *36* (22), 8260.

(63) Nicolas, J.; Charleux, B.; Guerret, O.; Magnet, S. *Angew. Chemie* **2004**, *116* (45), 6312.

(64) Chong, Y. K.; Ercole, F.; Moad, G.; Rizzardo, E.; Thang, S. H.; Anderson, A. G. *Macromolecules* **1999**, *32* (21), 6895.

(65) Bartholome, C.; Beyou, E.; Bourgeat-Lami, E.; Chaumont, P.; Lefebvre, F.; Zydowicz, N. *Macromolecules* **2005**, *38* (4), 1099.

(66) Bartholome, C.; Beyou, E.; Bourgeat-Lami, E.; Chaumont, P.; Zydowicz, N. *Polymer (Guildf).* **2005**, *46* (19 SPEC. ISS.), 8502.

(67) Brinks, M. K.; Studer, A. *Macromol. Rapid Commun.* **2009**, *30* (13), 1043.

(68) Chevigny, C.; Gigmes, D.; Bertin, D.; Jestin, J.; Boué, F. *Soft Matter* **2009**, *5* (19), 3741.

(69) Konn, C.; Morel, F.; Beyou, E.; Chaumont, P.; Bourgeat-Lami, E. *Macromol. Symp.* **2007**, *40*, 7464.

(70) Sill, K.; Emrick, T. *Chem. Mater.* **2004**, *16* (7), 1240.

(71) Husseman, M.; Malmstrom, E. E.; McNamara, M.; Mate, M.; Mecerreyes, D.; Benoit, D. G.; Hedrick, J. L.; Mansky, P.; Huang, E.; Russell, T. P.; Hawker, C. J. *Macromolecules* **1999**, *32* (5), 1424.

(72) Colombani, D. *Prog. Polym. Sci.* **1997**, *22* (8), 1649.

(73) Fristrup, C. J.; Jankova, K.; Hvilsted, S. *Soft Matter* **2009**, *5* (23), 4623.

(74) Singh, N.; Wang, J.; Ulbricht, M.; Wickramasinghe, S. R.; Husson, S. M. *J. Memb. Sci.* **2008**, *309* (1-2), 64.

(75) Marutani, E.; Yamamoto, S.; Ninjbadgar, T.; Tsujii, Y.; Fukuda, T.; Takano, M. *Polymer (Guildf).* **2004**, *45* (7), 2231.

(76) Chen, R.; Feng, W.; Zhu, S.; Botton, G.; Ong, B.; Wu, Y. *J. Polym. Sci. Part A Polym. Chem.* **2006**, *44* (3), 1252.

(77) Yang, W. J.; Neoh, K.-G.; Kang, E.-T.; Lee, S. S. C.; Teo, S. L.-M.; Rittschof, D. *Biofouling* **2012**, *28* (9), 895.

(78) Lee, S. H.; Dreyer, D. R.; An, J.; Velamakanni, A.; Piner, R. D.; Park, S.; Zhu, Y.; Kim, S. O.; Bielawski, C. W.; Ruoff, R. S. *Macromol. Rapid Commun.* **2010**, *31* (3), 281.

(79) Morandi, G.; Heath, L.; Thielemans, W. *Langmuir* **2009**, *25* (14), 8280.

(80) Sun, Y.; Ding, X.; Zheng, Z.; Cheng, X.; Hu, X.; Peng, Y. *Eur. Polym. J.* **2007**, *43* (3), 762.

(81) Keddie, D. J.; Moad, G.; Rizzardo, E.; Thang, S. H. *Macromolecules* **2012**, *45* (13), 5321.

(82) Moad, G.; Rizzardo, E.; Thang, S. H. *Aust. J. Chem.* **2005**, *58* (6), 379.

(83) Moad, G.; Rizzardo, E.; Thang, S. H. *Aust. J. Chem.* **2009**, *62* (11), 1402.

(84) Moad, G.; Rizzardo, E.; Thang, S. H. *Aust. J. Chem.* **2006**, *59* (10), 669.

(85) Zhu, M. Q.; Wang, L. Q.; Exarhos, G. J.; Li, A. D. Q. *J. Am. Chem. Soc.* **2004**, *126* (9), 2656.

(86) Yusa, S. I.; Fukuda, K.; Yamamoto, T.; Iwasaki, Y.; Watanabe, A.; Akiyoshi, K.; Morishima, Y. *Langmuir* **2007**, *23* (26), 12842.

(87) Boyer, C.; Whittaker, M. R.; Luzon, M.; Davis, T. P. *Macromolecules* **2009**, *42* (18), 6917.

(88) Hotchkiss, J. W.; Lowe, A. B.; Boyes, S. G. *Chem. Mater.* **2007**, *19* (1), 6.

(89) Fustin, C.-A.; Colard, C.; Filali, M.; Guillet, P.; Duwez, A.; Meier, M. A. R.; Schubert, U. S.; Gohy, J.-F. *Langmuir* **2006**, *22* (15), 6690.

(90) Aqil, A.; Qiu, H.; Greisch, J.-F.; Jérôme, R.; De Pauw, E.; Jérôme, C. *Polymer (Guildf).* **2008**, *49* (5), 1145.

(91) Kim, S.; Yoo, M.; Kang, N.; Moon, B.; Kim, B. J.; Choi, S. H.; Kim, J. U.; Bang, J. *ACS Appl. Mater. Interfaces* **2013**, *5* (12), 5659.

(92) Jiao, Y.; Chou, T.; Akcora, P. *Macromolecules* **2015**, *48* (14), 4910.

(93) Liang, M.; Lin, I.-C.; Whittaker, M. R.; Minchin, R. F.; Monteiro, M. J.; Toth, I. *ACS Nano* **2010**, *4* (1), 403.

(94) Zhu, L.; Yang, Y.; Farquhar, K.; Wang, J.; Tian, C.; Ranville, J.; Boyes, S. G. *ACS Appl. Mater. Interfaces* **2016**, *8* (7), 5040.

(95) Tao, P.; Viswanath, A.; Schadler, L. S.; Benicewicz, B. C.; Siegel, R. W. *ACS Appl. Mater. Interfaces* **2011**, *3* (9), 3638.

(96) Zhang, Y.; Luo, S.; Liu, S. *Macromolecules* **2005**, *38* (23), 9813.

(97) Li, C.; Benicewicz, B. C. *Macromolecules* **2005**, *38*, 5929.

(98) Li, C.; Han, J.; Ryu, C. Y.; Benicewicz, B. C. *Macromolecules* **2006**, *39* (9), 3175.

(99) Seitz, F. *Phys. Rev.* **1948**, *73* (6), 549.

(100) Seitz, F. *Phys. Rev* **1949**, *76* (9), 1376.

(101) Sparks, M.; Mills, D. L.; Warren, R.; Holstein, T.; Maradudin, A. A.; Sham, L. J.; Loh, E.; King, D. F. *Phys. Rev. B* **1981**, *24* (6), 3519.

(102) Brandstetter, S. S.; Drummy, L. F.; Horwath, J. C.; Schweickart, D. L.; Vaia, R. A. In *2008 IEEE International Power Modulators and High-Voltage Conference*; IEEE, 2008; pp 287–290.

(103) Tomer, V.; Manias, E.; Randall, C. A. *J. Appl. Phys.* **2011**, *110* (4), 0.

(104) Tomer, V.; Polizos, G.; Manias, E.; Randall, C. A. *J. Appl. Phys.* **2010**, *108* (7).

(105) Tomer, V.; Polizos, G.; Randall, C. A.; Manias, E. *J. Appl. Phys.* **2011**, *109* (7).

(106) Imai, T.; Sawa, F.; Nakano, T.; Ozaki, T.; Shimizu, T.; Kozako, M.; Tanaka, T. *IEEE Trans. Dielectr. Electr. Insul.* **2006**, *13* (2), 319.

(107) Tanaka, T.; Kozako, M.; Fuse, N.; Ohki, Y. *IEEE Trans. Dielectr. Electr. Insul.* **2005**, *12* (4), 669.

(108) Ma, D.; Hugener, T. a; Siegel, R. W.; Christerson, A.; Mårtensson, E.; Önneby, C.; Schadler, L. S. *Nanotechnology* **2005**, *16* (6), 724.

(109) Smith, R. C.; Liang, C.; Landry, M.; Nelson, J. K.; Schadler, L. S. *IEEE Trans. Dielectr. Electr. Insul.* **2008**, *15* (1), 187.

(110) Roy, M.; Nelson, J. K.; MacCrone, R. K.; Schadler, L. S.; Reed, C. W.; Keefe, R.; Zenger, W. *IEEE Trans. Dielectr. Electr. Insul.* **2005**, *12* (4), 629.

(111) Roy, M.; Nelson, J. K.; MacCrone, R. K.; Schadler, L. S. *J. Mater. Sci.* **2007**, *42*

(11), 3789.

(112) Gao, M.; Zhang, P.; Wang, F.; Li, L.; Li, Z. In *2013 Annual Report Conference on Electrical Insulation and Dielectric Phenomena*; IEEE, 2013; pp 234–237.

(113) Tkalya, E.; Ghislandi, M.; Otten, R.; Lotya, M.; Alekseev, A.; Van Der Schoot, P.; Coleman, J.; De With, G.; Koning, C. *ACS Appl. Mater. Interfaces* **2014**, *6* (17), 15113.

(114) Grabowski, C. a.; Fillery, S. P.; Westing, N. M.; Chi, C.; Meth, J. S.; Durstock, M. F.; Vaia, R. a. *ACS Appl. Mater. Interfaces* **2013**, *5* (12), 5486.

(115) Tan, D.; Cao, Y.; Tuncer, E.; Irwin, P. *Mater. Sci. Appl.* **2013**, *4* (April), 6.

(116) Kim, P.; Jones, S. C.; Hotchkiss, P. J.; Haddock, J. N.; Kippelen, B.; Marder, S. R.; Perry, J. W. *Adv. Mater.* **2007**, *19* (7), 1001.

CHAPTER 2

ONE POT GRAFTING-TO SYNTHESIS OF BIMODAL FUNCTIONALIZED SILICA FOR DIELECTRIC NANOCOMPOSITES

2.1 Abstract

A novel one pot grafting-to synthesis is presented to create bimodal ligand grafted silica nanoparticles, with the goal of improving the AC dielectric breakdown strength of silica-epoxy nanocomposites. Bimodal ligands consisted of long poly(glycidylmethacrylate) (PGMA) polymer chains that are compatible with the epoxy matrix and promote filler dispersion, as well as, short ligands consisting of terthiophene or ferrocene to add charge trapping functionality. Click chemistry was used as an efficient means for simultaneous attachment of ligands to the filler surface. Bimodal samples were then successfully cast into epoxy resin. TEM microscopy was used to monitor nanoparticle dispersion and dielectric breakdown testing was used to determine improvements in electrical strength. The synthesized composites were successful in improving AC dielectric breakdown strength compared to reference epoxy by as much as 44% with only 2 wt% SiO_2 loading. Text and figures are reproduced and adapted from *IEEE Trans. Dielectr. Electr. Insul.* **2014**, *21* (2), 563.

2.2 Introduction

It is now well established that polymers filled with nanoscale inorganic particles can show improvements in permittivity, loss, voltage endurance, and dielectric breakdown strength.[1–5] The central goal of the nanocomposite is to maintain the large interfacial surface area between the filler and matrix to tailor the properties of the composite. Enthalpic incompatibility of the inorganic filler and organic polymer can prevent mixing and cause filler agglomeration. The addition of matrix compatible polymeric species covalently bound to the filler surface has been shown to be an effective means to promote filler dispersion within a polymeric matrix, therefore maintaining the large interfacial area necessary to bring forth property enhancements.[6–8]

Many groups have investigated the effects of filler dispersion on the dielectric properties of nanocomposites.[9–13] It is now known that dielectric properties tend to improve with improved filler dispersion. Recent studies have also found that altering the electronic nature of the filler-matrix interface can affect the dielectric properties of the bulk composite.[14,15] Previously, when adding functionality to the surface of nanofillers, researchers had to choose between adding functionality to improve dispersion or functionality to alter the electronic nature of the filler surface. The use of a bimodal architecture allows for the modification of the filler surface with two separate populations so both parameters can be studied independently.

Covalent attachment of ligands at the substrate surface can be achieved in a variety of ways. One versatile method is “clicking” ligands onto the surface. Click chemistry defines a class of chemical reactions that are highly selective, efficient, produce high yields, and have easily isolated products.[16] This technique has established a means to effectively functionalize substrates pre or post polymerization.[17–22] Click chemistry combined with RAFT polymerization has provided a “toolbox” approach to synthesizing polymer nanocomposites.[23–26] Click defines many organic reactions but the most popular reaction used is the Huisgen Cycloaddition, a 1,3 dipolar cycloaddition between an azide and an alkyne.[27]

In this work click chemistry is utilized as a mild and efficient means to simultaneously attach two separate ligand species to the surface of silica nanoparticles. The attached ligands will serve the function of dispersing the nanoparticle (PGMA) and adding electronic functionality (terthiophene or anthracene). The selected ligands were synthesized to contain terminal alkyne groups for subsequent click attachment to the nanoparticle surface. This work aims to investigate the relationship between interfacial chemistry and bulk dielectric properties to further gain a fundamental understanding of the interface, so predictions can be made for further property enhancements.

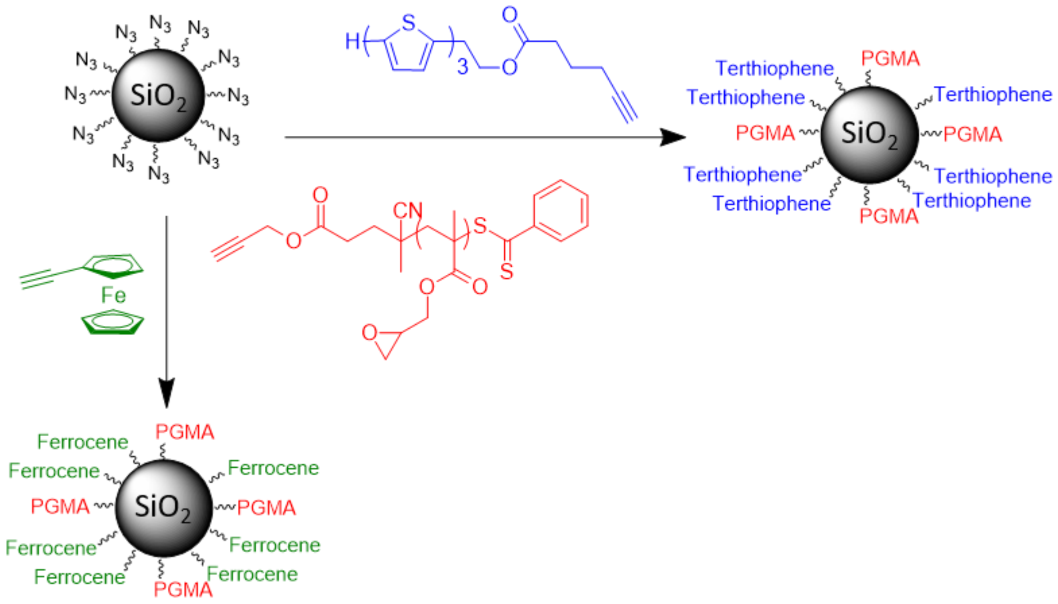

Figure 2.1: Synthesis of the bimodal grafted nanoparticles used in this study.

2.3 Experimental Section

Materials

All reagents were used as received from Fisher Scientific unless otherwise stated below. AIBN was purchased from Sigma Aldrich and recrystallized 3x from methanol. Glycidyl methacrylate was obtained from TCI and purified via passing through a column of neutral alumina. 4-Cyanopentanoic acid dithiobenzoate (CPDB) was received from Strem Chemical, Inc. 3-Aminopropyldimethylethoxysilane was obtained from Gelest. 3-(Chloropropyl)trimethoxysilane and ethynylferrocene was obtained from Sigma Aldrich.

Colloidal silica particles of 30 wt% dispersed in methyl ethyl ketone were kindly provided by Nissan Chemical. The average particle diameter, 14 ± 4 nm as measured by TEM and 20 nm as measured by light scattering.

Instrumentation

NMR spectra were recorded on a Varian 300 spectrometer using $CDCl_3$ as a solvent. Molecular weights and molecular weight distributions were determined using a Waters gel-permeation chromatograph equipped with a 515 HPLC pump, a 2410 refractive index detector, three Styragel columns (HR1, HR3, HR4 in the effective molecular weight range of 100-5000, 500-30000 and 5000-500000, respectively) with THF as eluent at 30°C and a flow rate of 1.0 mL/min. The GPC system was calibrated with poly(methyl methacrylate) and polystyrene standards obtained from Polymer Labs.

Synthesis of Alkyne CPDB

To a 100ml round bottom flask, a solution of 4-cyanopentanoic acid dithiobenzoate (CPDB) (0.5 g, 1.8 mmol), propargyl alcohol (0.1g, 2 mmol), and N,N, dicyclohexylcarbodiimide (DCC) (0.4 g, 2 mmol) in 40 ml dichloromethane was added. The solution was cooled to 0°C and flushed with N_2 for 15 min while stirring. Next a solution of 4-dimethylaminopyridine (18 mg, 0.2 mmol) in 5 ml dichloromethane was added dropwise to the CPDB solution over a period of 30 min. The reaction was then left to warm to room temperature and stir for 6 hours. The solids were filtered and the resulting solution was concentrated in vacuum. The product was then purified by column chromatography (SiO_2, hexanes:ethyl acetate, 4:1). Product was obtained as a dark red oil (yield 0.55 g, 96%). ^1H NMR (400 MHz, $CDCl_3$): δ (ppm) 7.90 (d, J = 6.3 Hz, 1H), 7.54 (t, J = 7.4 Hz, 1H), 7.37 (t, J = 8 Hz, 1H), 4.72 (d, J = 2.5 ,3H), 2.7 – 2.5 (m, 5H), 1.94 (s, 3H), ^{13}C NMR (400 MHz, $CDCl_3$): δ (ppm) 222.4, 171, 144.8, 133.3, 128.8, 127, 118.7, 77.5, 75.5, 52.7, 45.9, 33.5, 29.8, 24.4. HRMS (EI-DP) m/z: [M^+] Calcd for $C_{16}H_{15}NO_2S_2$ 316.0457; Found 316.0466.

Synthesis of Alkyne Terminated PGMA

In a side arm Schlenk tube alkyne CPDB (200mg, 63 μmol), AIBN (0.1 mg, 6.3 μmol), and glycidyl methacrylate (GMA) (8.9 g, 63 mmol) were dissolved into 10 ml THF. The solution was subjected to 3 freeze pump thaw cycles then placed in an oil bath for 5 hours at 60°C. The reaction was quenched by placing the Schlenk tube in ice water for 5 min. The polymer solution was poured into 200 ml hexanes to precipitate the product. The resultant polymer was centrifuged at 3,000 rpm for 5 min and the supernatant was discarded. The polymer was redissolved back into 5 ml THF before washing with hexanes 2 more times. Polymer was then characterized by GPC to determine molecular weight and dispersity. Mn: 12.8 kg/mol *Đ*: 1.14.

Synthesis of Alkyne Terminated Terthiophene

Terthiopheneethanol was prepared as outlined in the literature.[28] To 50 ml of dry DCM Terthiopheneethanol (0.47 g, 1.6 mmol), 5-hexynoic acid (0.20g, 1.8mmol) and 4-dimethylaminopyridine (16mg, 0.13 mmol) were added. The solution was cooled to 0°C and flushed with nitrogen before adding N,N'-dicyclohexylcarbodiimide (0.33 g, 1.6 mmol) in 10 ml of DCM dropwise over 30 min. The solution was allowed to warm to room temperature and react overnight. The resulting salts were filtered and the solvent removed under reduced pressure leaving a dark yellow solid. The resultant solid was then subjected to column chromatography (SiO_2, $CHCl_3$) yielding a bright yellow solid (0.54 g, 1.4 mmol) in 87% yield. MP: 76-78°C. 1H NMR (400 MHz, $CDCl_3$): δ (ppm) 7.21 (dd, J1 = 5.1 Hz, J2 = 1.1 Hz, 1H), 7.16 (dd, J1 = 3.6 Hz, J2 = 1.1 Hz, 1H), 7.06 (d, J = 3.8 Hz, 1H), 7.03 – 7.00 (m, 3H), 6.77 (d, J = 3.6 Hz, 1H), 4.32 (t, J = 6.6 Hz, 2H), 3.12 (t, J = 6.4 Hz, 2H), 2.47 (t, J = 7.4 Hz, 2H), 2.24 (t, J = 6.9, 2H), 1.97 (t, J = 2.9 Hz, 1H), 1.84 (t, J = 7.2 Hz, 2H) ^{13}C NMR (400 MHz, $CDCl_3$): δ (ppm) 172.2, 139.5, 137.2, 136.3, 136, 135.9, 135.8, 127.9, 126.5, 124.4, 124.3, 124, 123.7, 123.5, 83.3, 69.2, 64.4, 32.9, 29.6, 23.6, 17.9. HRMS (EI-DP) m/z: [M^+] Calcd for $C_{20}H_{18}O_2S_3$ 386.0470; Found 386.0469.

Synthesis of CPDB Grafted Silica

A solution of Colloidal silica (10 ml, 30 wt%) was added to 100 ml round bottom flask. The solution was diluted to 50 ml with THF. 3-Aminopropyldimethylethoxy silane (17 mg, 110 μmol) was then added to the solution. The reaction vessel was flushed with N_2 before refluxing for 4 hours. The particles were precipitated in a large amount of hexanes (300 ml) and isolated by centrifuge at 3,000 rpm and discarding supernatant. The washing was repeated 3 times before dispersing particles in 50 ml THF. Activated CPDB synthesis has been described previously.[29] A solution of activated CPDB in THF (50 mg, 132 μmol) was added dropwise to the particle solution and left to stir overnight at room temperature. The solution was precipitated into a large amount of hexanes (300 ml) and particles were isolated by centrifuging at 3,000 rpm for 5 minutes and discarding the supernatant. The particles were dissolved into THF and washing with hexanes was repeated two more times. The CPDB grafted particles were dried in vacuum for 2 hours before measuring CPDB graft density by UV-vis spectroscopy. Graft density was determined using a standard calibration curve of free CPDB ($\sigma = 0.15$ ch/nm^2).

Synthesis of Monomodal PGMA Grafted Silica (Grafting-From)

CPDB grafted silica nanoparticles (1 g, 36 μmol/g) GMA (5.2 g, 37 mmol), AIBN (0.6 mg, 3.7 μmol), and THF (5 ml) were added to a dried side arm Schlenk tube. The solution was degassed with 3 freeze pump thaw cycles and placed in an oil bath at 60°C for 4 hours. The reaction was quenched by placing the Schlenk tube in ice water for 5 minutes. The solution was poured into a large amount of hexanes (200 ml). The solution was centrifuged at 3,000 rpm for 5 minutes and supernatant was discarded. Recovered particles were redispersed into THF and washed with hexanes two more times. A small amount of the product was isolated and polymer chains were cleaved from the silica particles using a hydrofluoric acid solution. The resultant polymer chains were analyzed by GPC (Mn: 14kg/mol, *Đ*: 1.24)

Synthesis of Azide Surface Functionalized Nanoparticles

A solution of Colloidal silica (40 ml, 30 wt%) was added to 250 ml round bottom flask along with 3-(chloropropyl)trimethoxysilane (1.18 g, 6.0 mmol). The solution was refluxed under argon overnight before cooling to room temperature. The reaction mixture was precipitated into a large amount of hexanes (500 mL). The particles were recovered by centrifugation at 3000 rpm for 15 min. The particles were then redissolved in 20 mL of acetone and precipitated in 200 mL of hexanes. The functionalized particles were dispersed directly into 50 mL of DMF for subsequent use. An aliquot of the functionalized silica nanoparticles was dried and subjected to thermal gravimetric analysis to determine the amount of silane agent anchored onto the particles (4 wt%). 3-Chloropropyl)trimethoxysilane functionalized silica particles (0.59 g (3 mmol)) and sodium azide (0.3 g, 5.52 mmol) was added into 100 ml round bottom flask in DMF and refluxed at 100°C for 4 hours. After the reaction excess sodium azide was washed with deionized water three times. The particles were dissolved in THF to form a clear solution. An aliquot for TGA was taken (weight loss due to silane linker 5-6 %).

Synthesis of Bimodal Nanoparticles

0.8g Functionalized particles; azide (1 equiv) 0.08g alkyne terthiophene (10 equiv), 0.2 g alkyne terminated PGMA (1 eq), and PMDETA (40 microliters (0.5 equiv)) were added in 40 mL of dry THF. The mixture was degassed by bubbling argon gas for 5 minutes to get rid of oxygen before adding CuBr (7mg (0.5 equiv)) and stirred for 24 hrs. Particles were precipitated by deionized water and centrifuged at 4000 rpm for 10min to wash remaining catalyst then washed 2 times with hexanes to wash excess ligands.

Composite Preparation

Particles were mixed with Huntsman Araldite GY 2600; a bisphenol-A based epoxy resin using a Hauschild high shear mixer (FlackTek). Solvent residue was evaporated in vacuum. Loading of silica was determined via TGA, and the resin was diluted and combined with aliphatic amine based Huntsman Aradur 956-2 hardener to achieve the appropriate final composite loading. The composite resin and hardener mixture was likewise mixed in a high shear mixer and then cast into the appropriate shapes. Recessed samples[30,31] were used for breakdown tests, disks were created for dielectric spectroscopy, and microtome samples were created and processed for transmission electron microscopy (TEM) analysis.

2.4 Results and Discussion

Synthesis of Alkyne terminated PGMA (Long Brush)

PGMA long chains were chosen in this system for their demonstrated compatibility with commercial epoxy resin.[20,32] Scheme 2.1 outlines the synthesis of alkyne terminated PGMA. Synthesis of alkyne terminated PGMA was performed by first synthesizing the alkyne derivative of the commercially available RAFT agent, 4-cyanopentanoic acid dithiobenzoate (CPDB). Steglich Esterification was used to combine CPDB and propargyl alcohol in the presence of DCC to achieve the alkyne RAFT agent in one step. Next alkyne CPDB was used to polymerize glycidyl methacrylate (GMA) in the presence of AIBN. Post polymerization characterization of the alkyne functional group is difficult because the polymer repeat units dilute the chain end to the point where conventional NMR and IR techniques cannot detect its presence. However, previous efforts have demonstrated that the alkyne terminal group of the RAFT agent remained intact during the polymerizations of methyl methacrylate and glycidyl methacrylate. In these previous demonstrations the alkyne terminus was able to react in subsequent click reactions post polymerization.[33,34] Alkyne terminated PGMA was successfully synthesized at molecular weight of 12.8 kg/mol.

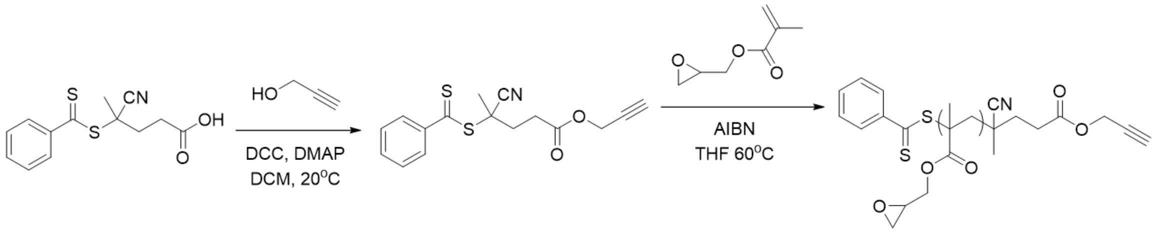

Scheme 2.1: Synthesis of alkyne terminated PGMA.

Synthesis of Alkyne Terminated Terthiophene

Short ligands were selected to add functionality to the overall composite. Conjugated polarizable ligands were selected as they are believed to act as electron traps at the composite interface. Alkyne ferrocene was commercially available and purchased from Sigma Aldrich. Alkyne terthiophene required synthesis of the desired product. The synthesis was achieved in three steps starting form commercially available thiopheneethanol and in one additional step from previously synthesized terthiopheneethanol.[28] Steglich Esterification was used to couple 5-hexynoic acid with terthiophene ethanol. The synthesis is outlined in Scheme 2.2. The resultant ester product was alkyne terminated terthiophene.

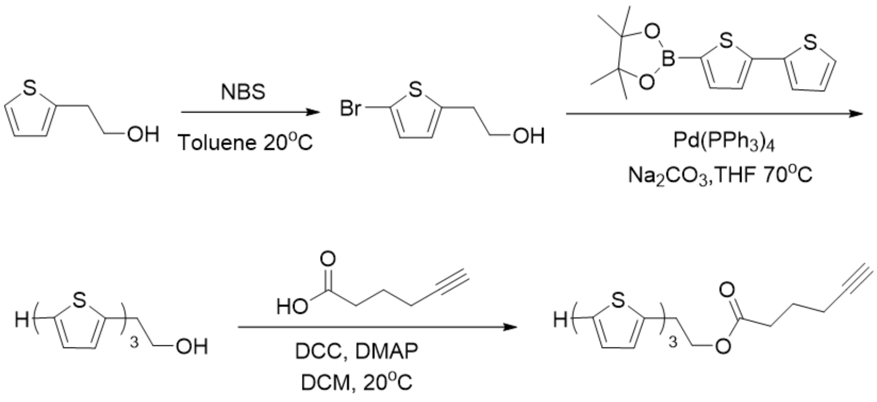

Scheme 2.2: Synthesis of alkyne terminated terthiopehene.

One Pot Synthesis of Bimodal Functionalized Silica Nanoparticles

The synthetic scheme for the synthesis of the bimodal particles is shown in Scheme 2.3. Azide surface modified nanoparticles were prepared as described before by Brittain et al.[17] In the first step, 3-(chloropropyl)trimethoxysilane was attached to the silica surface through a silane coupling reaction. Next, the chlorine group was substituted with an azide group using sodium azide. At this point FT-IR was used to verify the presence of azide groups on the silica surface. The presence of a peak at 2100 cm^{-1} was indicative of azide stretching[35] and confirmed the presence to the surface azide groups. Next grafting of the ligands to the particles was performed using the Huisgen Cycloaddition, click reaction. Alkyne terminated PGMA and one of the selected alkyne containing electroactive ligands was then grafted to the particle surface simultaneously. At the conclusion of the click reaction FT-IR, UV-vis, and TGA analysis were performed. FT-IR analysis confirmed the success of the reaction with the disappearance of the peak at 2100 cm^{-1} assigned to the stretching of the azide moiety. In addition, the appearance of a strong sharp peak at 1700 cm^{-1} characteristic of carbonyl group stretching[37] was observed in the FT-IR spectra upon completion of the reaction. Carbonyl groups are contained within the PGMA polymer as well as the terthiophene derivative. The presence of electroactive short ligands was confirmed by analysis with UV-vis spectroscopy. Terthiophene has an absorbance maxima of 360 nm and ferrocene 440 nm. The presence of these absorbance maxima after particle work up confirmed the attachment of the electroactive short ligands. TGA analysis was then used to verify weight gain due to surface groups and quantify polymer chain density. Accurate graft density determination by TGA is difficult because one is not able to distinguish weight loss attributed to short and long populations of grafted moieties. A range of possible polymer graft densities can be established by calculating polymer graft density assuming all weight loss is attributed to 12 kg/mol PGMA long chains then subtracting the theoretical maximum contribution of short ligands. Previous studies have shown that 15 nm silica nanoparticles have a maximum graft density of 0.7 ch/nm^2. Using this number, it was found that the maximum number of short ligands (0.7 ch/nm^2) equates to 0.02 ch/nm^2

of 12.5 kg/mol PGMA. The graft density assuming all surface groups were 12.5 kg/mol PGMA was found to be 0.05 ch/nm^2, establishing the possible PGMA graft density between 0.03 ch/nm^2 and 0.05 ch/nm^2. The obtained graft densities correlate with previously obtained graft densities using the grafting-to approach.[38]

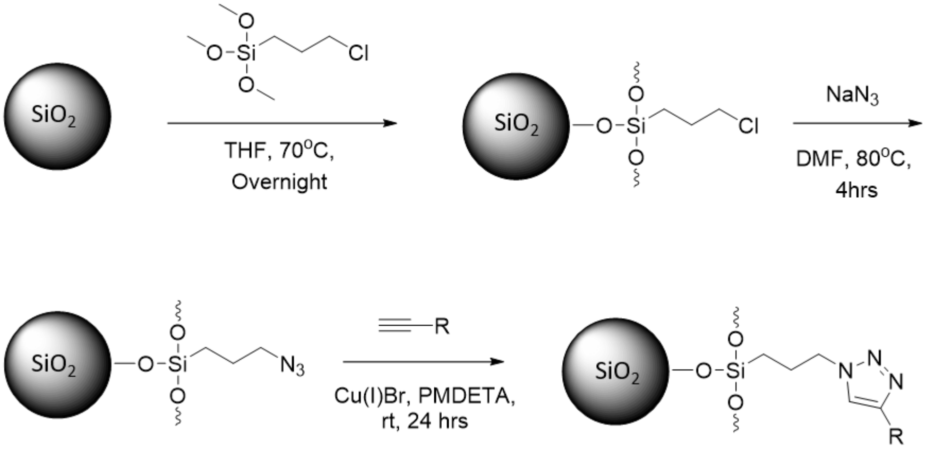

Scheme 2.3: Synthesis of azide grafted silica nanoparticles and subsequent click reaction.

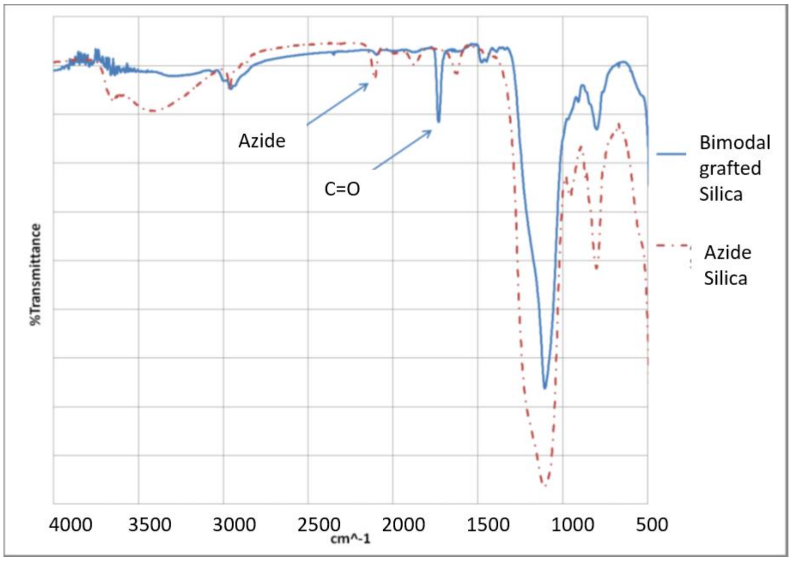

Figure 2.2: Comparison of FT-IR spectra for azide grafted silica and bimodal PGMA-terthiophene grafted silica. Note the disappearance of the azide peak at 2100 cm^{-1} and appearance of carbonyl peak at 1700 cm^{-1}.

Synthesis of Monomodal PGMA-Silica

Monomodal PGMA grafted silica was synthesized with a grating-from approach that has been outlined in literature previously.[29] The synthesis is outlined in Scheme 2.4. First, the surface of silica nanoparticles were amine functionalized using an aminosilane coupling reagent. CPDB was then attached through amidation of the activated acid. An excess of activated CPDB was added to ensure complete conversion of all the surface amine groups. CPDB graft density was determined with UV-vis spectroscopy. The CPDB surface functionalized nanoparticles were used to polymerize GMA in a surface initiated RAFT polymerization, yielding PGMA grafted silica nanoparticles.

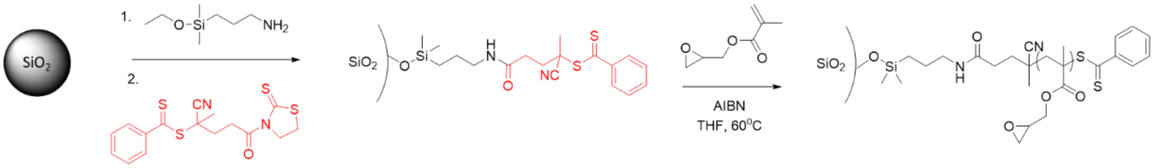

Scheme 2.4: Synthesis of PGMA grafted silica nanoparticles via grafting-from approach.

Composite Characterization

Casting and characterization of the composites was performed by collaborators at Rensselaer Polytechnic Institute. The synthesized composites were first characterized by TEM microscopy to monitor the dispersion of the added fillers. TEM images are shown in Figure 2.3. Dispersion of the synthesized composites was quantified by measuring the unreinforced polymer or free space length (L_f). L_f is calculated by tiling a statistically large number of boxes over a binarized TEM image and counting the number of particles in each box. The L_f corresponds to the width of the largest box for which the most likely particle count in a randomly placed box is zero. Thus, L_f provides a quantifier of the size of unreinforced polymer domains in the composite. Larger L_f then describes a less dispersed composite as phase separated filler will result in larger areas of unreinforced polymer.

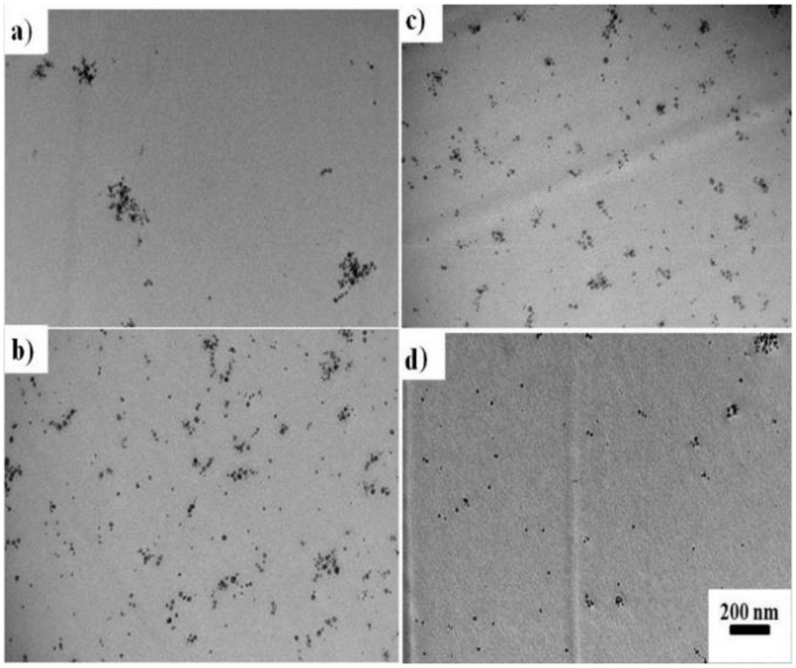

Figure 2.3: TEM micrographs of synthesized composites: a) 1 wt% bare silica in epoxy b) 2 wt% monomodal PGMA grafted silica in epoxy c) 2 wt% bimodal grafted PGMA-terthiophene silica in epoxy d) 2 wt% bimodal PGMA-ferrocene silica in epoxy.

Table 2.1: Free space length (L_f) and dielectric breakdown strength of synthesized composites (wt% represents silica in final casted samples).

	Sample	**L_f (nm)**	**α (kV/mm)**	**β value**	**Δ DBS**
	Neat epoxy	NA	185	4.2	NA
a)	Bare SiO_2 (1 wt%)	900	182	4.4	-2 %
b)	MM-PGMA-SiO_2 (2 wt%)	250	213	3.7	+15 %
c)	BM-PGMA-Terthiophene (2 wt%)	250	266	4.3	+44 %
d)	BM-PGMA-Ferrocene (2 wt%)	550	235	3.4	+27 %

Composite AC breakdown strength was measured with recessed samples, ball (1/4" thickness) and plane electrodes, and a ramp of 500 V/s as described previously.[39] The samples were created with a nominal thickness in the recess of 100 μm, with the exact thickness measured for each recess before breakdown. Breakdown was analyzed using a 2-parameter Weibull probability function.

$$P(E) = 1 - \exp\left[-\left(\frac{E}{\propto}\right)^{\beta}\right]$$

P(E) is the probability of failure, E is the breakdown strength determined through experimentation, α is the scale parameter, which describes the breakdown field at 63.2% probability of failure, and β is the shape parameter. %Δ breakdown strength was determined by comparison of the scale parameter composite sample versus the scale parameter from reference samples of neat epoxy. Results for (L_f) and breakdown strength are shown in Figure 2.3.

The neat commercial epoxy has breakdown strength of 185 kV/mm and was used as reference for all of the synthesized composites. Addition of unmodified silica nanoparticles to the epoxy resulted in filler agglomeration characterized by large phase separated regions visible in the TEM micrograph and a large L_f of 900 nm. Addition of the unmodified silica was detrimental to the electrical strength of the epoxy and caused a 2% decrease in dielectric breakdown strength compared to the neat reference epoxy. Modification of the silica nanoparticles with epoxy compatible PGMA chains was successful at promoting filler dispersion. TEM micrographs of the monomodal PGMA grafted silica showed the filler at an improved dispersion state compared to unmodified filler, but still containing small anisotropic clusters. L_f for the composite was 250 nm. The dispersed monomodal PGMA grafted silica sample saw an increase of 15% in dielectric breakdown strength. The increase in breakdown strength of PGMA modified compared to unmodified silica was assumed to be a result of increased dispersion as the chemistry of the PGMA chains is similar to the epoxy resin.

Bimodal grafted nanoparticles were then characterized. PGMA-terthiophene bimodal grafted nanoparticles were dispersed similarly to monomodal PGMA grafted silica particles with a L_f of 250 nm. PGMA-terthiophene bimodal grafted particles demonstrated the largest increase in breakdown strength with a 44% improvement. Analysis of TEM micrographs of PGMA-ferrocene bimodal grafted particles showed the L_f of the synthesized composite to be 550 nm. The breakdown strength of the composite was increased 27% compared to neat epoxy. The addition of short conjugated ligands to the nanoparticle surface was shown to contribute to increases in breakdown strength for the bimodal composites. Dispersion effects were ruled out because bimodal grafted particles were of similar dispersion or less dispersed than the monomodal sample according to L_f analysis of the TEM micrographs. It is then believed that the conjugated short ligands of the bimodal samples act as electron trapping groups that perturb migration of free electrons that are responsible for electrical breakdown. Comparison of PGMA-terthiophene and PGMA-ferrocene bimodal grafted particles is difficult as the quantified dispersions were dissimilar. However, there was correlation between increases in breakdown strength of the bimodal composites and reduction potential of the short ligands.[40] Further investigation is needed to divulge the individual contribution of filler dispersion and surface chemistry.

Permittivity measurements were also performed using dielectric spectroscopy. The obtained data for real and imaginary permittivity is shown in Figure 2.4. Terthiophene-

PGMA-SiO_2, PGMA-SiO_2, and bare-SiO_2 all exhibited an increase in real permittivity. A decrease in real permittivity was observed for the ferrocene-PGMA bimodal sample. No significant increases in imaginary permittivity (loss) were observed. All of the filled samples remained comparable to the neat epoxy.

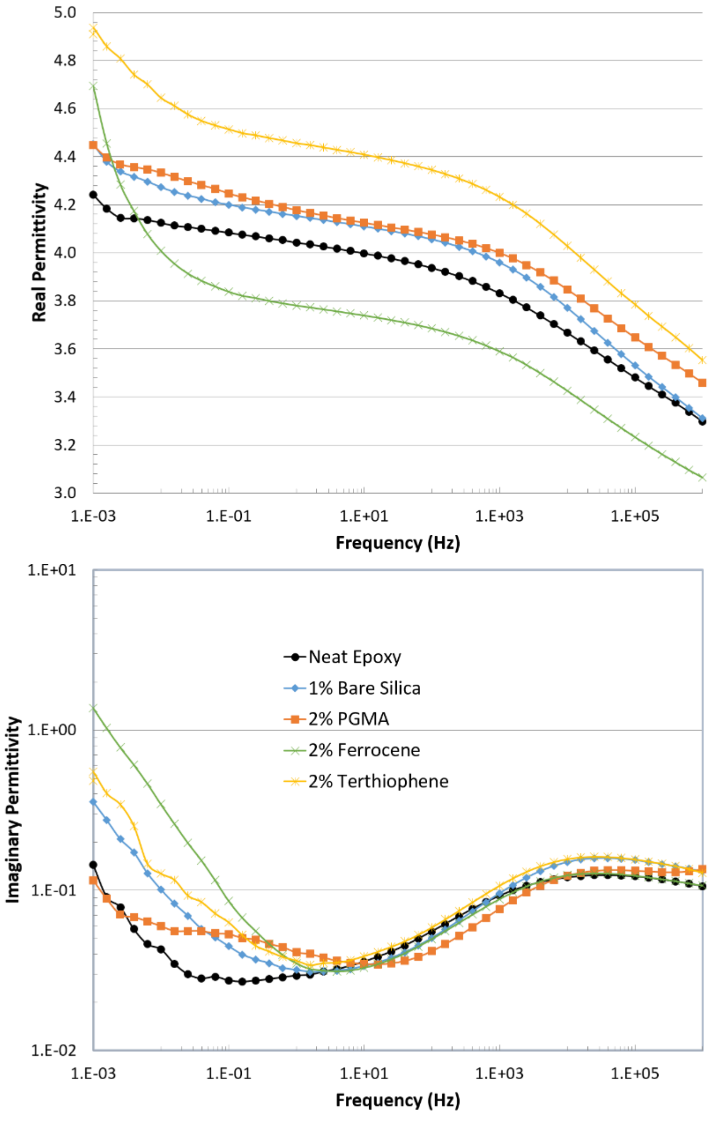

Figure 2.4: (top) Real permittivity measurements and (bottom) imaginary component of permittivity (loss) as a function of frequency for the synthesized composites.

2.5 Conclusion

A one pot grafting-to methodology was employed to synthesize two novel nanocomposites with the goal of improving the dielectric breakdown strength of a commercial epoxy resin. The multifunctional nanoparticles synthesized in this study were bimodal in nature, grafted with long PGMA chains and a short conjugated electroactive moiety. Click chemistry was employed as an efficient route to simultaneously attach the bimodal ligands to the silica nanoparticle surface. Two species of bimodal surface modified nanoparticles were synthesized, PGMA-terthiopehene and PGMA-ferrocene. Alkyne terminated PGMA chains were synthesized via RAFT polymerization. A novel alkyne derivative of terthiophene was synthesized and successfully employed in the one pot synthesis. Silica nanoparticles containing surface azide groups were synthesized as reported previously.[17] The synthesized composites were successful in improving AC dielectric breakdown strength by as much as 44% compared to reference epoxy.

Comparisons were made between the synthesized bimodal grafted composites, monomodal PGMA functionalized silica nanoparticles, bare silica, and neat epoxy. Evidence suggested that the chemistry at the particle interface as well as the dispersion state of the filler played a role in the dielectric enhancements of the novel composites. The methodology presented demonstrated an effective way to study electronic surface characteristics at well dispersed states. Further investigation is needed to determine what effects each of these parameters has on dielectric breakdown strength.

The one pot grafting-to approach is advantageous in that it uses a modular approach and limits the amount of synthetic steps necessary to functionalize the nanoparticle surface. For this reason, the synthetic methodology presented may be attractive for industrial applications. However, using the grafting-to approach limited the achievable polymer graft densities.[36] It has been presented in the literature that the dispersion state of the filler is known to play a role in dielectric enhancements.[2,9,11,41,42] It has also been demonstrated in the literature that increasing polymer chain density can be an effective means to increase enthalpic compatibility between filler and particle ultimately increasing filler dispersion.[43] Using the grafting-to approach, it may not be possible to achieve the polymer grafted chain density necessary to reach the ideal dispersion states that are postulated to bring forth greater property enhancements. A sequential addition method using a grafting-from approach may be more suitable for further investigation into such systems.

2.6 Acknowledgements

This work was performed in collaboration with Suvi Virtanen, Tim Krentz, and Linda Scadler of the Schadler research group at Rensselaer Polytechnic Institute, as well as, Su Zhao and Henrik Hillborg of ABB corporate research.

2.7 References

(1) Lewis, T. J. *IEEE Trans. Dielectr. Electr. Insul.* **1994**, *1* (5), 812.

(2) Rytoluoto, I.; Lahti, K.; Karttunen, M.; Koponen, M.; Virtanen, S.; Pettersson, M. In *2014 IEEE Conference on Electrical Insulation and Dielectric Phenomena (CEIDP)*; IEEE, 2014; pp 655–658.

(3) Tanaka, T. *IEEE Trans. Dielectr. Electr. Insul.* **2005**, *12* (5), 914.

(4) Lu, J.; Wong, C. P. *PORTABLE-POLYTRONIC 2008 - 2nd IEEE Int. Interdiscip. Conf. Portable Inf. Devices 2008 7th IEEE Conf. Polym. Adhes. Microelectron. Photonics* **2008**, 1.

(5) Nelson, J. K.; Hu, Y. *J. Phys. D. Appl. Phys.* **2005**, *38* (2), 213.

(6) Schadler, L. S.; Kumar, S. K.; Benicewicz, B. C.; Lewis, S. L.; Harton, S. E. *MRS Bull.* **2007**, *32* (04), 335.

(7) Winey, K. I.; Vaia, R. A. *MRS Bull.* **2007**, *32* (04), 314.

(8) Krishnamoorti, R. *MRS Bull.* **2007**, *32* (04), 341.

(9) Gao, M.; Zhang, P.; Wang, F.; Li, L.; Li, Z. In *2013 Annual Report Conference on Electrical Insulation and Dielectric Phenomena*; IEEE, 2013; pp 234–237.

(10) Payne, A. R. *J. Appl. Polym. Sci.* **1965**, *9* (6), 2273.

(11) Tan, D.; Cao, Y.; Tuncer, E.; Irwin, P. *Mater. Sci. Appl.* **2013**, *4* (April), 6.

(12) Schuman, T. P.; Siddabattuni, S.; Cox, O.; Dogan, F. *Compos. Interfaces* **2010**, *17* (8), 719.

(13) Roy, M.; Nelson, J. K.; MacCrone, R. K.; Schadler, L. S.; Reed, C. W.; Keefe, R.; Zenger, W. *IEEE Trans. Dielectr. Electr. Insul.* **2005**, *12* (4), 629.

(14) Siddabattuni, S.; Schuman, T. P.; Dogan, F. *ACS Appl. Mater. Interfaces* **2013**, *5* (6), 1917.

(15) Grabowski, C. a.; Fillery, S. P.; Westing, N. M.; Chi, C.; Meth, J. S.; Durstock, M. F.; Vaia, R. a. *ACS Appl. Mater. Interfaces* **2013**, *5* (12), 5486.

(16) Ganesh, V.; Sudhir, V. S.; Kundu, T.; Chandrasekaran, S. *Chem. - An Asian J.* **2011**, *6* (10), 2670.

(17) Ranjan, R.; Ranjan, R.; Brittain, W. J.; Brittain, W. J. *Macromolecules* **2007**, *40* (17), 6217.

(18) White, M. A.; Maliakal, A.; Turro, N. J.; Koberstein, J. *Macromol. Rapid Commun.* **2008**, *29* (18), 1544.

(19) Li, N.; Binder, W. H. *J. Mater. Chem.* **2011**, *21* (42), 16717.

(20) Tao, P.; Viswanath, A.; Schadler, L. S.; Benicewicz, B. C.; Siegel, R. W. *ACS Appl. Mater. Interfaces* **2011**, *3* (9), 3638.

(21) Mansfeld, U.; Pietsch, C.; Hoogenboom, R.; Becer, C. R.; Schubert, U. S. *Polym. Chem.* **2010**, *1* (10), 1560.

(22) Li, Y.; Benicewicz, B. C. *Macromolecules* **2008**, *41* (21), 7986.

(23) Li, D.; Zhu, J.; Cheng, Z.; Zhang, W.; Zhu, X. *React. Funct. Polym.* **2009**, *69* (4), 240.

(24) Ranjan, R.; Brittain, W. J. *Macromol. Rapid Commun.* **2007**, *28* (21), 2084.

(25) Ebbesen, M. F.; Schaffert, D. H.; Crowley, M. L.; Oupický, D.; Howard, K. A. *J. Polym. Sci. Part A Polym. Chem.* **2013**, *51* (23), 5091.

(26) Quémener, D.; Davis, T. P.; Barner-Kowollik, C.; Stenzel, M. H. *Chem. Commun. (Camb).* **2006**, No. 48, 5051.

(27) Amblard, F.; Cho, J. H.; Schinazi, R. F. *Chem. Rev.* **2009**, *109* (9), 4207.

(28) Li, W.; Yamamoto, Y.; Fukushima, T. *J. Am. Chem. Soc.* **2008**, *130*, 8886.

(29) Li, C.; Han, J.; Ryu, C. Y.; Benicewicz, B. C. *Macromolecules* **2006**, *39* (9), 3175.

(30) Ball, I. D. L. *Proc. IEE - Part I Gen.* **1951**, *98* (110), 84.

(31) Fava, R. A. *Proc. Inst. Electr. Eng.* **1965**, *112* (4), 819.

(32) Gao, J.; Li, J.; Benicewicz, B. C.; Zhao, S.; Hillborg, H.; Schadler, L. S. *Polymers (Basel).* **2012**, *4* (1), 187.

(33) Li, Y. Combining raft polymerization and click chemistry to prepare functionalized polymers and nanoparticles, PhD Thesis, Rensselaer Polytechnic Institute, 2008.

(34) Viswanath, A. Surface functionalization of inorganic substrates with polymeric

ligands using RAFT polymerization, PhD Thesis, University of South Carolina, 2014.

(35) Lieber, E.; Rao, C. N. R.; Chao, T. S.; Hoffman, C. W. W. *Anal. Chem.* **1957**, *29* (6), 916.

(36) Ligoure, C.; Leibler, L. *J. Phys.* **1990**, *51* (12), 1313.

(37) Mobaraki, N.; Hemmateenejad, B. *Chemom. Intell. Lab. Syst.* **2011**, *109* (2), 171.

(38) Li, Y.; Tao, P.; Viswanath, A.; Benicewicz, B. C.; Schadler, L. S. *Langmuir* **2013**, *29* (4), 1211.

(39) Bird, D. W.; Pelzer, H. *Proc. IEE - Part I Gen.* **1949**, *96* (97), 44.

(40) Virtanen, S.; Krentz, T.; Nelson, J.; Schadler, L.; Bell, M.; Benicewicz, B.; Hillborg, H.; Zhao, S. *IEEE Trans. Dielectr. Electr. Insul.* **2014**, *21* (2), 563.

(41) Takala, M.; Ranta, H.; Nevalainen, P.; Pakonen, P.; Pelto, J.; Karttunen, M.; Virtanen, S.; Koivu, V.; Pettersson, M.; Sonerud, B.; Kannus, K. *IEEE Trans. Dielectr. Electr. Insul.* **2010**, *17* (4), 1259.

(42) Kochetov, R.; Tsekmes, I. A.; Chmura, L. A.; Morshuis, P. H. F.; Iizuka, T.; Tatsumi, K.; Tanaka, T. In *2014 IEEE Conference on Electrical Insulation and Dielectric Phenomena (CEIDP)*; IEEE, 2014; pp 715–718.

(43) Akcora, P.; Liu, H.; Kumar, S. K.; Moll, J.; Li, Y.; Benicewicz, B. C.; Schadler, L. S.; Acehan, D.; Panagiotopoulos, A. Z.; Pryamitsyn, V.; Ganesan, V.; Ilavsky, J.; Thiyagarajan, P.; Colby, R. H.; Douglas, J. F. *Nat. Mater.* **2009**, *8* (4), 354.

CHAPTER 3

PREPARATION AND INVESTIGATION OF BIMODAL FILLERS FOR ENHANCED NANODIELECTRICS

3.1 Abstract

Epoxy based dielectrics are of great interest to the electronics and semiconductor industries for chip underfill, integrated circuit encapsulation, and electronics packaging among a variety of other applications.[1] Adding nano-sized fillers to epoxy has proven to be an effective method for improving dielectric breakdown strength (DBS). Evidence suggests that the dispersion state, as well as chemistry at the filler-matrix interface can play a crucial role in property enhancement.[2–8] Herein, we investigate the contribution of both filler dispersion and surface chemistry on the AC dielectric breakdown strength of silica-epoxy nanocomposites. Ligand engineering was used to synthesize bimodal ligands onto 15nm silica nanoparticles consisting of long epoxy compatible, poly(glycidyl methacrylate) (PGMA) chains, and short, π-conjugated, electroactive surface ligands. Surface initiated RAFT polymerization was used to synthesize multiple graft densities of PGMA chains, ultimately controlling the dispersion of the filler. Thiophene, anthracene, and terthiophene were employed as π-conjugated surface ligands that act as electron traps to mitigate avalanche breakdown. Investigation of the synthesized multifunctional nanoparticles was effective in defining the maximum particle spacing or free space length (L_f) that still leads to property enhancement, as well as giving insight into the effects of varying the electronic nature of the molecules at the interface on breakdown strength.

3.2 Introduction

Polymer based dielectrics have risen in popularity because of their low cost and processability compared to their inorganic counterparts. However, inorganic dielectrics remain superior in attainable dielectric properties.[9] The introduction of nano-sized inorganic fillers to polymers (nanodielectrics) can show improvements in permittivity, loss, voltage endurance, and dielectric breakdown strength compared to unfilled polymers.[2,6,10–13] Property enhancements found with nano-sized fillers are unseen or reversed with micron and larger sized fillers,[7,14] and it has been shown that preserving the large surface area (interfacial region) that nanoparticles create is critical to attaining improved properties. The large surface area that brings forth property enhancement in nanodielectrics creates a challenge for maintaining dispersion, as it increases unfavorable interactions between the inorganic filler and organic matrix resulting in nano-filler agglomeration.

Ligand engineering has emerged as a critical tool for the evolution of property enhancements in polymer nanocomposites. The addition of carefully selected ligands to the filler surface offers tunability over interfacial, and ultimately, bulk properties of the composite. A common challenge addressed through ligand engineering is reducing the enthalpic penalty associated with incorporating inorganic fillers into an organic polymer matrix.[15] Ligands ranging from short organic molecules to polymer brushes have been employed to overcome this obstacle with varying success.[16] Multifunctional surface ligand engineering offers a unique strategy for introducing additional functionality into a composite by utilizing chemically distinct ligands on the same filler surface. A bimodal architecture generally utilizes one long and one short surface population. Previous publications have reported bimodal brushes on the nanoparticle surface where two populations of polymer chains are present.[17–19] This work will utilize a bimodal architecture consisting of long polymer brushes and small molecule surface ligands that introduces additional functionality separate from the long brush. Additionally, mixed bimodal brushes will be explored where the short population is a functional polymer brush.

Thermochemical compatibility of isotropic nanoparticles in a polymer matrix was previously studied by Kumar et al.[20] Through theoretical and experimental studies, it was determined that the dispersion of polystyrene grafted isotropic silica nanoparticles in polystyrene was influenced by the long and short range enthalpic interactions of the nanoparticles and the entropic displacement of polymer chains on the nanoparticle surface. It was found by tuning the parameters of grafted polymer graft density (σ) and the ratio of grafted chain length to matrix polymer chain length (N_g/N), a variety of anisotropic self-assembled structures could be achieved by balancing the effects of particle core-core attraction and grafted chain elasticity. Multiple phases of filler dispersion including clusters, strings, and individually dispersed particles were realized by finely tuning the thermodynamic compatibility of the filler and matrix. Polymer graft densities of 0.01 – 0.1 ch/nm^2 were studied and results revealed that increasing the polymer graft density was effective at screening unfavorable particle core-core attraction resulting in a reduction of self-assembly and improved particle dispersion.

Control over grafted chain density and chain length has been achieved using reversible addition fragmentation chain transfer (RAFT) polymerization. RAFT is a popular controlled radical polymerization (CRP) technique that allows for precise control over polymer molecular weight, architecture, and end group chemistry.[21] The control found with RAFT polymerization is owed to the chain transfer agent, or CTA.[22] Surface initiated RAFT (SI-RAFT) polymerization utilizes a RAFT CTA covalently bound to a substrate surface as a means to outwardly grow polymer chains.[23] SI RAFT has become an integral part of ligand engineering because of the control it provides over a large selection of monomers, thus creating a vast toolbox of chemistries available for ligand design.[22]

It is common practice to incorporate polycyclic aromatic compounds, known as voltage stabilizers, into polymers to improve dielectric performance. Investigation into the role of voltage stabilizers determined that π-conjugated small molecules acted as electron traps, capturing free or "hot" electrons that are the precursors of avalanche breakdown.[24] The overall dielectric properties of the bulk polymer were shown to be altered depending on the electron nature of the additive.[24,25] Direct addition of voltage stabilizers can be problematic in that highly conjugated polycyclic compounds lack solubility and tend to crystallize in the polymer.[26,27] Previous reports found that the direct addition of 9-anthracenemethanol to epoxy was detrimental to breakdown strength, the underlying cause most likely being a conductive pathway created across the polymer.[6] Addition of conjugated molecules to the nanoparticle surface offers a means to include electron trapping moieties at isolated regions of the composite without a conductive pathway. The large interfacial area of nanocomposites ensures a high probability of interaction between hot electrons and trapping moieties.[10]

Schuman et al. presented a well correlated linear relationship of Hammett parameters to DBS for benzene derived functional groups on the surface of $BaTiO_3$ and TiO_2 in epoxy.[3] Much like Yamano's findings[24] regarding polycyclic voltage stabilizers, Schuman reported the addition of strong electron withdrawing groups (EWG) to the aromatic substituent to be most effective at improving overall DBS. Since Hammett parameters only define certain substituents on a benzene ring, it will be difficult to extend the utility of this model into further advanced systems. Predictions based on the sum of ionization energy (IE) and electron affinity (EA) should provide a much more generally applicable metric to predict DBS in surface modified composites.[28] Ionization energy and electron affinity describe the oxidation and reduction potential of a molecule, respectively. Koopman's theorem approximates IE and EA to corresponding HOMO and LUMO energies. The HOMO and LUMO levels of the small molecule surface ligands used in this work lie inside the band gap in the epoxy matrix. This leads to the introduction of spatially localized trap states for holes traveling in the valence band and electrons in the conduction band. The introduction of such traps in oil based insulations has been shown to lead to a reduction in hot carriers and affording improved DBS.[29]

In this material system, the literature indicates the mode of breakdown is through electron avalanche processes.[30] This phenomenon has been described in detail in the literature.[31–34] In general, electron avalanches develop when an electron gains sufficient energy to lead to impact ionization and subsequent charge multiplication. Seitz's model assumes that failure occurs when an avalanche forms that is large enough that the population of electrons can gain sufficient energy from the field to lead to large scale bond breaking. These principles lead to realistic order of magnitude estimates of breakdown strength. Furthermore, a critical size of avalanche is implied which contains sufficient energy to lead to breakdown of the bulk materials. Yamano's work shows that current spikes and electroluminescence allow for the detection of pre-breakdown avalanches, implying that the avalanche process occurs dynamically until the field is strong enough such that an avalanche proceeds to critical size.[25] Order of magnitude estimations determine that the critical size of an avalanche is ~200 nm. This prediction arises when the energy carried by the avalanche becomes sufficient to break the atomic bonds in the avalanche channel. Thus, the breakdown threshold is determined from the quantity of mobile charges, the field accelerating them, i.e. the breakdown field, and the hopping distances. Intuition indicates that adding extrinsic traps introduced via small molecules on nanoparticle surfaces should function best to improve breakdown strength when the arrangement of the filler can interfere with the growth of avalanches. Thus, the inter-particle spacing should be on the same length scale as that suspected for the critical avalanche sizes. Inter-particle spacings below 200 nm are very attainable with appropriate surface ligand engineering.

Nanodielectrics are a prime target for exploration using multifunctional surface ligand engineering with the need for independent investigation of dispersion and electroactive surface chemistry. Tang et al. used polymers containing terthiophene side chains as an effective means to create composite materials with increased permittivity and reduced loss.[35–37] Schuman et al. presented surface modified TiO_2 and $BaTiO_3$ nanoparticles that influenced dielectric properties of the composite depending on the electronic nature of the surface groups, but lacked insight into the dispersion of the particles.[3] Numerous studies have shown that reducing particle agglomeration is critical to achieving increases in breakdown strength but do not include investigation into the electronic nature of the surface ligands.[5,38–41] The previous chapter investigated bimodal multifunctional nanoparticles with varying surface chemistry at the filler interface, but did not fully address the independent impact of dispersion and surface chemistry on DBS.[2]

Inspired by the concept of mixed bimodal brushes, this work aims to developed a versatile ligand engineering strategy utilizing distinct surface populations that separately control filler dispersion and electron trapping abilities simultaneously. Our synthetic strategy uses long PGMA polymer chains for compatibilization with a commercial epoxy resin. Surface initiated RAFT polymerization provides control over polymer graft density and molecular weight, allowing for synthesis of composites at varying states of dispersion. Novel comparisons are drawn based on experimental results from TEM and dielectric breakdown measurements where a theoretical framework is presented to understand the DBS enhancements based on the inherent critical size of an avalanche and the dispersion of the filler. Short ligands were selected to be electroactive in nature, having conjugated π electrons. Ionization energy and electron affinity calculated using quantum computation was correlated with experimental values of DBS. The proposed metric could prove useful in further predictions of novel composite performance.

3.3 Experimental Section

Materials

All reagents were used as received from Fisher Scientific unless otherwise stated below. AIBN was purchased from Sigma Aldrich and recrystallized 3x from methanol. Glycidyl methacrylate was obtained from TCI and purified via passing through a column of neutral alumina. 4-Cyanopentanoic acid dithiobenzoate (CPDB) was received from Strem Chemical, Inc. 3-Aminopropyldimethylethoxysilane was obtained from Gelest. Colloidal silica particles of 30 wt% dispersed in methyl ethyl ketone were kindly provided by Nissan Chemical. The average particle diameter, 14 ± 4 nm as measured by TEM and 20 nm as measured by light scattering.

Instrumentation

NMR spectra were recorded on a Varian Mercury 400 spectrometer using $CDCl_3$ as the solvent. The molecular weights and molecular weight distributions were determined using a Waters gel-permeation chromatograph equipped with a 515 HPLC pump, a 2410 refractive index detector, three Styragel columns (HR1, HR3, HR4 in the effective molecular weight range of 100–5000, 500–30 000, and 5000–500 000, respectively). Tetrahydrofuran (THF) was used as the eluent at 30 °C and a flow rate of 1.0 mL min−1. The GPC system was calibrated with polymethyl methacrylate standards obtained from Polymer Laboratories. Samples were processed by filtration through microfilters with a pore size of 0.2 μm before analysis. FT-IR spectra were recorded on a Perkin Elmer Spectrum 100 using an attenuated total reflection diamond cell attachment. Quantification of surface groups was performed using either UV-vis or TGA. UV-vis absorption spectra were taken on a Perkin-Elmer Lamda 4C UV/vis spectrophotometer. TGA characterization was conducted using a TA Instruments Q5000 with a heating rate of 10°C/min from 25°C to 800°C~1000°C under nitrogen flow.

Synthesis of activated terthiophene ethoxy oxobutanoic acid

Terthiopheneethanol was synthesized as reported previously.[42] To a DCM solution (100ml) terthiopheneethanol (1.5 g, 5.13 mmol), succinic anhydride (2.05 g, 20.5 mmol), pyridine (2.03 g, 25.7 mmol), and DMAP (627 mg, 5.13 mmol) were successively added. The solution was allowed to stir at room temperature under N_2 for 24 hrs. Water (100 ml) was then added to the solution and the organic layer was separated. The resulting organic layer was then washed 3x with 1M HCl and once with brine before drying with $MgSO_4$. Solids were filtered and solvent removed in vacuum. The product (2 g, 5.13 mmol) was recovered without any further purification in 100% yield. Terthiopheneethoxy oxobutanoic acid (2.0 g, 5.13 mmol), 2-mercaptothiazoline (730 mg, 6.11 mmol), and DCC (1.26 g, 6.11 mmol), were dissolved into 200 ml THF. The solution was cooled to 0°C and flushed with N_2. DMAP (62.3 mg, 0.51 mmol) was dissolved into 5ml THF and added to the reaction mixture dropwise. The solution was allowed to warm to room temperature and stirred overnight. Solids were filtered and the solution was concentrated in vacuum. The resulting residue was purified via column chromatography (SiO_2, Hexanes:DCM, 3:2). The product was recovered as a yellow solid (2.3 g, 2.55 mmol) in 50% yield. MP: 130-132°C, ^1H NMR (400 MHz, $CDCl_3$): δ (ppm) 7.21 (dd, $J_1 = 5.1$ Hz, $J_2 = 1.1$ Hz, 1H), 7.16 (dd, $J_1 = 3.6$ Hz, $J_2 = 1.1$ Hz, 1H), 7.06 (d, $J = 3.8$ Hz, 1H), 7.03 – 7.00 (m, 3H), 6.77 (d, $J = 3.6$ Hz, 1H), 4.52 (t, $J = 7.6$ Hz, 2H), 4.32 (t, $J = 6.6$ Hz, 2H), 3.55 (t, $J = 6.4$ Hz, 2H), 3.24 (t, $J = 7.6$ Hz, 2H), 3.12 (t, $J = 6.4$ Hz, 2H), 2.71 (t, $J = 6.3$ Hz, 2H) ^{13}C NMR (400 MHz, $CDCl_3$): δ (ppm) 201.8, 173.3, 172.2, 139.5, 137.2, 136.3, 136, 135.9, 135.8, 127.9, 126.5, 124.4, 124.3, 124, 123.7, 123.5, 64.6, 55.9, 34.3, 29.6, 29.1, 28.4, HRMS (EI-DP) m/z: [M^+] Calcd for $C_{21}H_{19}NO_3S_5$ 492.9969; Found 492.9951.

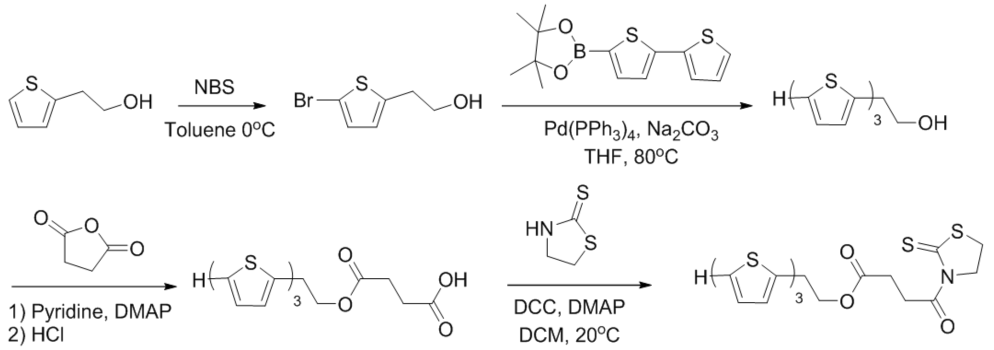

Scheme 3.1: Synthesis of activated terthiophene ethoxy oxobutanoic acid.

Synthesis of activated thiopheneacetic acid

2-Thiophenacetic acid (1.0 g, 7.80 mmol), 2-mercaptothiazoline (1.0 g, 8.58 mmol), and DCC (1.6 g, 7.80 mmol) were dissolved into DCM. The solution was cooled to 0°C and flushed with N_2. DMAP (22 mg, 800 μmol) was dissolved into 5ml DCM then added to the reaction mixture dropwise. Solids were filtered and the solution was concentrated in vacuum. The resulting residue was purified via column chromatography (SiO_2, $CDCl_3$). The product was recovered as a yellow Solid (1.52g, 80% yield). MP: 62-

63°C, ^{1}H NMR (400 MHz, $CDCl_3$): δ (ppm) 7.24 (d, *J* = 1.4 Hz, 1H), 6.98 (m, 2H), 4.88 (s, 2H), 4.61 (t, *J* = 7.5 Hz, 2H), 3.31 (t, *J* = 7.5 Hz, 2H) ^{13}C NMR (400 MHz, $CDCl_3$): δ (ppm) 201.8, 171.7, 134.7, 126.7, 125.4, 56.3, 38.7, 28.4. HRMS (EI-DP) m/z: [M^+] Calcd for $C_9H_9NOS_3$ 242.9846; Found 242.9847

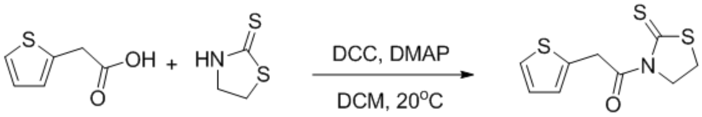

Scheme 3.2: Synthesis of activated thiophene acetic acid.

Activated 9-anthracene acetic acid

2-(Anthracen-9-yl)acetic acid was prepared as described previously.[43] 2-(Anthracen-9-yl)acetic acid (1.00 g, 4.2 mmol) was dissolved into 30ml dichloromethane along with 2-mercaptothiazoline (0.56 g, 4.7 mmol), and 4-dimethylaminopyridine (50 mg, 0.4 mmol). The solution was cooled to 0°C and flushed with N_2 for 20 minutes. N,N'-dicyclohexylcarbodiimide (0.87 g, 4.2 mmol) was dissolved into a minimal amount of dichloromethane and added dropwise to the anthracene acetic acid solution. The solution was allowed to warm to room temperature and stir over night. The solids were then removed via vacuum filtration and solvent was removed under reduced pressure. The crude product was purified via column chromatography (SiO_2, 7:3, dichloromethane: hexane) leaving the product as a yellow powder (0.62 g, 43% yield). MP: 200-203°C. ^{1}H NMR (400 MHz, $CDCl_3$): δ (ppm) 8.46 (s, 1H), 8.02 (d, *J* = 9.6 Hz, 4H), 7.49 (m, 4H), 5.64 (s, 2H), 4.63 (t, *J* = 7.6 Hz, 2H), 3.39 (t, *J* = 7.6 Hz, 2H), ^{13}C NMR (400 MHz, $CDCl_3$): δ (ppm) 202.3, 172.4, 131.5, 130.6, 129.3, 127.5, 126.4, 126.3, 124.9, 124, 56.3, 38.1, 28.5. HRMS (EI-DP) m/z: [M^+] Calcd for $C_{19}H_{15}NOS_2$ 330.9788; Found 330.9783

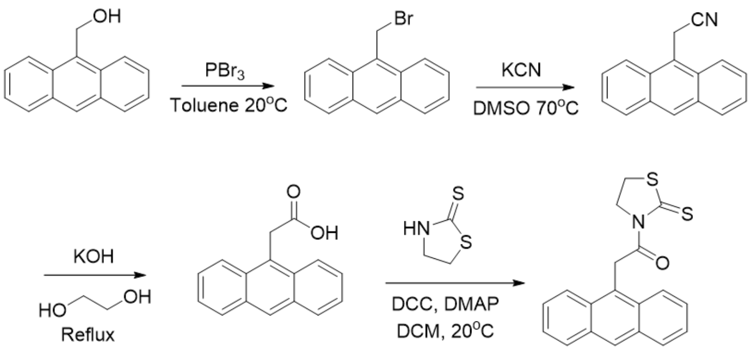

Scheme 3.3: Synthesis of activated anthracene methanol.

PGMA monomodal grafted silica nanoparticles

Activated CPDB and CPBD functionalized silica nanoparticles were prepared as described previously[23]. Glycidyl methacrylate (GMA) was purified by passing through a neutral alumina column. In a side arm Schlenk flask, CPDB grafted particles (1 g), GMA (500 eq to CPDB), AIBN (0.1 eq) and THF (3 ml) were combined. The solution was subjected to 3 freeze pump thaw cycles, and placed in an oil bath at 60°C for various intervals.

Bimodal ligand grafted nanoparticles

Silica nanoparticles (3 g) were dispersed into THF (50 ml). 3-Aminopropyldimethylethoxysilane (150 mg, 930 µmol) was then added to the solution at room temperature and the solution was stirred at 70°C for 3 hrs under N_2. The nanoparticles were precipitated in a large amount of hexanes and isolated via centrifuge at 5,000 rpm. The particles were re-dispersed into THF. The precipitation and dispersion was repeated three times. An excess of one of the previously synthesized conjugated surface ligands was added to the particle suspension and stirred overnight under N_2. The particles were precipitated in a large amount of hexanes, centrifuged, and re-dispersed in THF. Precipitation and isolation was repeated until supernatant was clear. The particles were redispersed into THF and a second population of 3-aminopropyldimethylethoxysilane was added just as described above. A THF solution of activated CPDB was added dropwise to the amine functionalized particle. The reaction was left to stir overnight at room temperature. Next the particles were precipitated and washed three times as described above. After the particles were dried in vacuum, quantification of surface groups was determined using UV-vis spectroscopy. PGMA was grown from the particle surface as described above.

Computation Methods

Computation was performed by Ke Wu and Curt Beneman of RPI. Quantum computation was performed using Guassian09. Quantum computation where the cation, anion and neutral molecule initial structures were first optimized using a PM3 model. The final optimized structure and zero-point-energy (ZPE) was calculated using B3lyp/6-31+G* with slight spin contamination. The optimized structure was then used to calculate the electronic energy using B3lyp/6-311++G**. The final energies were calculated as the sum of the electronic energy and the corrected ZPE (using a factor of 0.975).

Synthesis of Terthiopheneethylmethacrylate

To 50 ml of dry DCM terthiopheneethanol (5.22 g, 17.9 mmol), methacrylic acid (1.84 g, 21.4 mmol) and 4-dimethylaminopyridine (220 mg, 1.79 mmol) were added. The solution was then cooled to 0°C and flushed with nitrogen before adding N,N'-dicyclohexylcarbodiimide (3.68 g, 17.9 mmol) in 10 ml of DCM dropwise over 30 min. The solution was allowed to warm to room temperature and react overnight. The resulting salts were filtered and the solvent removed under reduced pressure leaving a dark yellow solid. The resultant solid was then subjected to column chromatography (SiO2, CHCl3) yielding a bright yellow solid (5 g, 13.9 mmol) in 78% yield. MP: 72 - 74°C, ^{1}H NMR (400 MHz, CDCl3): δ (ppm) 7.21 (dd, J1 = 5.1 Hz, J2 = 1.1 Hz, 1H), 7.16 (dd, J1 = 3.6 Hz, J2 = 1.1 Hz, 1H), 7.06 (d, J = 3.7 Hz, 1H), 7.03 – 7.00 (m, 3H), 6.78 (d, J = 3.6 Hz, 1H), 6.16 (s, 1H), 5.60 (t, J = 1.5 Hz, 1H), 4.36 (t, J = 6.5 Hz, 2H), 3.16 (t, J = 6.4, 2H), 1.97 (s,1H), ^{13}C NMR (400 MHz, CDCl$_3$): δ (ppm) 167.4, 139.8, 137.4, 136.5, 136.3, 136.2, 136.0, 128.2, 127.8, 126.4, 125.9, 124.4, 124.3, 123.6, 123.4, 64.9, 29.8, 18.6, HRMS (ESI-TOF) m/z: [M$^+$] Calcd for $C_{18}H_{16}O_2S_3$ 360.0313; Found 360.0312

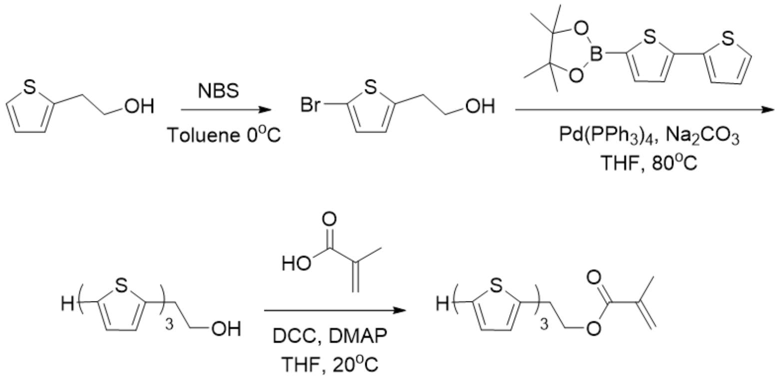

Scheme 3.4: Synthesis of terthiopheneethylmethacrylate.

Synthesis of PTTEMA Grafted silica

CPDB grafted particles (1 g), TTEMA (50 eq to CPDB), AIBN (0.1 eq) and THF (5 ml) were combined in a side arm Schlenk flask. The solution was subjected to 3 freeze pump thaw cycles, and placed in an oil bath at 60°C for 19 hrs. The reaction was quenched by placing the Schlenk tube in ice water for 5 minutes. The solution was poured into a large amount of hexanes (200 ml). The solution was centrifuged at 3,000 rpm for 5 minutes and supernatant was discarded. Recovered particles were redispersed into THF and washed with hexanes two more times. A small amount of the product was isolated and polymer chains were cleaved from the silica surface using a hydrofluoric acid solution. The resultant polymer chains were then analyzed by GPC (Mn: 6.4 kg/mol, *Đ*: 1.21).

Synthesis of PGMA-PTTEMA grafted bimodal brush particles

CPDB grafted particles ($\sigma = 0.19$ ch/nm^2) (1 g), TTEMA (50 eq to CPDB), AIBN (0.1 eq) and THF (5 ml) were combined in a side arm Schlenk flask. The solution was subjected to 3 freeze pump thaw cycles, and placed in an oil bath at 60°C for 19 hrs. The reaction was quenched by placing the Schlenk tube in ice water for 5 minutes. The solution was poured into a large amount of hexanes (200 ml). The solution was centrifuged at 3,000 rpm for 5 minutes and supernatant was discarded. Recovered particles were dispersed back into THF and washed with hexanes two more times. A small amount of the product was isolated and polymer chains were cleaved from the silica surface using a hydrofluoric acid solution. The resultant polymer chains were analyzed by GPC (Mn: 8 kg/mol, *Đ*: 1.2). PTTEMA grafted particles were dissolved into 50 ml THF with 50 mg of AIBN. The solution was refluxed for one hour before recovering the particles by crashing in hexanes and centrifuging at 3,000 rpm for 5 min. In 100 ml round bottom flask, PTTEMA grafted nanoparticles and 3-aminopropyldimethylethoxysilane (10 µL, 8.6 µmol) were dissolved into 50 ml THF. The solution was refluxed for 4 hours before recovering the nanoparticles as described earlier. The nanoparticles were dissolved into 100 ml THF and a solution of activated CPDB (22 mg, 60 µmol) was added to the particle solution and left to stir overnight under N_2. The particles were recovered as described previously. CPDB-PTTEMA Particles (0.5 g SiO_2), GMA (0.8 g, 5.5 mmol), and AIBN (17.6 mg, 1.1 µmol) were dissolved into 5 ml THF and added to a 25 ml side arm Schlenk tube. The solution was subjected to 3 freeze pump thaw cycles and placed in an oil bath at 60°C for 5 hours.

The reaction was quenched by placing in an ice water bath. The particles were recovered as described previously. A small portion of the bimodal brush grafted nanoparticles was isolated and polymer chains were cleaved with HF solution. Isolated polymer chains were characterized via GPC (Mn[PGMA]: 21 kg/mol, *Đ*: 1.3, σ: 0.25 ch/nm^2)

3.4 Results and Discussion

Synthesis of monomodal PGMA grafted particles

Scheme 3.5 shows the syntheses of monomodal PGMA grafted silica nanoparticles via surface initiated RAFT polymerization. Surface initiated RAFT polymerization using 4-cyanopentanoic acid dithiobenzoate (CPDB) grafted nanoparticles has been described previously in detail in literature[23] and in the previous chapter. Generally, in the first step, 3-aminopropyldimethylethoxy silane was attached to the silica nanoparticle surface using a silane coupling reaction, generating amine surface functionalized silica nanoparticles. Next, the activated derivative of the RAFT CTA, CPDB, was covalently attached to the amine functionalized nanoparticle through amidation of the activated acid. CPDB attachment was confirmed by the presence of a characteristic absorbance maxima at 302 nm in ultraviolet visible (UV-vis) spectroscopy. Quantification of attached CPDB was determined via standard calibration curve. Calculations for grafted polymer graft density (σ) in ch/nm^2 are outlined in previous literature.[44] Graft densities were controlled by altering the feed ratio of 3-aminopropyl dimethylethoxysilane during the first step of nanoparticle modification. Once CPDB was successfully attached to the particle surface, glycidyl methacrylate (GMA) was polymerized from the particle surface in the presence of AIBN in a grafting-from approach. Polymer characterization (M_n, M_w, and *Đ*) was performed using GPC analysis after PGMA chains were cleaved from the nanoparticle surface using a hydrofluoric acid solution.

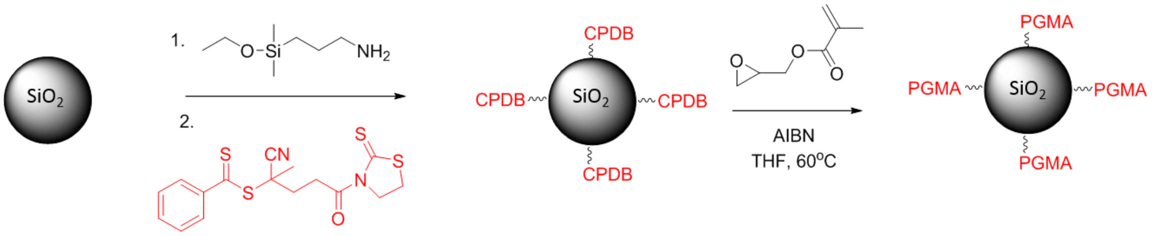

Scheme 3.5: Synthesis of PGMA monomodal grafted nanoparticles.

Activated ligand synthesis

Electroactive ligands were synthesized to contain 2-mercaptothiazoline activated acids for particle attachment. Previously, our group reported using azide-alkyne Huisgen cycloaddition, or the classic “click” reaction to attach surface ligands to silica nanoparticles.[2] While the click approach is advantageous in many instances for its efficiency, in this case the click reaction was unfavorable as it required: additional synthetic steps for azide functionalization of the silica surface, strict anaerobic conditions, and a copper catalyst that could remain bound to the silica surface and interfere with electrical activity. Using activated acids allowed for easy attachment to amine functionalized nanoparticles without a catalyst, metal contamination, or the need for anaerobic conditions. The only byproduct of amidation, 2-mercaptothiazoline, was washed away in subsequent particle work up. The activated acids were synthesized by reacting the selected carboxylic acid containing electroactive molecules with 2-mercaptothiazoline in a Steglich Coupling reaction. The molecules used in this study are shown in Figure 3.1. Synthesis of activated thiophene was successful in one step using commercially available thiopheneacetic acid. Synthesis of activated anthracene was achieved in four steps starting from commercially available 9-anthracenemethanol. Activated terthiophene was achieved in two additional steps from previously prepared terthiopheneethanol. Detailed synthetic schemes can be found in the experimental section.

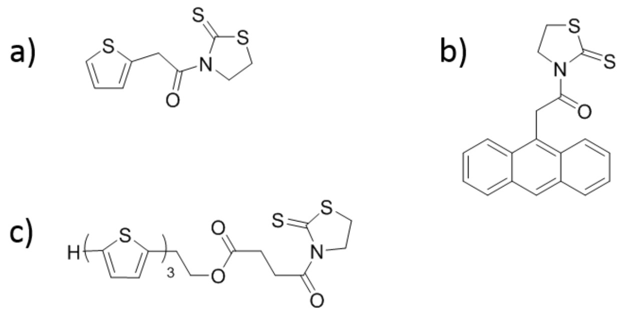

Figure 3.1: Activated short ligands synthesized a) activated thiopheneacetic acid b) activated 9-anthraceneacetic acid c) activated terthiopheneethoxy oxobutanoic acid.

Synthesis of bimodal ligand grafted particles

Bimodal ligand grafted nanoparticles were synthesized in multiple steps through sequential addition of surface groups. In general, 3-aminopropyldimethylethoxy silane was first attached to the particle surface. A higher concentration of silane was used in this step compared to the monomodal synthesis, as the target graft density (0.25 ch/nm^2) for the electroactive ligand population was higher than that of the PGMA population. Subsequent covalent bonding of the desired activated conjugated ligand through amidation was performed. Next, a second population of 3-aminopropyldimethylethoxy silane was added to the particle surface before attaching CPDB as described in the monomodal synthesis. Lastly, GMA was polymerized using surface initiated RAFT polymerization. Scheme 3.6 shows the synthetic process to achieve anthracene-PGMA bimodal particles. The synthetic methodology is the same for each bimodal species synthesized, only varying in the selection of the electroactive ligand added in the second step. Polymer graft densities were controlled through the feed ratio of the second 3-aminodimethylethoxy silane population. Samples containing only a short ligand population without PGMA were synthesized using the presented bimodal strategy only omitting the final polymerization step.

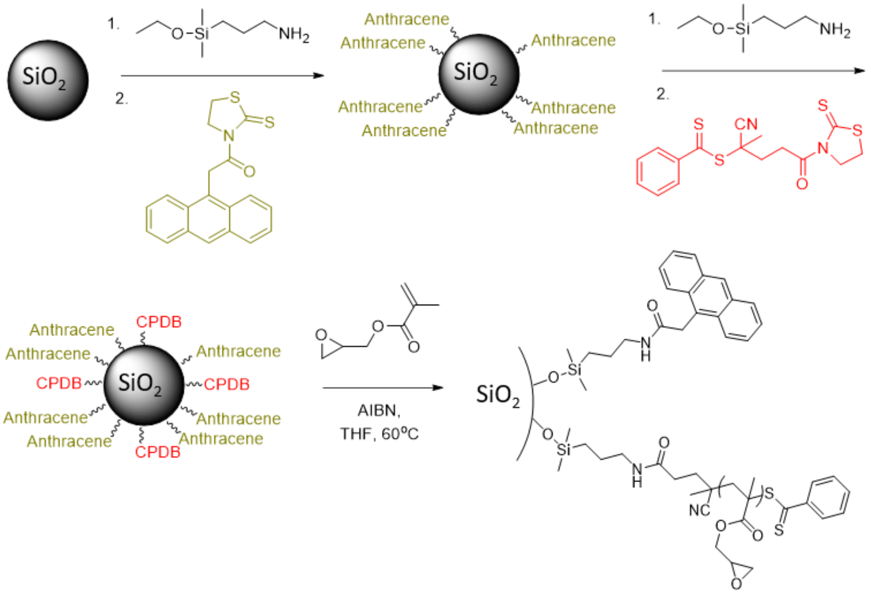

Scheme 3.6: Synthesis of bimodal anthracene-PGMA silica nanoparticles.

Attachment of the electroactive ligands was confirmed by UV-vis spectroscopy and quantified using a standard calibration curve. Target graft densities for the π-conjugated ligands were between 0.2 ch/nm^2 and 0.3 ch/nm^2. The UV-vis spectrum for anthracene functionalized particles is shown in Figure 3.2. The characteristic absorbance maxima for anthracene is represented by the peak at 365nm. The characteristic CPDB absorbance maxima at 302nm can also be seen along with anthracene, after addition of the RAFT agent. Both anthracene (365 nm) and thiophene (243 nm) have absorbance maximum values distinct from CPDB (302 nm), therefore individual graft densities can be quantified via UV-vis spectroscopy before polymerization.

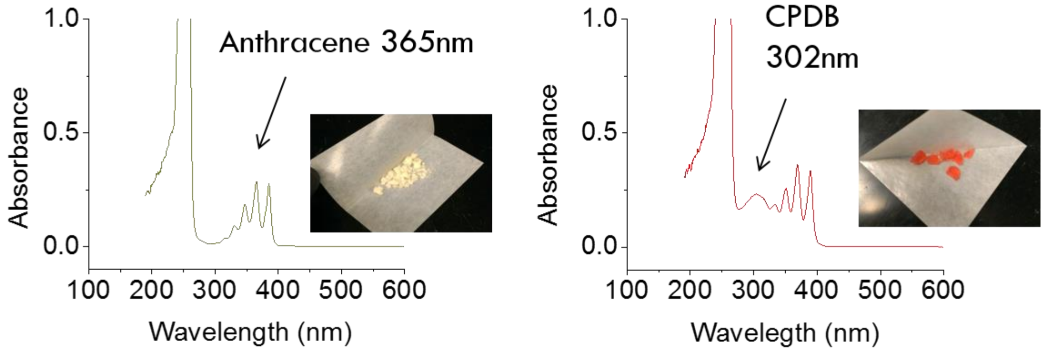

Figure 3.2: UV-vis spectrum of anthracene coated silica nanoparticles (left) and silica particles containing both anthracene and CPDB (right).

Terthiophene has a broad absorbance peak at 359 nm that overlaps the absorbance peak of CPDB, consequently CPDB graft density could not be quantified in addition to terthiophene via UV-vis spectroscopy. PGMA graft density was calculated by thermogravimetric analysis (TGA) after polymerization for terthiophene-PGMA bimodal samples. Experimental values for the synthesized surface functionalized particles are given in Table 3.1. Higher than targeted graft densities for thiophene grafted particles may be due to reduced steric constraint when attaching the substituent. Samples labeled MM-PGMA are monomodal in nature and contain only PGMA chains on the particle surface. Samples labeled BM-R are bimodal in nature and contain PGMA chains in addition to the noted conjugated short ligand. BM-R samples that contain NA in the PGMA column do not contain PGMA but CPDB and electroactive ligands. The PGMA chains were omitted in this case to create agglomerated filler composites.

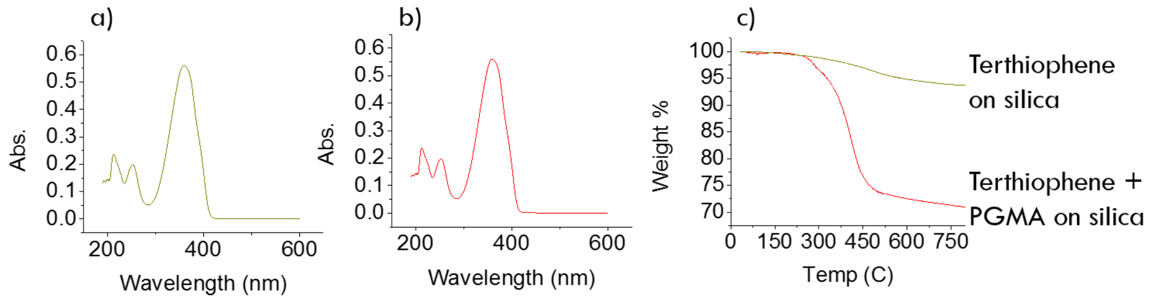

Figure 3.3: UV-vis spectra for a) terthiophene grafted silica b) terthiophene + CPDB grafted Silica and c) TGA analysis of both terthiophene and terthiophene + CPDB grafted particles.

Table 3.1: Synthetic characteristics of monomodal (MM) and bimodal (BM) grafted nanoparticles.

Sample	**Short Ligand σ (ch/nm^2)**	**PGMA σ (ch/nm^2)**	**PGMA M_n (Kg/mol)**	***Đ***
MM-PGMA(a)	NA	0.04	29	1.36
MM-PGMA(b)	NA	0.07	23	1.27
MM-PGMA(c)	NA	0.10	19	1.25
MM-PGMA(d)	NA	0.14	23	1.16
BM-Anthracene(a)	0.28	NA	NA	NA
BM-Anthracene(b)	0.28	0.06	30	1.61
BM-Anthracene(c)	0.24	0.07	26	1.37
BM-Anthracene(d)	0.28	0.15	20	1.20
BM-Anthracene(e)	0.22	0.12	23	1.31
BM-Anthracene(f)	0.28	0.11	10	1.36
BM-Thiophene(a)	0.44	NA	NA	NA
BM-Thiophene(b)	0.40	0.14	8	1.23
BM-Terthiophene(a)	0.22	NA	NA	NA
BM-Terthiophene(b)	0.22	0.10*	32	1.4

*Determined through TGA analysis.

To complete the composite, all of the synthesized grafted particles were mixed with a Huntsman bisphenol-A based epoxy resin using a shear mixer. The solvent was evaporated and silica loading was determined by TGA before crosslinking and casting final recessed samples for breakdown testing. L_f and dielectric breakdown data was obtained as described in the previous chapter. The L_f and DBS results are found in Table 3.2. Corresponding TEM micrographs are found in Figures 3.4-3.7

Table 3.2: L_f and Weibull scale (and 95% confidence interval CI) and shape parameters, along with percent change of DBS for synthesized monomodal (MM) and bimodal (BM) composites.

Sample	**L_f (nm)**	**α (kV/mm)**	**β Value**	**Δ DBS**	**95% CI**
MM-PGMA(a)	231	188	1.1	-5 %	107
MM-PGMA(b)	194	242	2.9	+22 %	43
MM-PGMA(c)	174	240	4.0	+21 %	23
MM-PGMA(d)	103	240	6.8	+21 %	20
BM-Anthracene(a)	294	178	1.6	-10 %	38
BM-Anthracene(b)	265	220	3.8	+11 %	19
BM-Anthracene(c)	171	244	8.0	+23 %	11
BM-Anthracene(d)	163	238	2.2	+20 %	44
BM-Anthracene(e)	126	240	3.1	+21 %	33
BM-Anthracene(f)	55	246	4.4	+24 %	20
BM-Thiophene(a)	616	192	3.7	-3 %	44
BM-Thiophene(b)	55	210	2.7	+6 %	35
BM-Terthiophene(a)	357	196	5.3	-1 %	22
BM-Terthiophene(b)	80	265	2.6	+34 %	61

Particle Dispersion

Compatibility of PGMA grafted nanoparticles with commercial grade epoxy resin has been established in previous publications.[2,45,46] Herein we demonstrate precise control over monomodal and bimodal polymer grafted nanoparticle dispersion in epoxy using the well-established methodology of controlling grafted chain density.[47] Bare 15 nm silica nanoparticles have been shown to agglomerate in epoxy resin in previous efforts.[2,6] Samples BM-anthracene(a), BM-thiophene(a), and BM-terthiophene(a) were synthesized containing only short ligands and no polymer coverage. As expected, filler aggregation characterized by relatively large L_f (>250 nm) and large phase separated regions shown in TEM micrographs was observed. The addition of small molecule organics to the particle surface in this case was not sufficient in overcoming the enthalpic penalty of mixing the nanoparticles in the matrix. Adding polymer chains to the nanoparticle in sufficient quantity to screen unfavorable enthalpic interactions should promote nanoparticle dispersion. Here we demonstrate with sample MM-PGMA(a) that a polymer graft density 0.04 ch/nm^2 does not provide adequate screening to prevent particle phase separation. Bimodal sample, BM-anthracene(b), with a PGMA graft density of 0.06 ch/nm^2 had a L_f of 265 nm and showed small anisotropic clusters in the corresponding TEM micrograph. The self-assembled structures observed for polymer grafted samples MM-PGMA(a) and BM-anthracene(b) are indicative of the sparse brush regime described previously by Kumar.[47] For the purpose of this work, we will define a well dispersed system based on Seitz's approximation for critical size of avalanche breakdown. Therefore, a L_f under 200 nm will be considered well dispersed. All samples synthesized containing PGMA polymer coverage of 0.07 ch/nm^2 or greater were well dispersed according to this definition. A plot of polymer graft density versus characterized L_f is shown in Figure 3.8. From the figure the general trend of improved dispersion with increasing PGMA long chain graft density is observed.

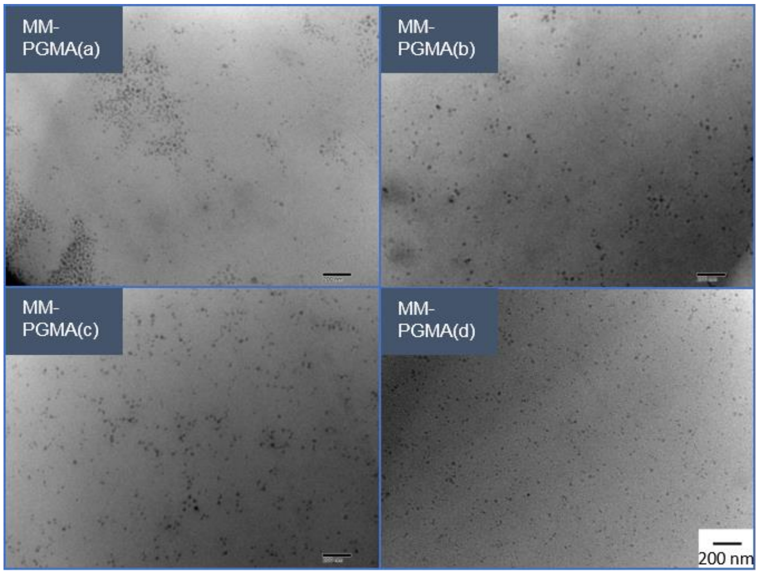

Figure 3.4: TEM micrographs of monomodal PGMA grafted silica at various states of dispersion.

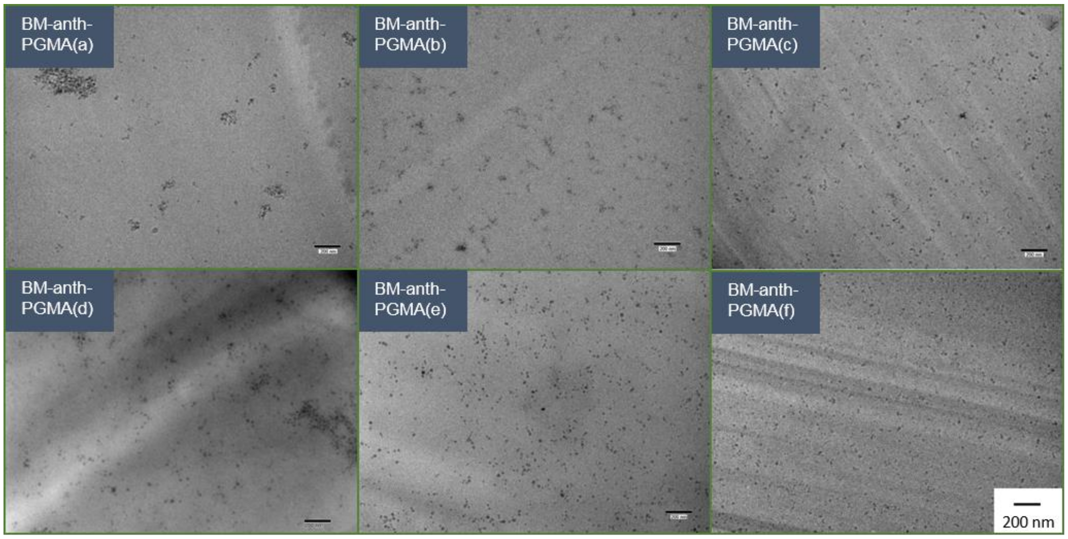

Figure3.5: TEM micrographs of bimodal PGMA-anthracene grafted silica at various states of dispersion.

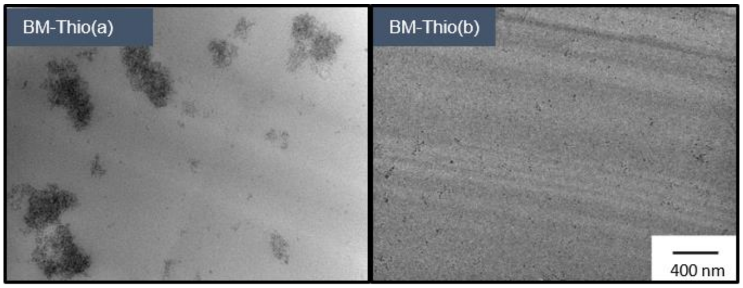

Figure 3.6: TEM micrographs of bimodal PGMA-thiophene grafted silica at non and well dispersed sates

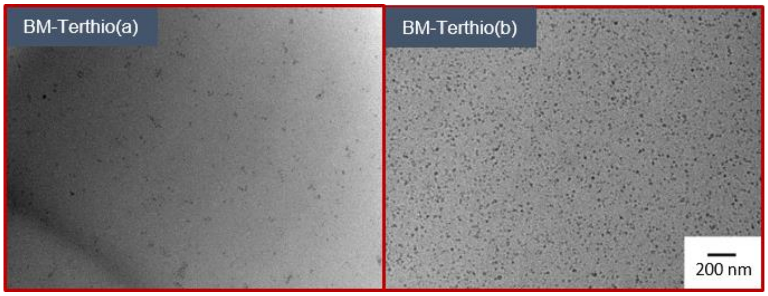

Figure 3.7: TEM micrographs of bimodal PGMA-terthiophene grafted silica at non and well dispersed sates

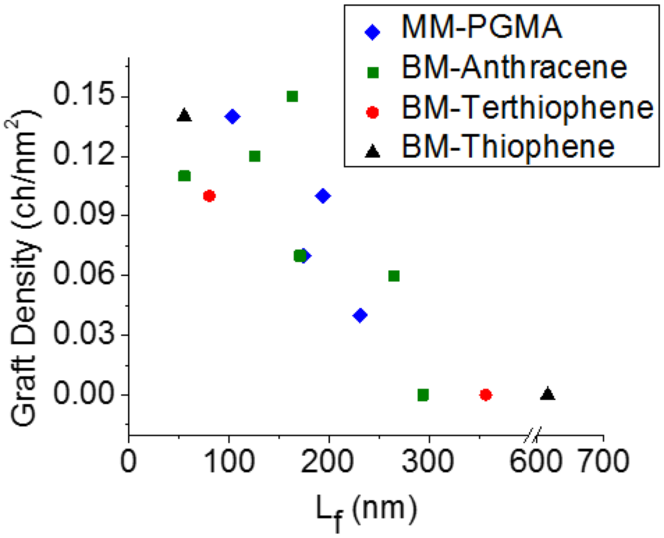

Figure 3.8: Plot of PGMA grafted chain density vs free space length (L_f) for the synthesized monomodal and bimodal composites.

Effect of particle dispersion on DBS

The data and correlation between L_f and DBS presented in Table 3.2 and Figure 3.9 respectively reveal a plateau in the dependence of DBS on quality of dispersion, specifically with the MM-PGMA and BM-anthracene samples where multiple samples of varying graft density were synthesized to explore dispersion effects on DBS. The literature has typically ignored dispersion, not achieved dispersion qualities sufficient to investigate this plateau, or not tested a sufficient variety of dispersion states to observe the plateau, and the assumption has been that improving dispersion will always improve DBS until a truly monodisperse system is achieved.[48–50] The results herein indicate instead that there is a diminishing return for improved dispersion after the L_f is reduced below 200 nm, a similar length scale to the estimates of avalanche size arising from Seitz's theory. This implicates electron avalanches as the dominant failure mode, and indicates that the filler acts to prevent nascent avalanches from reaching a critical size when it is sufficiently well dispersed.

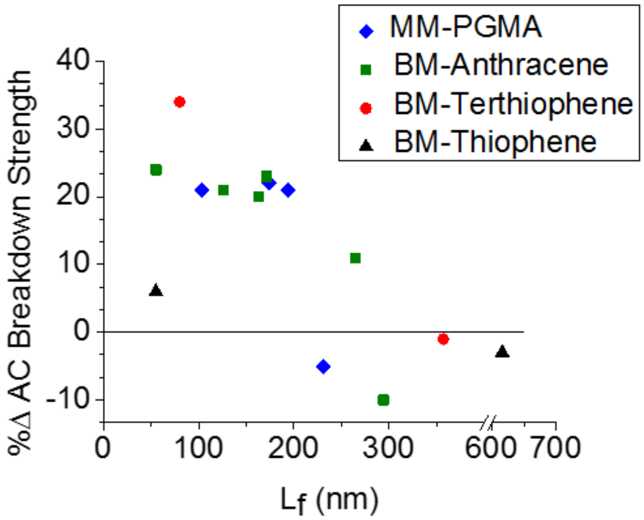

Figure 3.9: Plot of percent change in dielectric breakdown strength vs free space length (L_f) of the synthesized composites.

Effect of short ligand chemistry on DBS

In addition to the effects of dispersion on DBS, Figure 3.9 highlighted a second trend among well dispersed composite samples where surface chemistry was clearly contributing to overall performance. Bimodal terthiophene-PGMA composites saw the overall largest improvements in DBS followed by bimodal anthracene-PGMA and thiophene-PGMA samples. When considering the trapping mechanism in regards to avalanche breakdown it is intuitive that the longer conjugation length of anthracene and terthiophene would provide better trapping ability than thiophene. Bimodal anthracene-PGMA samples did not see significant improvements compared to well dispersed monomodal PGMA samples. Bimodal thiophene-PGMA sample saw a net decrease in DBS compared to well dispersed monomodal PGMA samples. It can therefore be assumed that the inherent trapping ability of the silica nanoparticle lies somewhere close to that of anthracene. It can also be assumed that the trapping ability of surface ligands supersedes the inherent trapping abilities of the particle. Quantification of the inherent trapping ability of the surface ligand was then necessary to explain this phenomenon.

Table 3.3: Calculated ionization energy (IE) and electron affinity (EA) for the synthesized conjugated electroactive ligands obtained by quantum computation.

Functional group	**IE (eV)**	**EA (eV)**	**IE+EA (eV)**
Thiophene	7.87	-0.43	7.44
Anthracene	6.8	-0.79	6.01
Terthiophene	6.75	-1.36	5.39

Calculated values of IE+EA for each of the short π-conjugated ligands used in this study are found in Table 3.3, IE and EA values were determined through quantum computation courtesy of Ke Wu and Dr. Curt Breneman of Rensselaer Polytechnic Institute. The IE and EA parameters offer a way to compare the energy levels related to the extrinsic traps introduced by the filler. In an identical matrix, the only difference in trap depth will be related to the differing electronic structure of the additive, and varying surface ligands offer a path for the introduction of significantly different traps, which lead to significantly different changes in DBS, seen in Figure 3.10. In general, a smaller IE+EA value suggests deeper traps, and deeper traps are shown to lead to better DBS performance. Figure 3.10 highlights the correlation between experimentally determined values for bimodal composites and calculated values for the sum of IE and EA. From the figure it can be seen that there is an excellent linear correlation between experimental and calculated values. The correlation between calculated and experimental values suggests that IE + EA could be a useful metric to predict the performance of future ligands to be used on the surface of nanodielectrics.

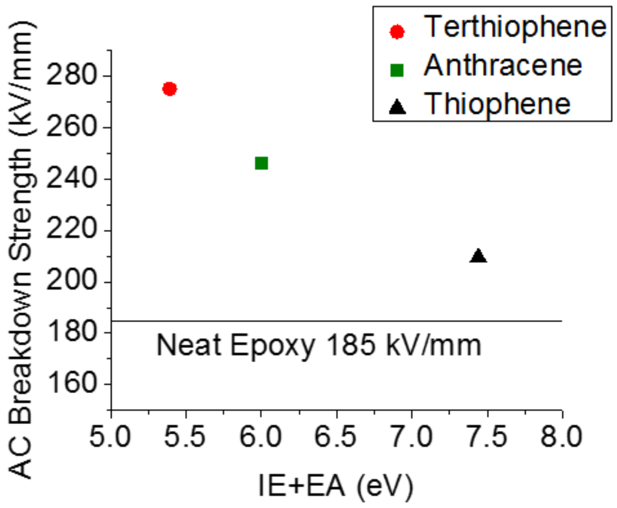

Figure 3.10: Plot of calculated ionization energy + electron affinity of the synthesized electroactive short ligands vs experimentally obtained values for the correlating nanocomposites.

Synthesis of PTTEMA grafted SiO_2 and PTTEMA-PGMA Mixed Bimodal Brush Grafted SiO_2

With the effects of dispersion and interfacial chemistry established, the effects of trapping group concentration was then considered. Increasing the filler concentration in the composite is problematic in that the increased concentration of filler can cause the system to approach the percolation threshold.[51,52] Increased concentration of trapping groups with an increase of silica was achieved by the incorporation of polymer brushes as opposed to small molecule surface ligands. Polymer brushes containing electroactive side chains offer a unique way of introducing increased trapping functionality at the composite interface. PTTEMA brushes were incorporated at nearly the same graft density as previously described for the short ligand population, however the use of a polymer brush enabled the short population to contain several repeat units. The polymer brushes used were polyterthiopheneethylmethacrylate or PTTEMA. The brushes are composed of a methacrylate backbone and terthiophene side chains. Surface initiated RAFT polymerization was used to polymerize the terthiopheneethylmethacrylate. Both monomodal PTTEMA grafted silica and bimodal PGMA-PTTEMA grafted silica were synthesized. PTTEMA compatibility with commercial epoxy has not been investigated but the two were not expected to be compatible due to dissimilar chemistry.

PGMA-PTTEMA grafted mixed bimodal brushes used a second polymer (PGMA) chain population for compatibility with the matrix. The parameters that govern bimodal brush grafted nanoparticles in polymer matrices have been investigated previously in our group. The utility of bimodal brushes of two populations of the same chemistry is now well established for improving filler dispersion and ultimately thermomechanical properties.[17–19,53] The concept of mixed bimodal brushes is relatively contemporary and is utilized in this work as a method to enhanced dielectric breakdown strength of epoxy composites.

The PGMA-PTTEMA mixed bimodal brush grafted nanoparticles were synthesized using sequential surface initiated RAFT polymerization. PTTEMA was polymerized first as it was intended to be the shorter more dense population. Following the polymerization of PTTEMA excess AIBN was used to cleave the living RAFT agent from the polymer chain ends. This step ensures that the first population of polymer chain ends is unable to reinitiate polymerization and prevents the formation of block copolymers. At this point the surface initiated RAFT polymerization procedure was performed again using PGMA. The synthesis of PGMA-PTTEMA bimodal grafted silica is shown in Scheme 3.11.

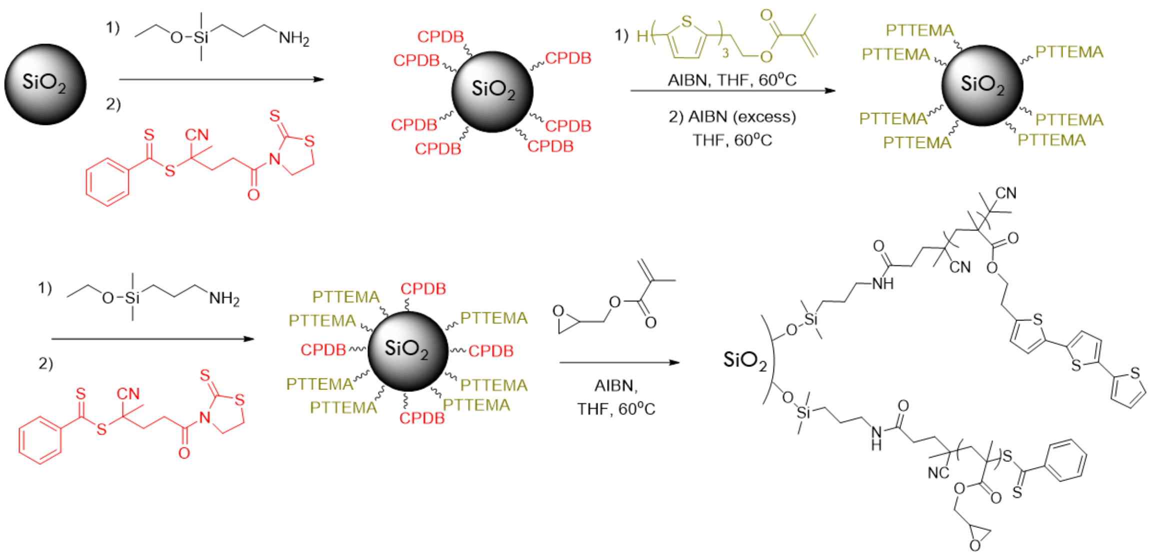

Scheme 3.7: Synthesis of PGMA-PTTEMA bimodal brush grafted nanoparticles.

The synthesized bimodal brush grafted nanoparticles were analyzed via GPC and TGA to determine grafted chain density and molecular weight. TGA and GPC traces are shown in Figure 3.12 In the GPC trace, one chain population can be seen after PTTEMA polymerization and the appearance of a second higher molecular weight peak after the polymerization of PGMA. The difference in molecular weight was not large enough to generate distinct peaks. Computer software was then used to deconvolute the peaks and obtain the necessary data for Mn and *Đ*. TGA weight loss data correlates with the GPC findings.

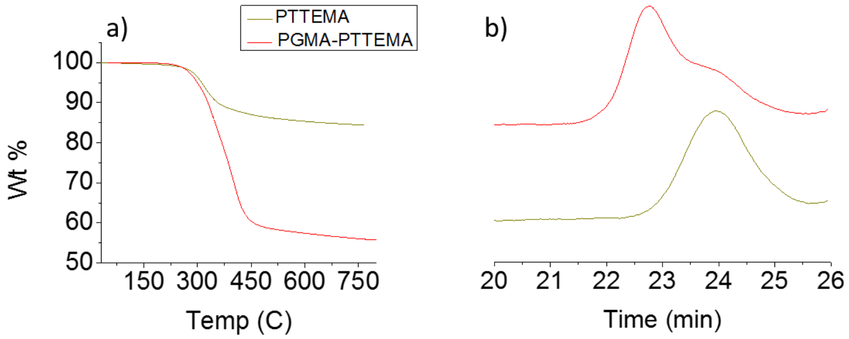

Figure 3.11: (a) TGA traces and (b) GPC chromatograms for PGMA-PTTEMA bimodal grafted SiO_2 after each polymerization step.

Table 3.4: Graft density (σ) and molecular weights of PGMA-PTTEMA bimodal brush grafted SiO_2 and PTTEMA monomodal brush grafted SiO_2.

Sample	**PTTEMA σ (ch/nm^2)**	**PTTEMAM_n (kg/mol)**	**PGMA σ (ch/nm^2)**	**PGMA M_n (kg/mol)**
BMB-PGMA-PTTEMA	0.19	8	0.25	21
PTTEMA-SiO_2	0.22	6.4	NA	NA

PTTEMA Grafted SiO_2 and PTTEMA-PGMA Mixed Bimodal Brush Grafted SiO_2 Dispersion and Electrical Breakdown

Both PTTEMA grafted and PGMA-PTTEMA bimodal grafted samples were then cast into commercial epoxy resin. TEM micrographs in Figure 3.13 show the dispersion of the polymer grafted samples in epoxy. PTTEMA was not expected to disperse well as the sample lacked epoxy compatible functionality. This hypothesis was confirmed upon viewing the TEM micrographs where the PTTEMA grafted nanoparticles were aggregated with a L_f of 365 nm. PGMA-PTTEMA bimodal grafted nanoparticles were also aggregated as shown by the corresponding TEM micrograph. The PTTEMA on the bimodal grafted nanoparticle surface has a Mn of ~ 8 kg/mol and the PGMA graft has a Mn of ~21 kg/mol. The ratio of long grafted chain length to short chain length may not be sufficient to allow entanglement of matrix and grafted long chains. The long chain graft density was calculated to 0.25 ch/nm^2 after polymerization. The long chain density is high relative to previous reports of bimodal brush grafted nanoparticles. The high, long chain graft density may also contribute lack of matrix entanglement. Further investigations are needed to to determine the appropriate grafted chain lengths and chain density for both and short ligands in the presented epoxy system.

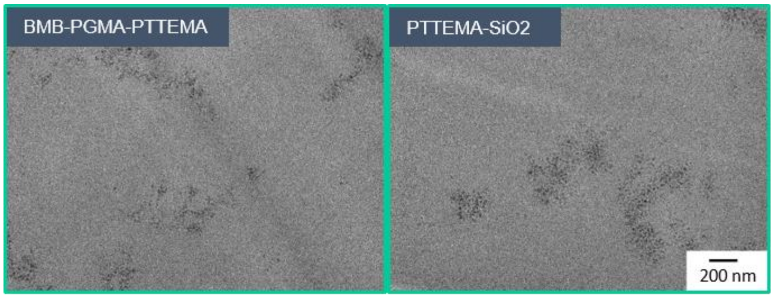

Figure 3.12: TEM micrographs for (left) PGMA-PTTEMA bimodal brush grafted SiO_2 and (right) PTTEMA monomodal grafted SiO_2.

Dielectric breakdown testing was performed on both the PTTEMA grafted and PGMA-PTTEMA bimodal grafted nanoparticles. Both samples showed improvements in dielectric breakdown strength compared to the reference epoxy. L_f and DBS improvements for the PTTEMA grafted samples are shown in Table 3.5. The results were not expected as the filler in both samples was aggregated with relatively high free space lengths (>250 nm). The data obtained suggests that the concentration of charge trapping groups at the particle interface may play an important role in dielectric breakdown strength even when the particles are not thoroughly dispersed.

Table 3.5: Observed free space length and % change in dielectric breakdown strength for PGMA-PTTEMA bimodal brush grafted SiO_2 and PTTEMA grafted SiO_2.

Sample	**L_f (nm)**	**Δ DBS**
BMB-PGMA-PTTEMA	316	+38 %
PTTEMA-SiO_2	364	+30 %

3.5 Conclusion

Multifunctional bimodal nanoparticles were successfully synthesized to contain π-conjugated electroactive short ligands and long matrix compatible PGMA brushes. Surface initiated RAFT polymerization served as a useful platform to control polymer chain length and graft density. Control over dispersion of the multifunctional nanoparticles in commercial epoxy was demonstrated effectively with varied polymer graft densities. L_f values, determined through analysis of TEM micrographs, were compared to changes in DBS. An inter-particle spacing of 200 nm was necessary to achieve a maximum increase in DBS and further property enhancements were not seen with decreasing particle spacing. The 200 nm L_f necessary to achieve maximum DBS was shown to correlate with predicted values of critical avalanche sizes based on Seitz's model, implicating the electron avalanche mechanisms for failure, and revealing a target quality of dispersion for optimal performance. Calculated IE+EA values for electroactive ligands proved to be a viable metric for composite performance based on excellent correlation with experimental values for DBS. Well dispersed bimodal PGMA-terthiophene nanoparticles showed the overall largest improvements in terms of breakdown strength as predicted based on calculated IE+EA values. Concentration of trapping groups was also considered with the synthesis of

PTTEMA and PGMA-PTTEMA grafted mixed bimodal showing considerable improvement in DBS.

3.6 Acknowledgements

This work was performed in collaboration with Timothy Krentz, Linda Schadler, Ke Wu, Curt Breneman, and J. Keith Nelson of Rensselaer Polytechnic Institute as well as, Su Zhao and Henrik Hillborg of ABB Corporate Research.

3.7 References

(1) Johari, G. P. *Chemistry and Technology of Epoxy Resins*; Ellis, B., Ed.; Springer Netherlands: Dordrecht, 1993.

(2) Virtanen, S.; Krentz, T.; Nelson, J.; Schadler, L.; Bell, M.; Benicewicz, B.; Hillborg, H.; Zhao, S. *IEEE Trans. Dielectr. Electr. Insul.* **2014**, *21* (2), 563.

(3) Siddabattuni, S.; Schuman, T. P.; Dogan, F. *ACS Appl. Mater. Interfaces* **2013**, *5* (6), 1917.

(4) Cheng, L.; Zheng, L.; Li, G.; Zeng, J.; Yin, Q. *Phys. B Condens. Matter* **2008**, *403* (17), 2584.

(5) Gao, M.; Zhang, P.; Wang, F.; Li, L.; Li, Z. In *2013 Annual Report Conference on Electrical Insulation and Dielectric Phenomena*; IEEE, 2013; pp 234–237.

(6) Krentz, T. M.; Huang, Y.; Nelson, J. K.; Schadler, L. S.; Bell, M.; Benicewicz, B. *2014 Annu. Rep. Conf. Electr. Insul. Dielectr. Phenom.* **2014**, 643.

(7) Roy, M.; Nelson, J. K.; MacCrone, R. K.; Schadler, L. S.; Reed, C. W.; Keefe, R.; Zenger, W. *IEEE Trans. Dielectr. Electr. Insul.* **2005**, *12* (4), 629.

(8) Tan, D.; Cao, Y.; Tuncer, E.; Irwin, P. *Mater. Sci. Appl.* **2013**, *4* (April), 6.

(9) Barber, P.; Balasubramanian, S.; Anguchamy, Y.; Gong, S.; Wibowo, A.; Gao, H.;

Ploehn, H. J.; zur Loye, H.-C. *Materials (Basel).* **2009**, *2* (4), 1697.

(10) Tanaka, T. *IEEE Trans. Dielectr. Electr. Insul.* **2005**, *12* (5), 914.

(11) Nelson, J. K. *Dielectric Polymer Nanocomposites*; Nelson, J. K., Ed.; Springer Science & Business Media, 2009.

(12) Tanaka, T.; Montanari, G. C.; Mulhaupt, R. *IEEE Trans. Dielectr. Electr. Insul.* **2004**, *11* (5), 763.

(13) Nelson, J. K.; Huang, Y.; Krentz, T. M.; Schadler, L. S.; Benicewicz, B. C.; Bell, M. *2015 IEEE 11th Int. Conf. Prop. Appl. Dielectr. Mater.* **2015**, 40.

(14) Nelson, J. K.; Fothergill, J. C. *Nanotechnology* **2004**, *15* (5), 586.

(15) Schadler, L. S.; Kumar, S. K.; Benicewicz, B. C.; Lewis, S. L.; Harton, S. E. *MRS Bull.* **2007**, *32* (04), 335.

(16) Li, Y.; Krentz, T. M.; Wang, L.; Benicewicz, B. C.; Schadler, L. S. *ACS Appl. Mater. Interfaces* **2014**, *6* (9), 6005.

(17) Natarajan, B.; Neely, T.; Rungta, A.; Benicewicz, B. C.; Schadler, L. S. *Macromolecules* **2013**, *46* (12), 4909.

(18) Rungta, A.; Natarajan, B.; Neely, T.; Dukes, D.; Schadler, L. S.; Benicewicz, B. C. *Macromolecules* **2012**, *45* (23), 9303.

(19) Li, Y.; Tao, P.; Viswanath, A.; Benicewicz, B. C.; Schadler, L. S. *Langmuir* **2013**, *29* (4), 1211.

(20) Akcora, P.; Liu, H.; Kumar, S. K.; Moll, J.; Li, Y.; Benicewicz, B. C.; Schadler, L. S.; Acehan, D.; Panagiotopoulos, A. Z.; Pryamitsyn, V.; Ganesan, V.; Ilavsky, J.; Thiyagarajan, P.; Colby, R. H.; Douglas, J. F. *Nat. Mater.* **2009**, *8* (4), 354.

(21) Chiefari, J.; Chong, Y. K. B.; Ercole, F.; Krstina, J.; Jeffery, J.; Le, T. P. T.;

Mayadunne, R. T. A.; Meijs, G. F.; Moad, C. L.; Moad, G.; Rizzardo, E.; Thang, S. H.; South, C. *Macromolecules* **1998**, *31* (16), 5559.

(22) Chong, B. Y. K.; Krstina, J.; Le, T. P. T.; Moad, G.; Postma, A.; Rizzardo, E.; Thang, S. H. *Macromolecules* **2003**, *36* (7), 2256.

(23) Li, C.; Han, J.; Ryu, C. Y.; Benicewicz, B. C. *Macromolecules* **2006**, *39* (9), 3175.

(24) Yamano, Y. *IEEE Trans. Dielectr. Electr. Insul.* **2006**, *13* (4), 773.

(25) Yamano, Y.; Endoh, H. *IEEE Trans. Dielectr. Electr. Insul.* **1998**, *5* (2), 270.

(26) Hanley, T. L.; Burford, R. P.; Fleming, R. J.; Barber, K. W. *IEEE Electr. Insul. Mag.* **2003**, *19* (1), 13.

(27) Sengupta, S. S.; Person, T. J.; Caronia, P. J. In *2010 IEEE International Symposium on Electrical Insulation*; IEEE, 2010; pp 1–6.

(28) Zhang, H.; Shang, Y.; Wang, X.; Zhao, H.; Han, B.; Li, Z. *J. Mol. Model.* **2013**, *19* (12), 5429.

(29) Du, Y.; Lv, Y.; Li, C.; Chen, M.; Zhou, J.; Li, X.; Zhou, Y.; Tu, Y. *J. Appl. Phys.* **2011**, *110* (10), 2.

(30) Champion, J. V; Dodd, S. J.; Stevens, G. C. *J. Phys. D. Appl. Phys.* **1994**, *27* (3), 604.

(31) Seitz, F. *Phys. Rev* **1949**, *76* (9), 1376.

(32) O’dwyer, J. *J. Phys. Chem. Solids* **1967**, *28* (7), 1137.

(33) Sparks, M.; Mills, D. L.; Warren, R.; Holstein, T.; Maradudin, A. A.; Sham, L. J.; Loh, E.; King, D. F. *Phys. Rev. B* **1981**, *24* (6), 3519.

(34) Sun, Y.; Boggs, S. A.; Ramprasad, R. In *2014 IEEE Conference on Electrical Insulation and Dielectric Phenomena (CEIDP)*; IEEE, 2014; pp 15–18.

(35) Qiao, Y.; Islam, M. S.; Han, K.; Leonhardt, E.; Zhang, J.; Wang, Q.; Ploehn, H. J.; Tang, C. *Adv. Funct. Mater.* **2013**, *23* (45), 5638.

(36) Qiao, Y.; Islam, M. S.; Wang, L.; Yan, Y.; Zhang, J.; Benicewicz, B. C.; Ploehn, H. J.; Tang, C. *Chem. Mater.* **2014**, *26* (18), 5319.

(37) Qiao, Y.; Yin, X.; Wang, L.; Islam, M. S.; Benicewicz, B. C.; Ploehn, H. J.; Tang, C. *Macromolecules* **2015**, *48* (24), 8998.

(38) Kuo, D. H.; Chang, C. C.; Su, T. Y.; Wang, W. K.; Lin, B. Y. *Mater. Chem. Phys.* **2004**, *85* (1), 201.

(39) Ma, D.; Hugener, T. a; Siegel, R. W.; Christerson, A.; Mårtensson, E.; Önneby, C.; Schadler, L. S. *Nanotechnology* **2005**, *16* (6), 724.

(40) Dou, X.; Liu, X.; Zhang, Y.; Feng, H.; Chen, J. F.; Du, S. *Appl. Phys. Lett.* **2009**, *95* (13), 132904.

(41) Kim, P.; Doss, N. M.; Tillotson, J. P.; Hotchkiss, P. J.; Pan, M. J.; Marder, S. R.; Li, J.; Calame, J. P.; Perry, J. W. *ACS Nano* **2009**, *3* (9), 2581.

(42) Li, W.; Yamamoto, Y.; Fukushima, T. *J. Am. Chem. Soc.* **2008**, *130*, 8886.

(43) Shah, J. R.; Mosier, P. D.; Roth, B. L.; Kellogg, G. E.; Westkaemper, R. B. *Bioorganic Med. Chem.* **2009**, *17* (18), 6496.

(44) Pyun, J.; Jia, S.; Kowalewski, T.; Patterson, G. D.; Matyjaszewski, K. *Macromolecules* **2003**, *36* (14), 5094.

(45) Tao, P.; Viswanath, A.; Schadler, L. S.; Benicewicz, B. C.; Siegel, R. W. *ACS Appl. Mater. Interfaces* **2011**, *3* (9), 3638.

(46) Gao, J.; Li, J.; Benicewicz, B. C.; Zhao, S.; Hillborg, H.; Schadler, L. S. *Polymers (Basel).* **2012**, *4* (1), 187.

(47) Kumar, S. K.; Jouault, N.; Benicewicz, B.; Neely, T. *Macromolecules* **2013**, *46* (9), 3199.

(48) Rytoluoto, I.; Lahti, K.; Karttunen, M.; Koponen, M.; Virtanen, S.; Pettersson, M. In *2014 IEEE Conference on Electrical Insulation and Dielectric Phenomena (CEIDP)*; IEEE, 2014; pp 655–658.

(49) Takala, M.; Ranta, H.; Nevalainen, P.; Pakonen, P.; Pelto, J.; Karttunen, M.; Virtanen, S.; Koivu, V.; Pettersson, M.; Sonerud, B.; Kannus, K. *IEEE Trans. Dielectr. Electr. Insul.* **2010**, *17* (4), 1259.

(50) Kochetov, R.; Tsekmes, I. A.; Chmura, L. A.; Morshuis, P. H. F.; Iizuka, T.; Tatsumi, K.; Tanaka, T. In *2014 IEEE Conference on Electrical Insulation and Dielectric Phenomena (CEIDP)*; IEEE, 2014; pp 715–718.

(51) Tkalya, E.; Ghislandi, M.; Otten, R.; Lotya, M.; Alekseev, A.; Van Der Schoot, P.; Coleman, J.; De With, G.; Koning, C. *ACS Appl. Mater. Interfaces* **2014**, *6* (17), 15113.

(52) Bauhofer, W.; Kovacs, J. Z. *Compos. Sci. Technol.* **2009**, *69* (10), 1486.

(53) Yan, J.; Kristufek, T.; Schmitt, M.; Wang, Z.; Xie, G.; Dang, A.; Hui, C. M.; Pietrasik, J.; Bockstaller, M. R.; Matyjaszewski, K. *Macromolecules* **2015**, *48* (22), 8208.

CHAPTER 4

SURFACE MODIFIED METAL OXIDE NANOPARTICLES FOR IMPROVED DIELECTRIC COMPOSITES

4.1 Abstract

Nanocomposites with metal oxide fillers are known to exhibit enhancements in optical, electrical, and thermomechanical properties.[1] Metal oxide composite dielectrics can show improvements in dielectric breakdown strength, permittivity, and energy density.[2] Previous work has shown that the modification of nanoparticle surfaces with conjugated electroactive groups can induce additional improvements upon both permittivity and dielectric breakdown strength.[3–5] The performance of the composite can be further altered by adding electron donating or withdrawing functionality to the conjugated electroactive molecules present at the surface.[3] Presented herein is the synthesis of two polycyclic anthracene surfaces ligands varying in electronic nature for attachment to metal oxide surfaces. The anthracene ligands were synthesized to contain phosphonic acid moieties to take advantage of the hydrolytic stable P-O-C and M-O-P bonds for nanoparticle attachment. The anthracene phosphonic acid ligands were successfully attached to TiO_2 along with a bimodal population of polydimethylsiloxane (PDMS) chains before dispersing into a commercial silicone matrix (Sylgard 184). Dielectric breakdown testing was performed to determine the effect of adding an electron withdrawing group to the anthracene on overall composite breakdown strength. Also presented is the synthesis of a novel phosphate containing RAFT agent for SI RAFT polymerization from metal oxides. The kinetics of SI RAFT polymerization from ZrO_2 was used to determine the efficacy of the novel RAFT agent. Text and figures are reproduced and adapted from *2015 IEEE Electrical Insulation Conference (EIC)*; IEEE: Seattle, WA, **2015**; pp 325–328.

4.2 Introduction

The surface modification of metal oxide nanoparticles has been performed using carboxylic acid, silane, amine, phosphate, and phosphonic acid groups.[6–8] Carboxylic acid and amine linkages are noncovalent and use chemisorption for surface attachment. Ligands attached using amines or carboxylic acids are generally for stabilization in organic media and can be easily displaced by covalent bonding molecules.[6] The use of silanes for the modification of metal oxide nanoparticles is well documented in the literature. The bond produced is covalent in nature and formed through condensation with hydroxyl groups on the metal oxide surface. There are several commercially available silane options that bear functionalities for subsequent functionalization, making them a popular choice for metal oxide surface functionalization. Competition for the formation of the M-O-Si bond is encountered with homocondensation of the organosilane coupling reagent to form Si-O-Si bonds. Conditions can be altered to favor heterocondenstion however once formed the bond is readily hydrolyzed compared to phosphorous derivatives.

The use of phosphates and phosphonic acids is being realized as a method for robust attachment to metal oxide surfaces. The resultant M-O-P bond is readily formed and hydrolytically stable. Heterocondensation of the phosphorous derivatives is the kinetically and thermodynamically favored reaction while homocondensation only is viable under high temperatures and dehydrating conditions. Functional organophosphorus derivatives need to be explored as the availability and popularity is not yet equal to that of organosilane derivatives.[7]

Several metal oxide nanofillers exist, each with unique properties, allowing for the synthesis of precisely tailored composite materials with appropriate ligand engineering.[9]

Organophosphorus reagents offer a robust covalent attachment method for metal oxide surface modification. Functional dielectric ligands consisting of phosphorous derived linkers have been explored previously where functionality has included small molecule stabilizing ligands,[10] polymeric ligands,[11–14] and small molecule electroactive ligands.[3,15,16] Multi-functional ligands on metal oxide surfaces have been explored for optical properties[17,18] however, exploration of multifunctional ligands for dielectrics has been limited to silica nanoparticles.[4,5] In this work, well dispersed multifunctional surface modified TiO_2 nanoparticles in commercial silicone are investigated for enhancements in dielectric breakdown strength.

Polymer functionalization for matrix compatibility is an important component for multifunctional ligand engineering. Polymer attachment using the grafting-to approach has been successful using polymers containing phosphorous derived end groups[19,20] or click functionality.[21–23] The use of the click reaction increases the number of required synthetic steps where the metal oxide surface requires appropriate functionality as well as the polymer chain end. Grafting-to dominates the literature for metal oxides however, precise morphological control over nanoparticles in a matrix has been most effectively demonstrated using a grafting-from approach.[24] The majority of grafting-from on metal oxide surfaces in the literature uses initiators or CTA's bound through chemisorption with carboxylic acids or with silane attachment. In order to create a hydrolytically stable bond an initiator containing a phosphorous derived linker is needed. Presented here is the synthesis of a phosphate containing RAFT agent for easy robust attachment of the CTA to metal oxide surfaces for SI RAFT polymerization.

4.3 Experimental Section

Materials

All reagents were purchased from Fisher Scientific unless stated otherwise below. Titanium(IV) butoxide (97%), oleic acid (90%), and tert- butylamine (98%) were purchased from Sigma Aldrich and used for the synthesis of titanium dioxide NPs. Phosphorus(V) oxychloride ($POCl_3$) and triethylamine (Et_3N) were obtained from Sigma Aldrich and used for modification of hydroxyl-terminated PDMS. Monocarbinol terminated PDMS MCR-C22 (Mw = 10 000 g/mol), and silanol-terminated PDMSDMS-S32 (Mw = 36 000 g/mol) were purchased from Gelest and were used as brush polymers. Sylgard 184 (Mw estimated as 100 000 g/mol) was purchased from Dow Corning, and used as matrix material for nanocomposite preparation. Methylhydrosiloxane-dimethylsiloxane copolymer (HMS-301) and platinum-divinyltetramethyldisiloxane complex (SIP6831.2) were purchased from Gelest and used as cross-linking agent and catalyst, respectively. 4-Cyano-4-(dodecylsulfanylthiocarbonyl)sulfanylpentanoic acid was received from Boron Molecular.

Instrumentation

NMR spectra were recorded on a Varian Mercury 400 spectrometer. FT-IR spectra were recorded on a Perkin Elmer Spectrum 100 using an attenuated total reflection diamond cell attachment. Quantification of surface groups was performed using UV-vis and TGA. UV-vis absorption spectra were taken on a Perkin-Elmer Lamda 4C UV/vis spectrophotometer. TGA characterization was conducted using a TA Instruments Q5000 with a heating rate of 10°C/min from 25°C to 800°C~1000°C under nitrogen flow. The molecular weights and molecular weight distributions were determined using a Waters gel-permeation chromatograph equipped with a 515 HPLC pump, a 2410 refractive index detector, three Styragel columns (HR1, HR3, HR4 in the effective molecular weight range of 100–5000, 500–30 000, and 5000–500 000, respectively). Tetrahydrofuran (THF) was used as the eluent at 30 °C and a flow rate of 1.0 mL min^{-1}. The GPC system was calibrated with polymethyl methacrylate standards obtained from Polymer Laboratories. Samples were processed by filtration through microfilters with a pore size of 0.2 μm before analysis.

Synthesis of 9-anthracenemethylbromide

In a 250 ml round bottom flask, 9-anthracenemethanol (2 g, 9.6 mmol) was dissolved into 40ml of toluene at room temperature before cooling to 0°C and flushing with nitrogen for 20 min. Phosphorus tribromide (3.12 g, 11.5 mmol) was added dropwise over 30 minutes. The solution was allowed to warm to room temperature and stirred overnight. Next 30 ml of 2M aqueous sodium carbonate was added dropwise. The mixture was allowed to stir for one hour after complete addition. The reaction mixture was then added to a separatory funnel where the aqueous layer was removed. The remaining organic layer was washed with two more portions of water. The organic layer was dried overnight with sodium sulfate. The solids were filtered and the solvent removed under reduced pressure. 9-Anthracenemethylbromide was obtained as a yellow solid (2.22 g, 85% yield) MP: 139-141°C, ^{1}H NMR (400 MHz, $CDCl_3$): δ (ppm) 8.51 (s, 1H), 8.30 (d, *J* = 8.9 Hz, 2H), 8.04 (d, *J* = 8.5 Hz, 2H), 7.63 (t, *J* = 7 Hz 2H), 7.49 (t, *J* = 7.7 Hz 2H), 5.56 (s, 2H), ^{13}C NMR (400 MHz, $CDCl_3$): δ (ppm) 131.6, 129.7, 129.3, 129.2, 127.9, 126.8, 125.4, 123.5, 27.0, MS (m/z): 271 [M^{+}].

Synthesis of 9-anthracenemethylphosphonate

To a 100 ml round bottom flask 9-anthracenemethylbromide (2.22 g, 8.19 mmol) and triethyl phosphate (5 g, 30 mmol) were refluxed overnight under nitrogen. The reaction was allowed to cool to room temperature where solid 9-anthracenemethylphosphonate began to precipitate out of solution. The product was further precipitated by placing in the freezer for two hours. The solid product was isolated via vacuum filtration and washed with cold ether. 9-Anthracenemethylphosphonate was obtained as a yellow crystalline solid (2.41g, 90% yield) ^{1}H NMR (400 MHz, $CDCl_3$): δ (ppm) 8.40 (d, *J* = 3.7 Hz, 1H), 8.32 (d, *J* = 8.9 Hz, 2H), 7.99 (d, *J* = 8.4 Hz, 4H), 7.59 – 7.45 (m, 4H), 4.26 (s, 1H) 4.19 (s, 1H), 3.94 – 3.76 (m, 4H), 1.07 (t, *J* = 7.1 Hz, 6H), ^{31}P NMR (400 MHz, ($CDCl_3$): δ (ppm) 25.69.

Synthesis of 9-anthracenemethylphosphonic acid

9-Anthracenemethylphosphonate (2.41 g, 7.31 mmol) was dissolved into 30 ml of DCM. The solution was cooled to 0°C and flushed with nitrogen before adding bromotrimethylsilane (3.35 g, 21.9 mmol) dropwise over 30 minutes. The solution was allowed to warm to room temperature and stirred overnight. Solvent and volatiles were removed under reduced pressure. The product was dissolved back into 30 ml DCM before adding 10 ml of methanol and stirring for two hours. The solvent was removed under reduced pressure leaving 9-anthracenemethylphoshonic acid as yellow crystalline solid (2g, 100% yield). MP: 254-255°C, ^{1}H NMR (400 MHz, (CD_3OD) δ (ppm) 8.45 (d, J = 3.7 Hz, 1H), 8.39 (d, *J* = 8.9 Hz, 2H), 7.03 (d, *J* = 8.3 Hz, 4H), 7.58 – 7.46 (m, 4H), 4.28 (s, 1H) 4.20 (s, 1H), ^{13}C NMR (400 MHz, (CD_3OD): δ (ppm) 131.5, 130.2, 129.1, 127.0, 126.9, 126.0, 125.5, 29.2, 27.9, ^{31}P NMR (400 MHz, (CD_3OD): δ (ppm) 24.15, HRMS (ESI) [M + H] Calcd for $C_{15}H_{13}O_3P$ 273.0676; Found 273.0675.

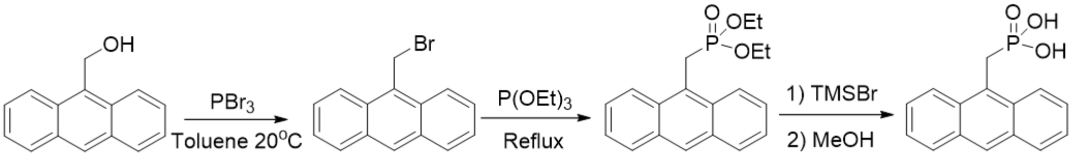

Scheme 4.1: Synthesis of 9-anthracenemethylphosphonic acid

Synthesis 10-bromo-9-anthracenemethylbromide

In a 250 ml round bottom flask, 9-anthracenemethanol (2g, 9.6 mmol) was dissolved into 100ml carbon tetrachloride. Bromine (1.53g, 9.6mmol) was added to the solution before bringing to reflux and stirrng for two hours. The reaction was cooled to room temperature and moved to a separatory funnel where the organic solution was washed three times with DI water. The organic layer was isolated and dried with $MgSO_4$. Solids were filtered and the solvent was removed in vacuum. The resultant yellow solid was recrystallized three times in toluene yielding 10-bromo-9-anthracenemethylbromide (1.2g, 76% yield). MP: 193-196°C, ^1H NMR (400 MHz, $CDCl_3$): δ (ppm) 8.62 (d, $J = 8$ Hz, 2H), 8.30 (d, $J = 8.4$ Hz, 2H), 7.70 – 7.61 (m, 4H), 5.50 (s, 2H) ^{13}C NMR (400 MHz, $CDCl_3$): δ (ppm) 130.6, 130.3, 128.9, 128.6, 127.2, 127, 125.8, 123.9, 26.6, MS (m/z): 350 [M^+].

Synthesis 10-bromo-9-anthracenemethylphosphonate

To a 100 ml round bottom flask 10-bromo-9-anthracenemethylbromide (0.95 g, 2.71 mmol) and triethyl phosphate (5 g, 30 mmol) were refluxed overnight under nitrogen. The reaction was allowed to cool to room temperature where solid 10-bromo-9-anthracenemethylphosphonate began to precipitate out of solution. The product was further precipitated by placing in the freezer for two hours. The solid product was isolated via vacuum filtration and washed with cold ether. 10-bromo-9-anthracenemethylphosphonate was obtained as a yellow crystalline solid (1 g, 91% yield) ^{1}H NMR (400 MHz, $CDCl_3$): δ (ppm) 8.59 (d, *J* = 9.4 Hz, 2H), 8.35 (d, *J* = 10 Hz, 2H), 7.62 - 7.59 (m, Hz, 4H), 4.24 (s, 1H) 4.18 (s, 1H), 3.95 – 3.79 (m, 4H), 1.08 (t, *J* = 7.1 Hz, 6H), ^{31}P NMR (400 MHz, $CDCl_3$): δ (ppm) 24.76.

Synthesis 10-bromo-9-anthracenemethylphosphonic acid

10-Bromo-9-anthracenemethylphosphonate (1 g, 2.46 mmol) was dissolved into 30 ml of DCM. The solution was cooled to 0°C and flushed with nitrogen before adding bromotrimethylsilane (1.5 g, 9.82 mmol) dropwise over 30 minutes. The solution was allowed to warm to room temperature and stirred overnight. Solvent and volatiles were removed under reduced pressure. The product was dissolved back into 30 ml DCM before adding 10 ml of methanol and stirring for two hours. The solvent was removed under reduced pressure. The resultant yellow powder was recrystallized in THF leaving 10-bromo-9-anthracenemethylphoshonic acid as yellow crystalline solid (0.864 g, 98% yield). MP:272-274°C ^{1}H NMR (400 MHz, $(CD_3)_2SO$): δ (ppm) 8.48 (t, *J* = 8.6 Hz, 4H), 7.73–7.61 (m, 4H), 4.13 (s, 1H), 4.08 (s, 1H) ^{13}C NMR (400 MHz, $(CD_3)_2SO$): δ (ppm) 131, 130.1, 128.8, 128.7, 128, 127.8, 126.9, 126.4, 121.6, 29.5 28.2, ^{31}P NMR (400 MHz, $(CD_3)_2SO$): δ (ppm) 19.5, HRMS (ESI) [M+H] Calcd for $C_{15}H_{12}BrO_3P$ 348.9629; Found 348.9635.

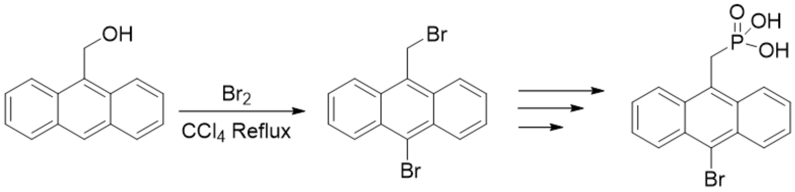

Scheme 4.2: Synthesis of 9-anthracenemethylphosphonic acid

Synthesis of PDMS Grafted TiO_2

The synthesis of TiO_2 nanoparticles and PDMS grafted TiO_2 nanoparticles was documented previously.[19] Nanoparticles were synthesized by collaborators at Rensselaer Polytechnic Institute. The TiO_2 nanoparticle were anatase with a narrow size distribution of 5 nm in diameter. Two populations of PDMS chains were sequentially grafted to the nanoparticles, the first having a molecular weight of 36 kg/mol at a graft density of 0.01 ch/nm^2 and the second, 10 kg/mol at 0.1 ch/nm^2.

Synthesis of PDMS-Anthracene Grafted Particles

In a typical synthesis procedure, one of the anthracenemethylphosphonic acids (0.16 mmol) was dissolved in 50 ml THF and a solution of PDMS grafted TiO_2 nanoparticles in THF was added to the solution dropwise at 0°C. The mixture was allowed to warm to room temperature and stir overnight. The nanoparticles were recovered by precipitation in methanol, and redispersed in THF for subsequent use in composite preparation. Using the presented procedure, the obtained graft density was found to be 0.3 ch/nm^2 for anthracene groups.

Composite Preparation

Sylgard® 184 silicone rubber was obtained from Dow Corning and used as the polymer matrix. Sylgard® 184 contains 40 wt% fumed silica as a reinforcing filler. The resin was mixed in THF along with the TiO_2 nanoparticles before removing the solvent under vacuum. Cross-linker was added at a 10:1 weight ratio before shear mixing at 3500 rpm for 1 min. The resin was cast in a flat aluminum dish and cured at 110°C under vacuum for 1.5 h. The cured samples were stored in a desiccator and conditioned at 70°C under vacuum overnight before dielectric testing.

Synthesis of RAFT alcohol (CDSS-OH)

In a 250 ml round bottom flask 4-cyano-4-(dodecylsulfanylthiocarbonyl) sulfanylpentanoic acid (CDSS) (2.00 g, 4.95 mmol), 1,6-hexanediol (3.50 g, 29.7 mmol), and DCC (1.12 g, 5.45 mmol) were dissolved in 50 ml of THF. The solution was cooled to 0°C and flushed with N_2 for 10 min. A solution of DMAP (30 mg, 0.25 mmol) in 5 ml THF was added dropwise over 20 min. The solution was allowed to warm to room temp and stirred over night. The solids formed during the reaction were filtered off and the solvent was removed at reduced pressure. The resultant residue was dissolved in 100 ml DCM and washed three times with DI water. The organic layer was isolated and dried with $MgSO_4$. Solids were filtered and solvent removed under reduced pressure. The residue was then subjected to column chromatography (SiO_2 5:4, hexanes:ethyl acetate) The product was recovered as a yellow oil (2.00 g, 80 % yield). ^{1}H NMR (400 MHz, $CDCl_3$): δ (ppm) 4.10 (t, J = 6.6 Hz, 2H), 3.65 (t, J = 6.4 Hz, 2H), 3.33 (t, J = 7.4 Hz, 2H) 2.64 – 2.60 (m, 2H). 2.55 – 2.48 (m, 1H), 2.40 – 2.33 (m, 1H), 1.88 (s, 3H), 1.69 – 1.57 (m, 8H), 1.39 (t, J = 3.6 Hz, 6H), 1.26 (s, 18H), 0.88 (t, J = 6.6 Hz 3H) ^{13}C NMR (400 MHz, $CDCl_3$): δ (ppm) 217, 171.6, 119, 65.1, 62.7, 46.4, 37, 33.9, 32.6, 31.9, 29.8, 29.6, 29.5, 29.4, 29.3, 29.1, 28.9, 28.5, 27.7, 25.7, 25.4, 24.9, 22.7 IR: 1700 cm^{-1} sharp (C=O), 3500cm^{-1} broad (O-H). HRMS (EI) [M+H] Calcd for $C_{25}H_{45}NO_3S_3$ 503.2562; Found 503.2573

Synthesis of RAFT Phosphate (CDSS-Phosphate)

In a flame dried 250 ml round bottom flask CDSS-OH (2.00 g, 3.96 mmol), and triethylamine (600 mg, 5.95 mmol) were dissolved in 40 ml of dry THF. The solution was cooled to 0°C and flushed with dry N_2 for 20 min before adding phosphoryl chloride (2.7 g, 17.4 mmol) dropwise over one hour. The solution was allowed to warm to room temperature and stirred overnight under N_2 atmosphere. DI water (100 ml) was then added to the solution and stirred for two hours. DCM (100 ml) was added and the solution was moved to separatory funnel and allowed to separate into organic and aqueous portions. The organic layer was isolated and washed with three portions of DI water. The organic layer was isolated and dried with $MgSO_4$. The solids were filtered and the solvent was removed under reduced pressure. The product was recovered as a thick yellow to brown oil. (1.8 g, 73% yield) ^{1}H NMR (400 MHz, $CDCl_3$): δ (ppm) 6.37 (s, 2H) 4.12 – 4.03 (m, 3H), 3.33 (t, *J* = 7.4 Hz, 2H) 2.63 (t, *J* = 7.4 Hz, 2H) 2.55 – 2.48 (m, 1H), 2.40 – 2.32 (m, 1H), 1.88 (s, 3H), 1.71 – 1.65 (m, 6H), 1.41 (m, 6H), 1.26 (s, 16H), 0.88 (t, *J* = Hz, 3H). ^{13}C NMR (400 MHz, $CDCl_3$): δ (ppm) 217, 171.7, 119, 67.4, 65.1, 46.4, 37.1, 33.9, 31.9, 29.8, 29.6, 29.4, 29.3, 29.1, 29, 28.4, 27.7, 25.4, 25, 24.8, 22.7. ^{31}P NMR (400 MHz, $CDCl_3$): δ (ppm) 1.74, 1.64, IR: 1190 cm^{-1} (P=O) HRMS (ESI) [M+H] Calcd for $C_{25}H_{46}NO_6PS_3$ 584.2300; Found 584.2298.

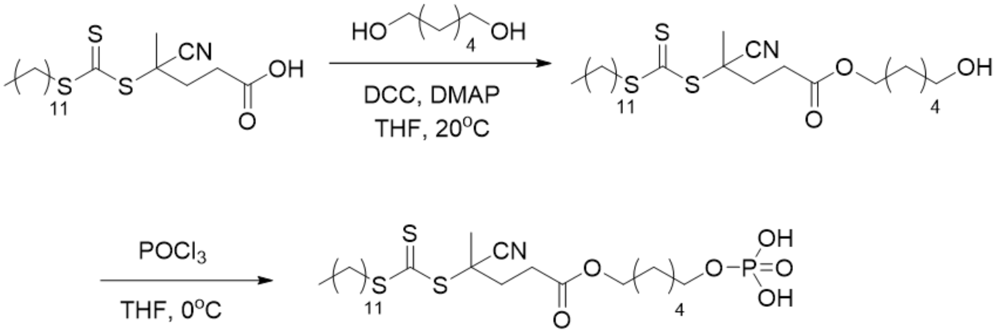

Scheme 4.3: Synthesis of CDSS phosphate.

CDSS Grafted Zirconia

Zirconia nanoparticles were synthesized by collaborators at Rensselaer Polytechnic Institute using methodology described previously.[25] The zirconia nanoparticles had a diameter of 5 nm. Zirconia nanoparticles (0.25g) and CDSS-phosphate (45 mg, 77 µmol) were dissolved into 25 ml THF. The solution was subjected to three freeze pump thaw cycles and placed in an oil bath at 80°C for six hours. The solution was allowed to warm to room temperature and grafted particles were recovered by precipitation in methanol and centrifuging at 10,000 RPM for 15 minutes. The recovered particles were washed two more time with methanol before dispersing in THF for subsequent use.

PMMA Grafted Zirconia

CDSS grafted zirconia (114 mg), methylmethacrylate (MMA) (2.34 g, 23 mmol), and AIBN (2 mg, 12 µmol) were combined in 5 ml of anhydrous THF. The solution was subjected to three freeze pump thaw cycles and placed in an oil bath at 60°C. samples (1 ml) were taken at 3 hr intervals. Polymer grafted particles were isolated by precipitating in methanol and centrifuging at 10,000 RPM for 15 minutes. Additional precipitations and recovery were performed to remove residual monomer. Polymer chains were cleaved from the ZrO_2 surface using a hydrofluoric acid solution. NMR and GPC analysis were performed on the polymer samples.

4.4 Results and Discussion

Synthesis of 9-anthracenemethylphosphonic acid

9-Anthracenemethylphosphonic acid was achieved in three synthetic steps from commercially available 9-anthracenemethanol. The synthesis is outlined in Scheme 4.1. 9-Anthracenemethanol was first converted to 9-anthracenemethylbromide using phosphorous tribromide. The procedure was followed from Westkaemper et al.[26] Product was confirmed by ^1H NMR where the protons from the benzylic carbon shifted upfield because of electronic shielding from the less electronegative bromine group. NMR comparison of 9-anthracenemethaol and 9-anthracenemethylbromide is shown in Figure 4.1. IR also confirms success of the reaction with the disappearance of the broad peak at 3400 cm^{-1} representative of hydroxyl group stretching. Triethyl phosphate was then used to substitute the benzylic bromine generating 9-anthracenemethylphosphonate. Next the phosphonate moiety was converted to the phosphonic acid using TMSBr. The conversion was successful in excellent yield and purity requiring no column chromatography.

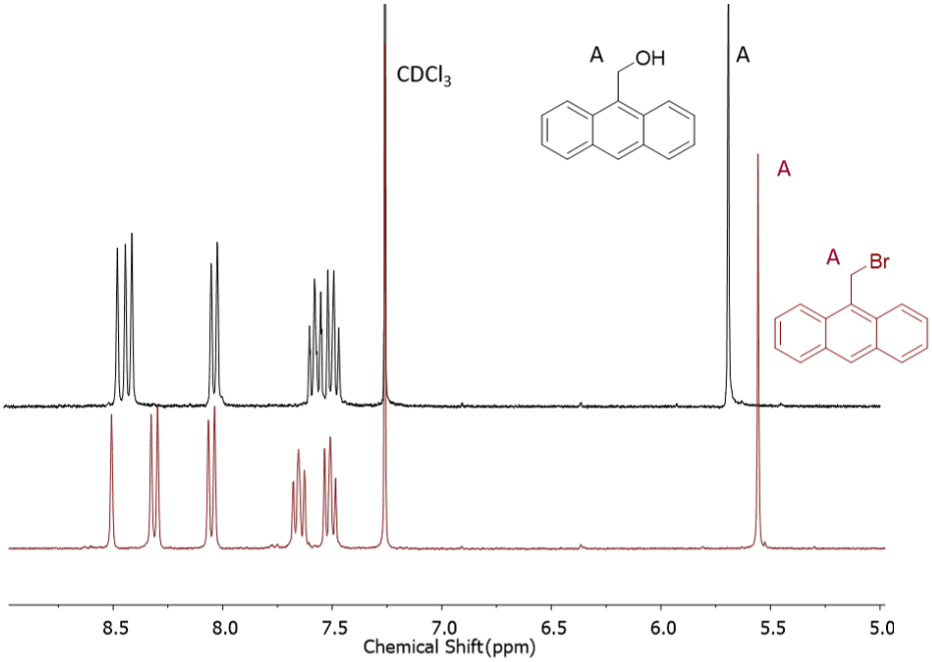

Figure 4.1: ^{1}H NMR of comparison of 9-anthracenemethanol and 9-anthracenemethyl bromide.

Synthesis of 10-bromo-9-anthracenemethylphosphonic acid

Synthesis of 10-bromo-9-anthracenemethylphosphonic acid is outlined in Scheme 4.2. Bromination of the 10 position of anthracene has been demonstrated previously.[27,28] Bromination of 9-anthracenemethanol in this study used a modified version of previous literature. Upon completion of the aromatic bromination reaction, it was found that in addition to aromatic substitution at the 10 position, the benzylic hydroxyl group also underwent substitution with bromide functionality. The byproduct of aromatic substitution was HBr which subsequently facilitated substitution at the benzylic position. This was useful in eliminating an additional synthetic step of converting the alcohol to a bromide using PBr_3 as described earlier. ^{1}H NMR spectra for these products are shown in Figure 4.2. Proton NMR shows the disappearance of the aromatic H at the 10 position and the upfield shift of benzylic hydrogens. Substitution of the benzylic bromine was then performed with triethyl phosphate and subsequent conversion to the phosphonic acid species was performed using the same procedure as described earlier for 9-anthracenemethylphosphonic acid. The product was recovered in excellent yield without the need for column chromatography.

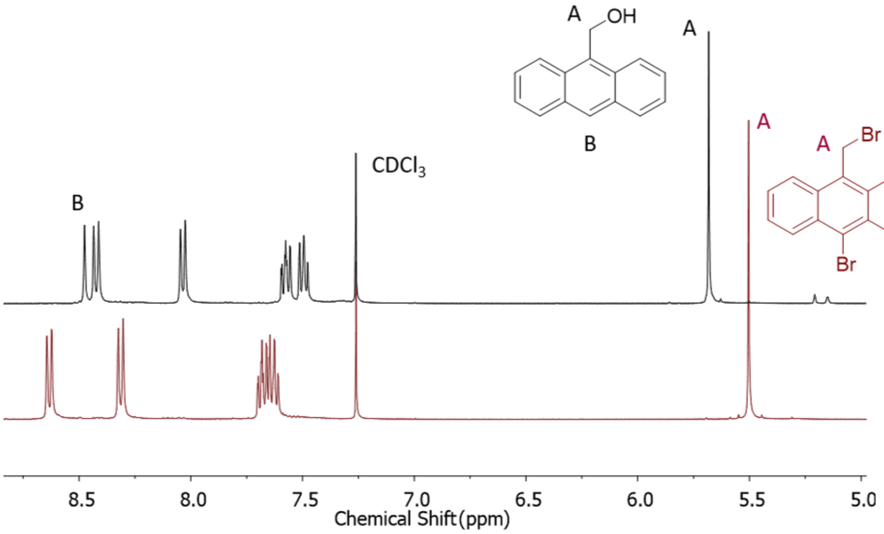

Figure 4.2: ^{1}H NMR comparison of 9-anthracenemethanol and 10-bromo-9-anthracenemethylbromide.

Composite Preparation

The synthesis of PDMS grafted nanoparticles and composite preparation in Sylgard 184 has been outlined in detail previously in the literature.[19] PDMS was purchased containing hydroxyl terminal groups that were then converted to phosphate end groups using $POCl_3$ under anhydrous conditions. The phosphate terminated PDMS polymers were grafted to the nanoparticle surface sequentially, short chains (10kg/mol) followed by long chains (36 kg/mol). TGA analysis determined the graft density for each grafted species.

Following the addition of polymer chains, one of the anthracene derivatives was added to the particle surface. After washing the particles, anthracene attachment was verified and quantified using UV-vis spectroscopy. Matrix polymer, grafted particles and crosslinking agents were then mixed in solution and final samples were dried and cast for dielectric measurements. Synthesis of the grafted particles is outlined in Scheme 4.4.

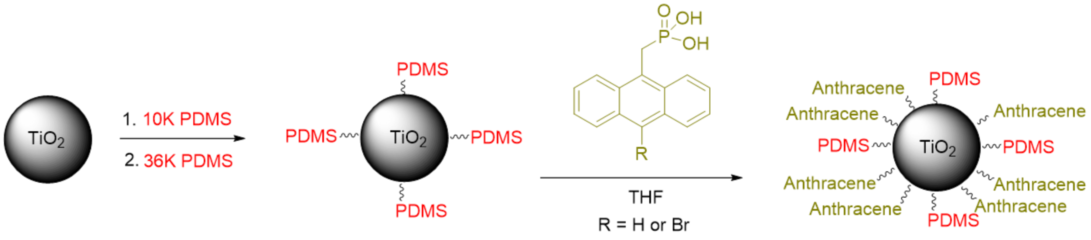

Scheme 4.4: Assembly of TiO_2 nanoparticles containing bimodal brush PDMS and anthracene surface groups.

Composite Characterization

Upon casting the composites, TEM microscopy was used to monitor dispersion of the particles. TEM images for ungrafted and grafted TiO_2 nanoparticles in Sylgard 184 are shown in Figure 4.3. Bare TiO_2 (Figure 4.3 a) was not compatible with the polymeric matrix and phase separated upon mixing. These results were consistent with our previous findings using silica nanoparticles in epoxy and several literature publications. The addition of bimodal PDMS brushes (Figure 4.3 b, c) allowed for nanoparticle dispersion in the matrix. Bimodal grafted brushes were utilized in this case because of their tendency to improve thermodynamic compatibility with polymer matrices. Previous literature shows that nanoparticles grafted with bimodal brushes disperse well over a larger range of polymer molecular weights and graft densities than nanoparticles grafted with a single population of polymer brushes. The two populations independently overcome enthalpic and entropic incompatibility where the long polymer brushes promote entanglement with the polymer matrix while the short polymer brushes screen particle core-core attraction.[19,29,30]

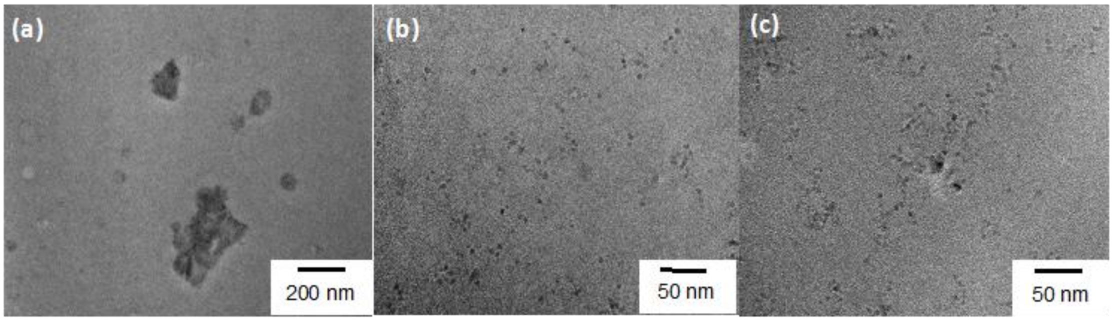

Figure 4.3: TEM micrographs of a) bare TiO_2 b) TiO_2 grafted with bimodal PDMS brushes and c) TiO_2 grafted with bimodal PDMS brushes and anthracene phosphonic acid. All samples contain 2 wt% TiO_2 in Sylgard 184.

Synthesized TiO_2 filled composites were compared to neat Sylgard 184 for variations in dielectric breakdown strength. Dielectric breakdown measurements of the synthesized composites showed similar trends as previous chapters where agglomerated samples demonstrated a decrease in breakdown strength compared to the neat matrix and well dispersed samples containing charge trapping functionality showed improvements. Unmodified TiO_2 in silicone showed a 3 % decrease in breakdown strength compared to neat silicone. Trends deviated from previous findings where, well dispersed PDMS modified TiO_2 also showed a decrease in breakdown strength with a 2% loss compared to neat silicone. However, well dispersed PDMS-anthracene modified samples demonstrated improvements in dielectric breakdown strength compared to neat silicone. Figure 4.4 shows the Weibull plots for probability of dielectric breakdown at an applied voltage. The plot highlights the trend of added increased breakdown strength with added trapping functionality.

Increasing the filler concentration of PDMS-anthracene grafted TiO_2 from 2 wt% to 4 wt% had no effect on the overall composite breakdown strength. Increasing the filler concentration to 6 wt% had a negative impact on composite dielectric breakdown strength compared to 2 and 4 wt% filled samples. The increase in filler concentration may have decreased the inter-particle distances to the percolation threshold, where a conducting pathway can be formed across the composite ultimately reducing breakdown strength. Values from dielectric breakdown measurements for all samples are shown in Table 1.

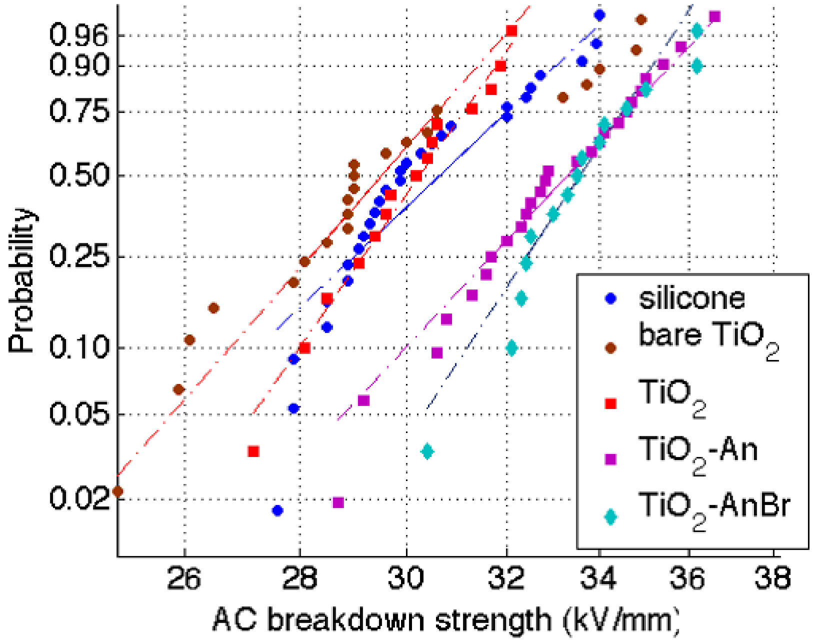

Figure 4.4: Weibull probability plot for silicone composite samples containing 2 wt% TiO_2 with varied interfacial chemistries.

Table 4.1: AC dielectric breakdown values for TiO_2 nanoparticles in commercial Sylgard 184 silicone (wt% values represent TiO_2 in the final casted composite).

Sample	**AC DBS (kV/mm)**	**Δ DBS**
Neat Sylgard 184	31.2	NA
4 wt% TiO_2-Unmodified	30.3	-3 %
2 wt% TiO_2-PDMS	30.6	-2 %
2 wt% TiO_2-PDMS-Anthracene	33.9	+9 %
4 wt% TiO_2-PDMS-Anthracene	33.9	+9 %
6 wt% TiO_2-PDMS-Anthracene	31	0 %
2 wt% TiO_2-PDMS-AnthraceneBr	34.3	+10 %

Previous literature has shown that the addition of electron withdrawing groups to conjugated polycyclic voltage stabilizers[31] and nanoparticle surface ligands[3] can show improvements in overall dielectric breakdown strength. Bromination of the 10 position of anthracene was an easy and effective means to add electron withdrawing functionality to the polycyclic anthracene molecule. Comparisons were then made between the brominated and non-brominated species of anthracene for their effect on composite dielectric breakdown strength. Experimental data shows only a slight increase in breakdown strength for the brominated species compared to the non-brominated species. These findings are consistent with Yamano's finding regarding polycyclic voltage stabilizers in LDPE.[31] The addition of the weakly withdrawing bromine group may not be sufficient to significantly alter the charge trapping properties of anthracene. The Breneman group at RPI provided calculations for IE+EA values of the synthesized molecules. Calculated values IE+EA were 5.74 eV and 5.62 eV for 9-anthracenemethylphosphonic acid and 10-bromo-9-anthracenemethylphosphonic acid respectively. The decrease in IE+EA from non-brominated to brominated species suggests better charge trapping ability though the difference is minor relative to previously studied molecules. The small decrease in calculated IE+EA is consistent with the small increase in experimentally obtained breakdown strength values.

Synthesis of CDSS-Phosphate

Synthesis of the phosphate containing RAFT agent was achieved in two synthetic steps, the synthesis is outlined in Scheme 4.3. In the first step, an excess of 1,6-hexanediol was used in the esterification of the acid containing commercial RAFT agent CDSS. The excess of diol in dilute solution prevented crosslinking of RAFT agents. The alcohol moiety was converted to the phosphate using $POCl_3$. FT-IR, ^{1}H NMR and ^{31}P NMR analysis confirmed conversion of the alcohol to the phosphate moiety. UV-vis analysis of the commercial RAFT agent compared to the synthesized phosphate RAFT agent suggested successful conversion of the acid to phosphate without degradation of the trithiocarbonate moiety. ^{1}H NMR spectra for CDSS-OH and CDSS-phosphate are shown in Figure 4.5. The downfield shift of adjacent protons is shown when going from alcohol functionality to phosphate.

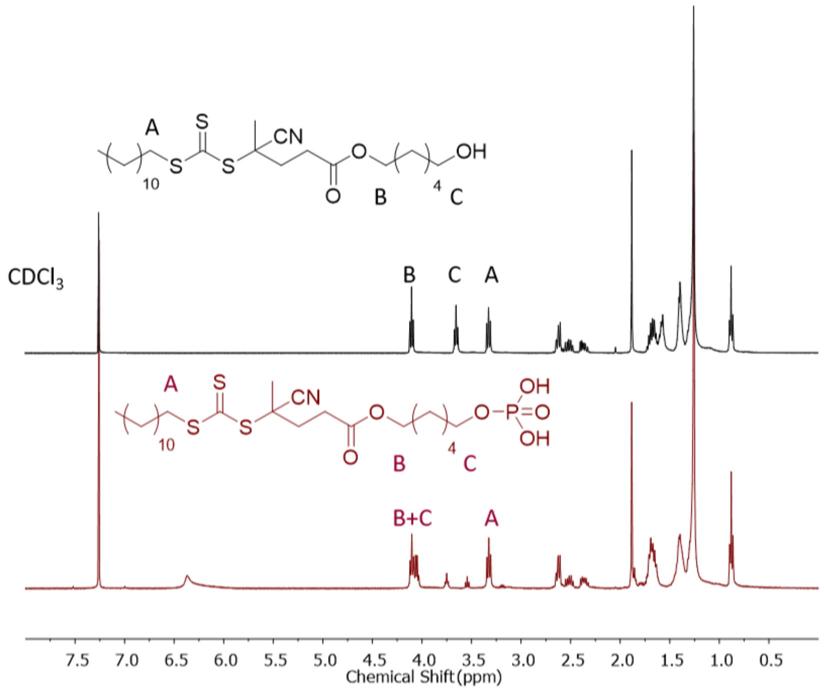

Figure 4.5: ^{1}H NMR spectra for CDSS-OH and CDSS-phosphate.

Surface Initiated RAFT Polymerization from ZrO_2

The RAFT agent was successfully attached to 4 nm ZrO_2 nanoparticles and confirmed by UV-vis and TGA analysis after particle workup. Polymerization of methyl methacrylate was then performed to determine the effectiveness of the grafted RAFT agent. The kinetics of the polymerization are shown in Figure 4.5. When monitoring conversion with time, there was a linear increase as the reaction progressed to approximately 40% conversion over 17 hours. Molecular weight increased linearly with time, however it largely deviated from theoretically calculated molecular weight. The Dispersity index (*Đ*) for the synthesized polymers was also high in regards to controlled radical polymerization ranging from 1.3 to 1.8. *Đ* values typically fall in the range of 1 -1.3 for the SI-RAFT polymerization of MMA.[32] The polymerization reached experimentally high molecular weight early in the reaction and maintained a slight increase through progress of the polymerization. The early increase in molecular weight was indicative of conventional free radical polymerization where polymer chains reach high molecular weight early in the reaction and conversion is dependent upon initiator decomposition.

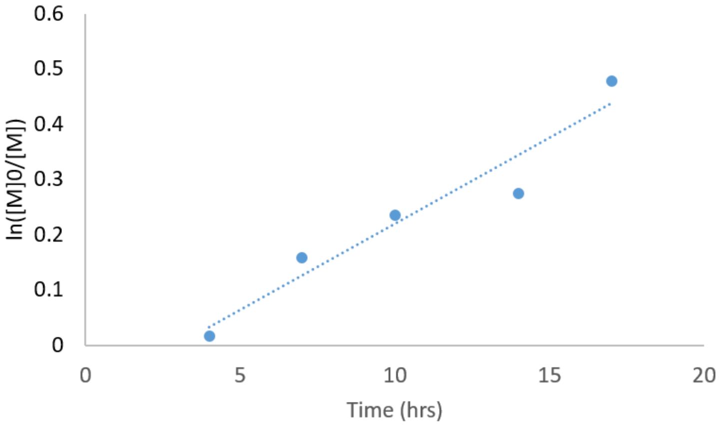

Figure 4.6: MMA conversion with time for SI RAFT polymerization from 4 nm ZrO_2 using phosphate RAFT agent.

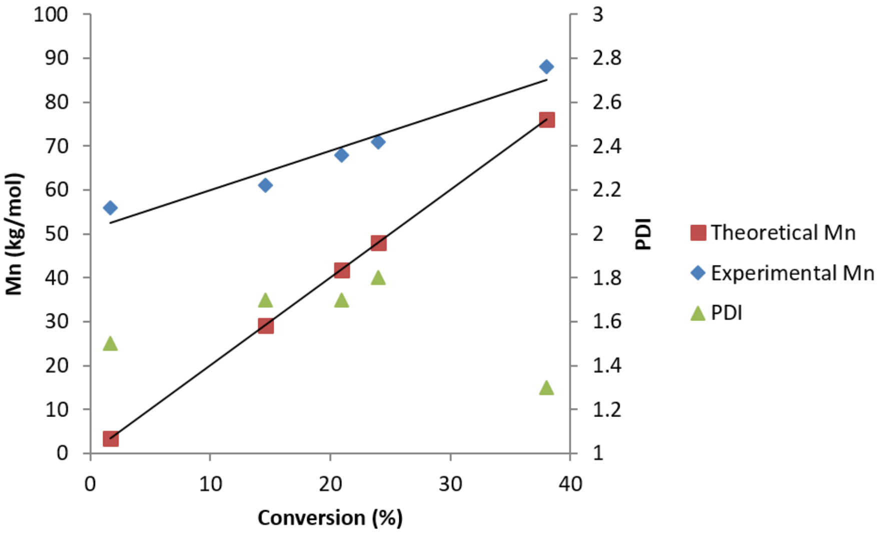

Figure 4.7: Theoretical and experimental MMA molecular weight with monomer conversion for SI RAFT polymerization from 4 nm ZrO_2 using phosphate RAFT agent.

The evidence presented suggests that the RAFT agent was not successful in controlling the polymerization. Evidence obtained from UV-vis measurements show that the trithiocarbonate remained intact throughout RAFT agent synthesis and attachment, therefore it is not believed RAFT agent degradation is responsible for poor control. Kinetic experiments were also conducted on BaTiO3 nanoparticles and using free CDSS-phosphate in solution. The results of the additional kinetic studies demonstrated similar results, eliminating the substrate as a possible cause of the lack of molecular weight control. Contaminates may have remained with the RAFT agent after converting the alcohol to the phosphate moiety. The phosphate product could not be purified by column chromatography and an appropriate solvent system was not found for recrystallization. Further investigation is required into determine the appropriate method for purification.

4.5 Conclusion

Functional phosphonic acid ligands were successfully synthesized and attached to TiO_2 nanoparticles. The nanoparticles were made compatible with commercial silicone by grafting a bimodal population of PDMS chains to the surface. Two anthracene phosphonic acid species were synthesized differing in substitution at the 10 position. The anthracene ligands were attached to the TiO_2 surface following PDMS attachment creating two well dispersed composites differing in electronic functionality. Comparisons were then made in overall dielectric breakdown strength of the two composites. The composite containing TiO_2 modified with brominated anthracene showed a minor increase in dielectric breakdown strength that was consistent with calculations of IE+EA. Comparisons of anthracene modified TiO_2 vs TiO_2 without anthracene modification demonstrated that anthracene attachment was necessary to achieve very significant improvements in DBS for this system. In addition, a novel phosphate containing RAFT agent was also synthesized for attachment to metal oxide surfaces. The RAFT agent was successfully attached to 4 nm zirconia nanoparticles however, kinetic studies of surface initiated RAFT polymerization of MMA showed that the polymerization was not controlled.

4.6 Acknowledgements

This work was performed in collaboration with Yanhui Huang of the Schadler research group and Ke Wu of the Breneman research group at Rensselaer Polytechnic Institute.

4.7 References

(1) Li, Y.; Krentz, T. M.; Wang, L.; Benicewicz, B. C.; Schadler, L. S. *ACS Appl. Mater. Interfaces* **2014**, *6* (9), 6005.

(2) Barber, P.; Balasubramanian, S.; Anguchamy, Y.; Gong, S.; Wibowo, A.; Gao, H.; Ploehn, H. J.; zur Loye, H.-C. *Materials (Basel).* **2009**, *2* (4), 1697.

(3) Siddabattuni, S.; Schuman, T. P.; Dogan, F. *ACS Appl. Mater. Interfaces* **2013**, *5* (6), 1917.

(4) Virtanen, S.; Krentz, T.; Nelson, J.; Schadler, L.; Bell, M.; Benicewicz, B.; Hillborg, H.; Zhao, S. *IEEE Trans. Dielectr. Electr. Insul.* **2014**, *21* (2), 563.

(5) Krentz, T. M.; Huang, Y.; Nelson, J. K.; Schadler, L. S.; Bell, M.; Benicewicz, B. *2014 Annu. Rep. Conf. Electr. Insul. Dielectr. Phenom.* **2014**, 643.

(6) Neouze, M.-A.; Schubert, U. *Monatshefte für Chemie - Chem. Mon.* **2008**, *139* (3), 183.

(7) Mutin, P. H.; Guerrero, G.; Vioux, A. *J. Mater. Chem.* **2005**, *15* (35-36), 3761.

(8) Ulman, A. *Chem. Rev.* **1996**, *96* (4), 1533.

(9) Corr, S. A. *Nanoscience*; O'Brien, P., Ed.; Nanoscience; Royal Society of

Chemistry: Cambridge, 2012; Vol. 1.

(10) Kim, P.; Jones, S. C.; Hotchkiss, P. J.; Haddock, J. N.; Kippelen, B.; Marder, S. R.; Perry, J. W. *Adv. Mater.* **2007**, *19* (7), 1001.

(11) Qiao, Y.; Islam, M. S.; Wang, L.; Yan, Y.; Zhang, J.; Benicewicz, B. C.; Ploehn, H. J.; Tang, C. *Chem. Mater.* **2014**, *26* (18), 5319.

(12) Qiao, Y.; Yin, X.; Wang, L.; Islam, M. S.; Benicewicz, B. C.; Ploehn, H. J.; Tang, C. *Macromolecules* **2015**, *48* (24), 8998.

(13) Xie, L.; Huang, X.; Wu, C.; Jiang, P. *J. Mater. Chem.* **2011**, *21* (16), 5897.

(14) Yang, K.; Huang, X.; Huang, Y.; Xie, L.; Jiang, P. *Chem. Mater.* **2013**, *25* (11), 2327.

(15) Hanson, E. L.; Guo, J.; Koch, N.; Schwartz, J.; Bernasek, S. L. *J. Am. Chem. Soc.* **2005**, *127* (28), 10058.

(16) Hotchkiss, P. J.; Jones, S. C.; Paniagua, S. a; Sharma, A.; Kippelen, B.; Armstrong, N. R.; Marder, S. R. *Acc. Chem. Res.* **2012**, *45* (3), 337.

(17) Li, Y.; Tao, P.; Siegel, R. W.; Schadler, L. S. *MRS Proc.* **2013**, *1547*, 161.

(18) Tahir, M. N.; Eberhardt, M.; Theato, P.; Faiß, S.; Janshoff, A.; Gorelik, T.; Kolb, U.; Tremel, W. *Angew. Chemie - Int. Ed.* **2006**, *45* (6), 908.

(19) Li, Y.; Tao, P.; Viswanath, A.; Benicewicz, B. C.; Schadler, L. S. *Langmuir* **2013**, *29* (4), 1211.

(20) Li, J.; Khanchaitit, P.; Han, K.; Wang, Q. *Chem. Mater.* **2010**, *22* (18), 5350.

(21) White, M. A.; Maliakal, A.; Turro, N. J.; Koberstein, J. *Macromol. Rapid Commun.* **2008**, *29* (18), 1544.

(22) White, M. a.; Johnson, J. a.; Koberstein, J. T.; Turro, N. J. *J. Am. Chem. Soc.* **2006**,

128 (35), 11356.

(23) Tao, P.; Viswanath, A.; Schadler, L. S.; Benicewicz, B. C.; Siegel, R. W. *ACS Appl. Mater. Interfaces* **2011**, *3* (9), 3638.

(24) Akcora, P.; Liu, H.; Kumar, S. K.; Moll, J.; Li, Y.; Benicewicz, B. C.; Schadler, L. S.; Acehan, D.; Panagiotopoulos, A. Z.; Pryamitsyn, V.; Ganesan, V.; Ilavsky, J.; Thiyagarajan, P.; Colby, R. H.; Douglas, J. F. *Nat. Mater.* **2009**, *8* (4), 354.

(25) Li, Y.; Wang, L.; Natarajan, B.; Tao, P.; Benicewicz, B. C.; Ullal, C.; Schadler, L. S. *RSC Adv.* **2015**, *5* (19), 14788.

(26) Shah, J. R.; Mosier, P. D.; Roth, B. L.; Kellogg, G. E.; Westkaemper, R. B. *Bioorganic Med. Chem.* **2009**, *17* (18), 6496.

(27) Bachmann, W. E.; Kloetzel, M. C. *J. Org. Chem.* **1938**, *03* (1), 55.

(28) Wright, O. L.; Mura, L. E. *J. Chem. Educ.* **1966**, *43* (3), 150.

(29) Rungta, A.; Natarajan, B.; Neely, T.; Dukes, D.; Schadler, L. S.; Benicewicz, B. C. *Macromolecules* **2012**, *45* (23), 9303.

(30) Natarajan, B.; Neely, T.; Rungta, A.; Benicewicz, B. C.; Schadler, L. S. *Macromolecules* **2013**, *46* (12), 4909.

(31) Yamano, Y. *IEEE Trans. Dielectr. Electr. Insul.* **2006**, *13* (4), 773.

(32) Li, C.; Han, J.; Ryu, C. Y.; Benicewicz, B. C. *Macromolecules* **2006**, *39* (9), 3175.

CHAPTER 5

SURFACE INITIATED AQUEOUS FREE RADICAL POLYMERIZATION FOR FRACKING ADDITIVES WITH ENHANCED SUSPENSION

5.1 Abstract

Fracking fluids are composed of primarily water, proppant (sand), and a small percentage of chemical additives. The additives serve multiple functions, one of which is suspending the proppant in the aqueous solution. Polyacrylamide (PAM) is a common chemical additive that serves this function, as well as, friction reducer. Hydrocarbon feedstocks have become less accessible as of late and require longer and more advanced drilling techniques to be able to access them. With the implementation of advanced drilling techniques like horizontal drilling, proppants need to stay suspended in solution longer and under more rigorous conditions. A surface initiated free radical polymerization in aqueous conditions is presented. The methodology is intended to be an industrially applicable alternative to current hydraulic fracturing proppants. Surface initiated free radical polymerization offers an inexpensive, effective platform for covalent attachment of water soluble polyacrylamide to the surface of 5μm silica. Proppants incorporating covalently bound polyacrylamide were shown to increase suspension time compared to solutions of unmodified silica.

5.2 Introduction

Hydraulic fracturing is a method of hydrocarbon extraction that uses fluids injected at high pressure to cause fractures in shale rock at drilling sites. Incorporated in the fluid, among other additives, is a proppant. The proppant’s function is to create and hold open small fissures in the shale rock so trapped hydrocarbon can be released.[1] Common proppants used in industry include sand, bauxite, and various ceramics.[2] A problem with current fracking technology is that proppants tend to settle out of solution before reaching the intended fracture location.[3] This problem is exacerbated by newer directional drilling methods where fluids may have to travel horizontally.[4] Current protocol to combat this phenomenon is to increase pumping rates or include additives to increase solution viscosity. Thickening agents can be costly compared to their efficacy and increased pumping rates consume larger amounts of water.

Polyacrylamide is a hydrogel polymer that is often used as a thickener or suspending agent in fracking fluids.[5] The thickening of fracking solution reduces turbulence when water is pumped down a borehole and helps to keep the proppant suspended, though current formulations still allow for relatively quick settling without agitation. Polyacrylamide can be synthesized via emulsion, solution, dispersion, and CRP methods.[6–13] Polyacrylamide with high molecular weights (> 1 million g/mol) can show flocculation properties and is common in municipal waste water treatment. Amide groups are known to adsorb onto particle surfaces and the long chain length of high molecular weight polymers can cause multiple particles to adsorb onto a single chain causing aggregation.[14,15]

Because of the scale of hydrocarbon extraction, cost is a large contributing factor to the viability of fracking technology. Using controlled radical polymerization techniques may be prohibitive because of the relative high cost of chain transfer agents. The precise control over polymerization parameters is also not necessary. Surface initiated free radical polymerization has been demonstrated in the past where an azo initiator was covalently bound to a substrate surface and subsequent polymerization was performed. Prucker et al. performed free radical SI polymerization of styrene from the surface of silica gels.[16] Bruening et al. performed the same task from the surface of gold nanoparticles.[17]

A current investigation into self-suspending proppants uses hydrogel polymers applied to the proppant through noncovalent means and crosslinked to create a core-shell type morphology.[18] The presented methodology was shown to increase hydrocarbon yield by as much as 45%. The synthesis of the core-shell proppants requires processing where the polymer is applied in a thin coating and later crosslinked. Details of the process are proprietary but polymerization directly from the substrate surface may be an effective alternative with less processing.

Along with concerns of the efficacy of fracking fluids, environmental concerns have emerged over chemical additives being released into strata and fresh water aquifers in the event of an accidental release.[19–21] Covalent bonding of the chemical additive to the proppant surface has been shown to be an effective method for preventing migration of the additives through simulated strata.[22] This could be useful in the event of an industrial spill where chemical additives attached to the proppant surface could be recovered without leeching into groundwater.

The current research aims to improve upon the proppants ability to remain suspended in solution using proppants grafted with water soluble polymers. Covalent attachment of the polymer to the proppant is suspected to increase suspension in aqueous solution as the water soluble chains are grafted to the surface and cannot separate from the substrate. Relatively low molecular weight PAM was investigated as to not promote flocculation of the proppants and to the limit volume of materials used. Materials of low cost were utilized so the process could be an industrially viable method for low cost enhanced fracking additives.

5.3 Experimental Section

Materials

All reagents were used as received from Fisher Scientific unless otherwise stated below. ACVA was purchased from Alfa Aesar and used without further purification. Acrylamide was obtained from Fluka and was recrystallized 3x in acetone prior to use. Syloid-244 was obtained from Syloid Silicas, average diameter ~ 5.5 µm. 3-Aminopropyldimethylethoxysilane were obtained from Gelest.

Instrumentation

NMR spectra were recorded on a Varian 400 spectrometer using $CDCl_3$ as a solvent. Transmittance measurements were taken on a Perkin-Elmer Lamda 4C UV/vis spectrophotometer. TGA characterization was conducted using a TA Instruments Q5000 with a heating rate of 10°C/min from 25°C to 800°C~1000°C under nitrogen flow. FT-IR spectra were recorded on a Perkin Elmer Spectrum 100 using an attenuated total reflection diamond cell attachment.

Synthesis of Activated 4,4'-Azobis(4-cyanovaleric acid)

To a 250 ml round bottom flask, a solution of 4,4'-azobis(4-cyanovaleric acid) (ACVA) (10 g, 35.7 mmol), 2-mercaptothiazoline (9.36g, 78.5 mmol), and N,N, dicyclohexylcarbodiimide (DCC) (16.2 g, 78.5mmol) in 100 ml dichloromethane was added. The solution was cooled to 0°C and flushed with N_2 for 15 min while stirring. Next a solution of 4-dimethylaminopyridine (436 mg, 3.57 mmol) in 10 ml dichloromethane was added dropwise to the ACVA solution over a period of 30 min. The reaction was then left to warm to room temperature and stirred for 6 hours. The solids were filtered and the resulting solution was concentrated in vacuum. The product was a yellow solid that was then purified by 3x recrystallization in ethanol (yield 13.1 g, 76%). MP: 123 - 124°C. ^{1}H NMR (400 MHz, $CDCl_3$): δ (ppm) 4.61 (t, J = 7.6 Hz, 4H), 3.56 – 3.20 (t, J = 7.4 Hz, 8H), 2.55 (m, 4H), 1.79 (d, J = 4.7 ,6H), ^{13}C NMR (400 MHz, $CDCl_3$): δ (ppm) 202, 172.3, 117.7, 72.1, 56.1, 34.1, 33.2, 28.5, 24.3. HRMS (PI-ESI) m/z: [M+H] Calcd for $C_{18}H_{22}N_6O_2S_4$ 483.0760; Found 483.0760.

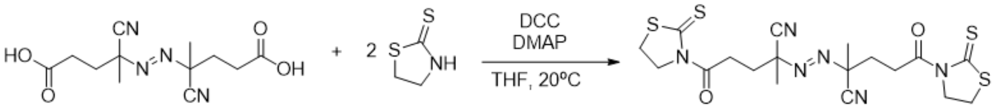

Scheme 5.1: Synthesis of activated 4,4’-azobis(4-cyaanovaleric acid)

Synthesis of Amine Functionalized Syloid

In a 250 ml round bottom flask, Syloid-244 silica particles (0.5 g) and 3-aminopropyldimethylethoxysilane (50µL, 0.27 mmol) were combined in 100 ml THF. The solution was refluxed overnight. The particle solution was allowed to cool to room temperature. The amine functionalized particles were recovered by centrifuging at 3,000 rpm for five minutes. The recovered particles where resuspended in THF. The recovery process was then repeated 2 more times. Next the particles were suspended in 100 ml THF for subsequent modification.

Synthesis of ACVA surface Functionalized Syloid

Amine functionalized Syloid-244 silica particles (0.5 g) in 100 ml THF were added to a 250 ml round bottom flask along with AACVA (100 mg, 0.21 mmol). The solution was stirred at room temperature overnight. The particles were recovered by centrifuging at 3,000 rpm for five minutes. The particles were dispersed back into THF and recovered two more times. The ACVA surface modified particles were then dried in vacuum overnight.

Synthesis of Polyacrylamide (PAM) Grafted Syloid

In a 1,000 ml 3-neck round bottom flask, ACVA functionalized Syloid-244 silica particles (0.5 g) were suspended in 600 ml DI water. The suspension was sparged with a large flow of N_2 for 30 minutes before adding acrylamide in varying amounts. The solution was heated to 80°C and stirred for 24 hours. The solution was allowed to cool to room temperature before recovering the PAM grafted particles by centrifuging at 3,000 rpm for five minutes. The particles were then suspended back into water and recovered two more times.

Transmittance measurements of Syloid solutions

Syloid (100 mg) was diluted into 20 ml water yielding a 5 mg/ml Syloid in water solution for each sample. Syloid loading of PAM grafted particles was determined through TGA analysis. For preparation of free PAM + bare Syloid solution, a portion of free polymer recovered from MHB2-205 was dried before combining the free polymer (25 wt%) and bare Syloid (100 mg) in 20 ml water to make the resulting Syloid + bare PAM solution. The samples were sonicated for 20 minutes before transferring an aliquot of each sample to a polystyrene cuvette. A lid was placed on the cuvette and sealed in place with parafilm. Transmittance at 300 nm was measured immediately (t = 0) then again at timed intervals for 100 hours.

5.4 Results and Discussion

Synthesis of Activated AVCA (AACVA)

The activated derivative of 4,4’-azobis(4-cyanovaleric acid) has been synthesized previously.[23–26] The product was obtained through a DCC coupling reaction between commercially available 4,4’-azobis(4-cyanovaleric acid) and two equivalents of 2-

mercaptothiazoline. The reaction did not require a column for purification as the product was recrystallized in ethanol. FT-IR analysis of the product showed the disappearance of the broad peak at approximately 3000 cm^{-1} indicative of OH stretching of carboxylic acids. Figure 5.2 compares FT-IR spectra of ACVA and activated ACVA. Proton and carbon NMR further confirmed the product by showing the addition of the mercaptothiazoline groups.

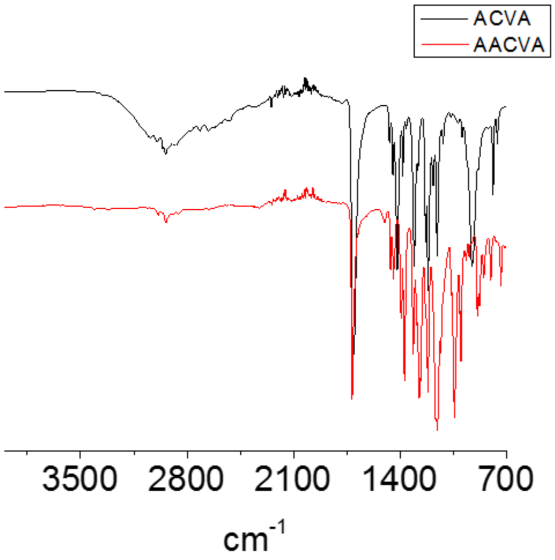

Figure 5.1: FT-IR spectra comparison of ACVA and activated ACVA (AACVA).

Synthesis of ACVA Surface Functionalized Syloid

It is now well established that silica surfaces can be amine functionalized using aminiosilane coupling reagents as long as the silica surface contains hydroxyl groups. The amount of amino groups that could be attached to Syloid-244 had not been previously studied. The use of symmetrically activated initiator introduced the possibility of bidentate bonding to the Syloid surface or crosslinking of particles. ACVA is not UV active therefore its concentration could not be determined by UV-vs spectroscopy. An investigation was performed using a UV active model compound to determine the maximum amount of groups that could be grafted to the Syloid surface. Aliquots of aminosilane coupling reagent were added to the particle surface before adding an excess of the known UV active compound CPDB. Attached CPDB was then quantified using UV-vis spectroscopy and a standard calibration curve. When the maximum amount of surface groups were implemented, the UV data showed a plateau in graft density vs added aminosilane. The plateau was found at 138 μmol/g. Amine functionalized particles were then synthesized to contain the maximum number of surface groups for this study. A large excess of AAVCA was added to the amine functionalized particles to prevent bidentate bonding or particle crosslinking. TGA analysis confirmed attachment of the initiator on the surface.

PAM Grafted Syloid

The number of ACVA molecules converted to PAM chains on the surface of the Syloid is dependent on initiator efficiency and the length of time the reaction is allowed to proceed. Unlike living polymerization, progress of free radical polymerization is dependent on the decomposition of initiator. The decomposition rate (k_d) of ACVA in water at 80°C is 9.0×10^{-5} making the half-life approximately 130 minutes.[27] The 24 hour reaction time allotted for the polymerization was ample for the decomposition of all the surface initiators. The polymerization process produced free polymer in solution in addition to the bound PAM. PAM grafted Syloid was isolated from free polymer by centrifuging the particles and washing 3x with water. It should be noted that the polymerization solution became very viscous at the conclusion of the reactions and the gelation of the solution could have inhibited later reaction progress.

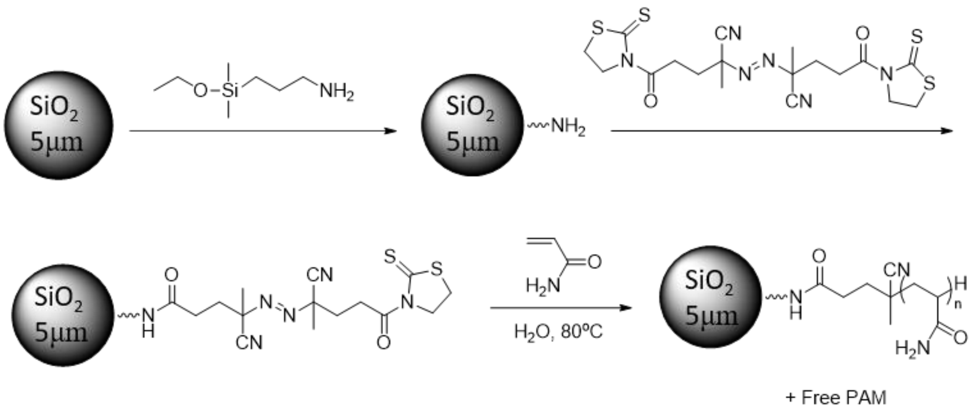

Scheme 5.2: Synthesis of PAM functionalized Syloid.

Three polymer grafted samples were investigated for their suspension charcteristics in aqueous solution and compared to bare Syloid. The feed ratio of monomer to initiator was varied for the three samples. Theoretically, the average molecular weight of the grafted polymer increases with increased monomer to initiator ratio. The monomer feed ratio for the three samples can be seen in Table 5.1. The PAM grafted particles were characterized via FT-IR and TGA. FT-IR spectra are shown in Figure 5.3. With addition of PAM to the substrate surface an increase in intensity of a sharp peak at 1700 cm^{-1} and a bread peak at 3400 cm^{-1} was observed, both indicative of the amide functional group.[28] The intensity of the peak was increased with increasing monomer feed ratio.

Table 5.1: Feed ratio of monomer to initiator and percent weight loss for the Syloid samples synthesized in this study.

Sample	Equivalents of acrylamide to initiator	% wt loss at 800°C
Bare Syloid	NA	3
Syloid-ACVA	NA	13
MHB2-198	204	12
MHB2-202	1019	28
MHB2-205	1631	35

TGA analysis determined the wt % of polymer on the Syloid surface by measuring weight loss at 800°C. TGA traces are shown in Figure 5.4 An increase in polymer weight was observed for samples as the monomer feed ratio increased. Comparison of MHB2-198 to Syloid-ACVA shows a decrease in weight % of surface groups, however initiator decomposition needs to be considered. FT-IR spectra showed the presence of amide functionality in MHB2-198. The sample most likely contained small oligomeric groups grafted to the surface. It should be noted that aqueous GPC is required for the molecular weight characterization of the PAM chains. An aqueous GPC was not accessible in house and external analysis was cost prohibitive.

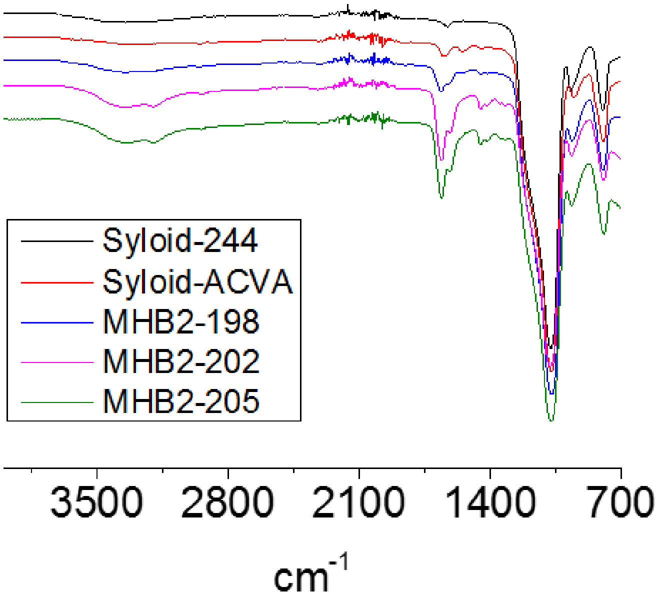

Figure 5.2: IR spectra of the synthesized surface modified Syloid particles.

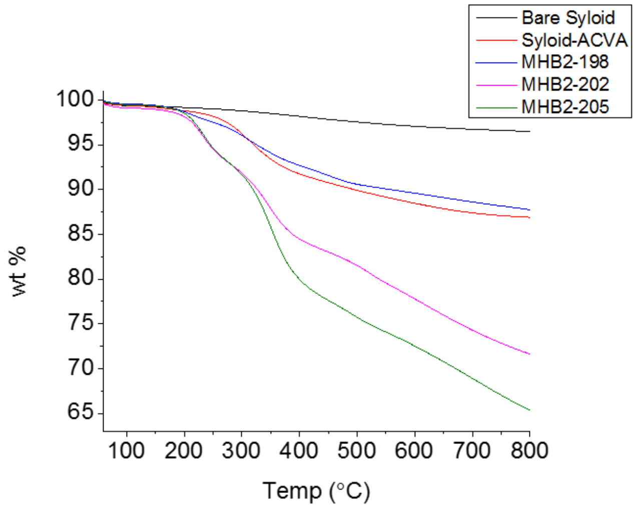

Figure 5.3: TGA traces showing weight loss for the grafted Syloid samples.

Suspendability of PAM Grafted Syloid

Initial tests determined that PAM grafted Syloid remained suspended in aqueous solution at longer durations of time than ungrafted Syloid. Figure 5.5 shows a picture of ungrafted Syloid suspensions and grafted Syloid suspensions. The photographs visually demonstrated the suspension times for the Syloid were enhanced with polymer grafting. The visual analysis was qualitative in nature and transmittance was used quantify and compare suspension times of the turbid Syloid suspensions. Comparisons were made between suspensions of bare Syloid, bare Syloid + free PAM, and three PAM grafted Syloid samples. The PAM grafted samples differed in wt% of PAM grafted to the surface. The samples were suspended in water at equal concentration of core Syloid and transmittance measurements were taken over a period of 100 hours. The bare Syloid suspension reached 100 % transmittance by the conclusion of the tests meaning all of the Syloid had settled out of solution. Comparisons of the slope of the remaining transmittance curves in Figure 5.6 demonstrates that PAM grafted samples were suspended longer than bare Syloid and Syloid solutions containing free PAM. The suspension time of the three PAM grafted samples correlated with the wt% of polymer present on the substrate surface.

Start

Day 4

Figure 5.4: Suspensions of Syloid-244 in water from left to right: PAM grafted Syloid + free PAM, PAM grafted Syloid, bare Syloid + free PAM, and bare Syloid.

.

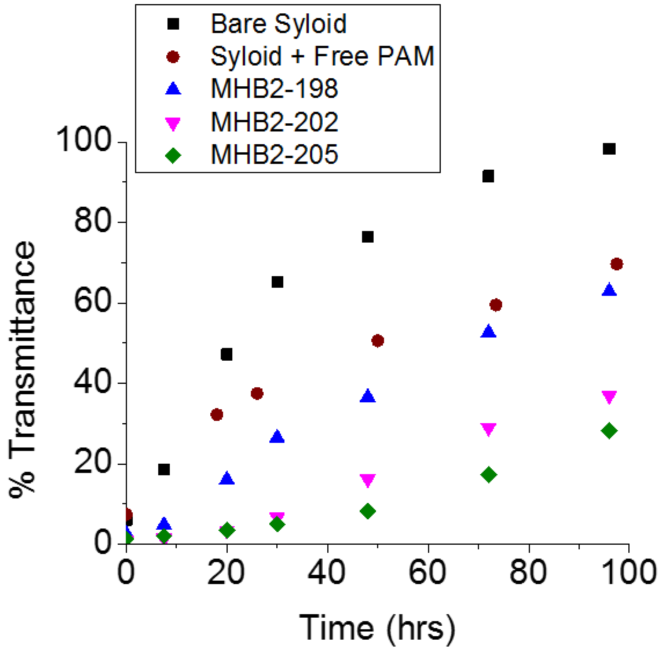

Figure 5.5: Transmittance of aqueous Syloid solutions over 100 hours.

Reusing the Free Polymer

The synthesis of PAM grafted particles produced free polymer in addition to the polymer grafted to the Syloid surface. The free polymer potentially contained an activated chain end as shown in Figure 5.7. The free polymer could potentially be used in a grafting-to approach with amine functionalized silica to produce PAM grafted Syloid. Attempts were made to reuse the free polymer, however surface PAM surface attachment was not successful. The aqueous conditions and elevated temperature of the PAM polymerization most likely hydrolyzed the activated acid end group back to a carboxylic acid.

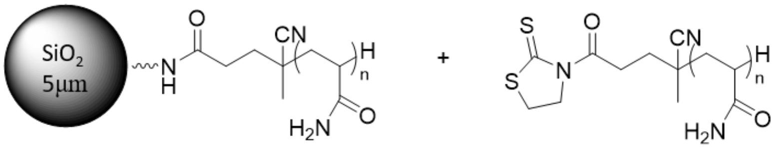

Figure 5.6: Grafted PAM and PAM free chains generated during polymerization reaction.

Future Work

The variety of available proppants requires surface initiated free radical polymerization to be explored beyond using silica as a substrate. Free radical initiators need to be synthesized for the attachment to metal oxides like bauxite and ceramics. Phosphates are a known to bond to metal oxide surfaces creating the robust metal oxygen phosphorus bond. A proposed synthesis for a phosphate containing free radical azo initiator is shown in Scheme 5.3. Investigation into the effectiveness of phosphate azo initiators from metal oxide surfaces in aqueous solutions will need to be explored.

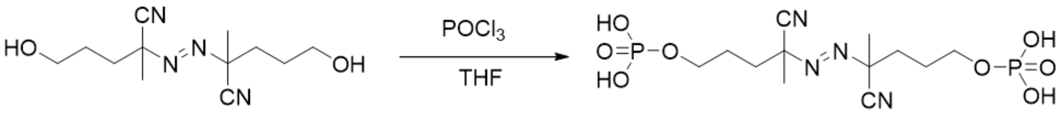

Scheme 5.8: Synthesis of phosphate azo free radical initiator.

The efficacy of the polymer grafted proppants will also need to be determined in drilling conditions. Measurements to determine the suspension, conductivity, and hydrocarbon yield compared to existing technology needs to be determined in real world conditions.

5.5 Conclusion

A surface initiated free radical polymerization in water was presented for the covalent grafting of polyacrylamide chains to commercial grade 5μm silica (Syloid) particles. The polymer grafted particles were successful in improving suspension times in water compared to untreated particles and particle solutions containing free PAM chains. An activated azo initiator was synthesized and grafted onto the Syloid surface. PAM was then grown from the Syloid surface along with free PAM in solution. The free PAM was recovered however it was discovered that the activated chain ends did not survive the reaction conditions and the free polymer could not be used for subsequent grafting-to reactions. The materials used were not cost prohibitive and were in laboratory experiments to offer improvements over existing technology.

5.6 Acknowledgement

This work was performed in collaboration with Anand Viswanath.

5.7 References

(1) Sovacool, B. K. *Renew. Sustain. Energy Rev.* **2014**, *37*, 249.

(2) Liang, F.; Sayed, M.; Al-Muntasheri, G. A.; Chang, F. F.; Li, L. *Petroleum* **2016**, *2* (1), 26.

(3) Sharma, M. M.; Gadde, P. B. In *SPE Annual Technical Conference and Exhibition*; Society of Petroleum Engineers, 2005; pp 1–12.

(4) Gu, M.; Dao, E.; Mohanty, K. K. *Fuel* **2015**, *150*, 191.

(5) Zoveidavianpoor, M.; Gharibi, A. *J. Nat. Gas Sci. Eng.* **2015**, *24*, 197.

(6) Kuru, E. A.; Orakdogen, N.; Okay, O. *Eur. Polym. J.* **2007**, *43* (7), 2913.

(7) Tanaka, H. *J. Polym. Sci. Part A Polym. Chem.* **1986**, *24* (1), 29.

(8) Mabire, F.; Audebert, R.; Quivoron, C. *Polymer (Guildf).* **1984**, *25* (9), 1317.

(9) Lin, H. R. *Eur. Polym. J.* **2001**, *37* (7), 1507.

(10) Chen, D.; Liu, X.; Yue, Y.; Zhang, W.; Wang, P. *Eur. Polym. J.* **2006**, *42* (6), 1284.

(11) Xiao, D.; Wirth, M. J. *Macromolecules* **2002**, *35*, 2919.

(12) Dainton, F. S.; Tordoff, M. *Trans. Faraday Soc.* **1956**, *53*, 499.

(13) Thomas, D. B.; Convertine, A. J.; Myrick, L. J.; Scales, C. W.; Smith, A. E.; Lowe, A. B.; Vasilieva, Y. a.; Ayres, N.; McCormick, C. L. *Macromolecules* **2004**, *37*, 8941.

(14) Sharma, B. R.; Dhuldhoya, N. C.; Merchant, U. C. *J. Polym. Environ.* **2006**, *14* (2), 195.

(15) Wisniewska, M. *Appl. Surf. Sci.* **2012**, *258* (7), 3094.

(16) Prucker, O.; Rühe, J. *Macromolecules* **1998**, *31* (3), 592.

(17) Huang, W.; Skanth, G.; Baker, G. L.; Bruening, M. L. *Langmuir* **2001**, *17* (5), 1731.

(18) Kincaid, K. P.; Snider, P. M.; Herring, M.; Mahoney, R. P.; Soane, D. In *SPE Hydraulic Fracturing Technology Conference*; Society of Petroleum Engineers, 2013; pp 1–12.

(19) Vengosh, A.; Jackson, R. B.; Warner, N.; Darrah, T. H.; Kondash, A. *Environ. Sci. Technol.* **2014**, *48* (15), 8334.

(20) Jacquet, J. B. *Environ. Sci. Technol.* **2014**, *48* (15), 8321.

(21) Burton, G. A.; Basu, N.; Ellis, B. R.; Kapo, K. E.; Entrekin, S.; Nadelhoffer, K. *Environ. Toxicol. Chem.* **2014**, *33* (8), 1679.

(22) Viswanath, A. Surface functionalization of inorganic substrates with polymeric ligands using RAFT polymerization, University of South Carolina, 2014.

(23) Jiangtao, T. P. X.; Cyrille, B.; Volga, B.; Davis. *J. Polym. Sci. Part A Polym. Chem.* **2009**, *47*, 4302.

(24) Hruby, M.; Subr, V.; Kucka, J.; Kozempel, J.; Lebeda, O.; Sikora, A. *Appl. Radiat. Isot.* **2005**, *63* (4), 423.

(25) Karir, T.; Sarma, H. D.; Samuel, G.; Hassan, P. A.; Padmanabhan, D.; Venkatesh, M. *J. Appl. Polym. Sci.* **2013**, *130* (2), 860.

(26) Šubr, V.; Koňák, Č.; Laga, R.; Ulbrich, K. *Biomacromolecules* **2006**, *7* (1), 122.

(27) *Polymer Handbook*, 4th ed.; Brandrup, J., Immergut, E. H., Grulke, E. A., Eds.; Wiley, 2003.

(28) Sivy, G. T.; Coleman, M. M. *Carbon N. Y.* **1981**, *19* (2), 137.

CHAPTER 6

CONCLUSION AND OUTLOOK

Multifunctional surface modified nanoparticles were synthesized, characterized and investigated for their property enhancements pertaining to dielectric breakdown strength. Surface modified microparticles were synthesized and characterized to determine suspendability in aqueous solution for fracking additives.

A one-pot synthetic strategy using click chemistry to simultaneously anchor two separate chemical populations to 15 nm silica nanoparticles was presented. RAFT polymerization was employed to synthesize well-defined alkyne terminated PGMA chains. Alkyne terminated terthiophene was synthesized in three synthetic steps while alkyne ferrocene was available from a commercial source. PGMA + a selected electroactive ligand, were simultaneously attached to the surface of an azide functionalized silica NP surface. The bimodal assembly of the surface functionalized particles was confirmed by FT-IR, UV-vis, and TGA. The particles were then incorporated into a commercial epoxy resin. The dispersion of the resultant composites was monitored by TEM. Dielectric characterization was performed using dielectric breakdown testing and dielectric spectroscopy. Analysis of the multifunctional nanoparticles demonstrated that having two functional ligand populations present (one for dispersion and one for trapping) on the nanoparticle surface was an effective means to improve upon dielectric breakdown strength of silica-epoxy composites by as much as 44% with only 2 wt% loading SiO_2. Variations in permittivity were observed depending on the trapping ligand chemistry.

Further investigation into the parameters that govern dielectric breakdown strength in composite materials was then performed. A grafting from strategy was used for surface initiated RAFT polymerization of PGMA from the surface of 15 nm silica nanoparticles. SI RAFT allowed for precise control of polymer graft density and molecular weight. By varying the graft density of polymer chains on the nanoparticle surface, control was achieved over the degree of nanoparticle dispersion in the epoxy matrix. It was found that increasing the polymer graft density generally resulted in decreased particle free space lengths or more dispersed particles. Dielectric breakdown strength was shown to improve with improved nanoparticle dispersion but demonstrated diminishing returns with free space lengths under 200 nm. Three activated short ligands were synthesized differing in electronic character. Thiophene, terthiophene, and anthracene were synthesized to contain activated acid groups for attachment to amine functionalized silica nanoparticles. Dielectric breakdown strength of composites containing the three ligands was measured at well-dispersed states. Excellent correlation was observed for calculated IE+EA values of the conjugated ligands and experimentally obtained composite DBS values. The correlation could prove useful for prediction of performance for future composite materials based on ligand chemistry. Mixed bimodal brushes containing poly(terthiopheneethyl methacrylate) short brushes and PGMA long brushes were explored for their impact on dielectric breakdown strength in epoxy resin. The results showed improvements in breakdown strength even at non-dispersed states leading to the hypothesis that the composite breakdown strength is also depended on charge trapping group concentration.

Based on the experimental results of this work, predictions can be made for surface chemistries that are effective at increasing composite dielectric breakdown strength beyond what was achieved in this study. The best performing surface chemistry in terms of improving dielectric breakdown strength was found to be the terthiophene trimer. The synthesis of the trimer species is expensive in terms of reagent cost and requires column chromatography at nearly every synthetic step. Quantum computation could be used to calculate IE+EA values of alternative polycyclic molecules that possesses equally low or lower IE+EA values at reduced costs. Investigation of free voltage stabilizers in LDPE showed that anthracene containing a nitro group improved dielectric breakdown strength by 1.65x that of the unsubstituted athracene. Perhaps further investigation of substituted anthracene molecules is warranted. Investigation into mixed bimodal brush grafted nanoparticles for nanodielectrics is an attractive avenue for the synthesis of dielectric nanocomposites. If trends from this work hold true, the bimodal brush system could show even further improvements at a well-dispersed state. Multiple monomers can be investigated for the short electroactive brush. Monomer selection can be determined by calculated values of IE+EA.

Surface modification of metal oxide nanoparticles for enhanced dielectrics was then investigated. TiO_2 nanoparticles were made compatible with a commercial silicone matrix using a bimodal population of PDMS chains. PDMS chains were obtained from a commercial supplier and end functionalized with phosphate moieties for grafting to the particle surface. Two species of anthracene phosphonic acids were synthesized differing in substitution at the 10 position. 9-anthracenemethyl phosphonic acid and 10-bromo-9-anthracenemethyl phosphonic acid were synthesized and attached to the PDMS-TiO_2 nanoparticles. Well-dispersed PDMS-TiO_2 samples did not show DBS improvements compared to neat silicone. PDMS-anthracene-TiO_2 samples improved breakdown strength by 9% compared to neat silicone at 2 wt% TiO_2. Addition of electron withdrawing bromine to the 10 position of the anthracene ligand had little effect on overall composite dielectric breakdown strength compared to PDMS-anthracene-TiO_2 samples. Investigation of filler concentration showed 2-4 wt% TiO_2 to be optimal for DBS enhancements. A novel phosphate containing trithiocarbonate RAFT agent was synthesized and attached to the surface of zirconia nanoparticles. The RAFT agent was tested for SI RAFT polymerization. Kinetic studies for the SI RAFT polymerization of MMA from 4 nm ZrO_2 nanoparticles demonstrated that polymerization was not well controlled with the synthesized RAFT agent.

Surface modified hydrolytic fracturing proppants were explored where polyacrylamide was covalently bound to a 5µm silica substrate via surface initiated free radical polymerization in water. The polymer grafted proppants were shown to suspend in water longer than proppants without surface modification. Correlation of wt% of polymer present on the substrate surface with suspension time was also observed. Because of the success of laboratory scale experiments and the low cost of materials the presented methodology may be viable for industrial fracking operations.

Further investigation of the synthesized fracking proppants is required where the proppants are tested in complete blends of fracking fluid additives. The additives package will generally include biocides, salts, and acid additives. The additional compounds or variations in pH of the solution could be problematic to the stability of the PAM grafted Syloid. Laboratory scale experiments should be performed to study the effects of said additives on PAM grafted Syloids. Because the proposed process produces a large amount of free polymer, a process should be developed that can reuse the free polymer generated. Separation of the free polymer is easy on a laboratory scale; however industrial process will need to be equipped for large scale separation as well as application for the recovered polymer. Post polymerization modification of the recovered polymer chain ends could be explored. If successful, the recovered polymer could be used in a grafting-to synthesis to the Syloid surface. The efficacy of such a process will need to be explored since the obtainable polymer graft density will theoretically be much lower for PAM grafted particles using the grafting-to approach.

Finally, the synthetic methodologies performed in this thesis could be could be applied to applications beyond nanodielectrics and fracking additives. Thermoresponsive, photoresponsive, and, pH responsive applications can be imagined from the implementation of multifunctional grafted nanoparticles at well dispersed states with functional ligands that impart novel functionality.

BIBLIOGRAPHY

(1) Schadler, L. S.; Kumar, S. K.; Benicewicz, B. C.; Lewis, S. L.; Harton, S. E. *MRS Bull.* **2007**, *32* (04), 335.

(2) Winey, K. I.; Vaia, R. A. *MRS Bull.* **2007**, *32* (04), 314.

(3) Hule, R. A.; Pochan, D. J. *MRS Bull.* **2007**, *32* (04), 354.

(4) Krishnamoorti, R. *MRS Bull.* **2007**, *32* (04), 341.

(5) Baur, J.; Silverman, E. *MRS Bull.* **2007**, *32* (04), 328.

(6) Li, Y.; Krentz, T. M.; Wang, L.; Benicewicz, B. C.; Schadler, L. S. *ACS Appl. Mater. Interfaces* **2014**, *6* (9), 6005.

(7) Nelson, J. K.; Hu, Y. *J. Phys. D. Appl. Phys.* **2005**, *38* (2), 213.

(8) Sunday, D.; Ilavsky, J.; Green, D. L. *Macromolecules* **2012**, *45* (9), 4007.

(9) Maillard, D.; Kumar, S. K.; Rungta, A.; Benicewicz, B. C.; Prud'Homme, R. E. *Nano Lett.* **2011**, *11* (11), 4569.

(10) Kumar, S. K.; Jouault, N.; Benicewicz, B.; Neely, T. *Macromolecules* **2013**, *46* (9), 3199.

(11) Akcora, P.; Liu, H.; Kumar, S. K.; Moll, J.; Li, Y.; Benicewicz, B. C.; Schadler, L. S.; Acehan, D.; Panagiotopoulos, A. Z.; Pryamitsyn, V.; Ganesan, V.; Ilavsky, J.; Thiyagarajan, P.; Colby, R. H.; Douglas, J. F. *Nat. Mater.* **2009**, *8* (4), 354.

(12) Natarajan, B.; Neely, T.; Rungta, A.; Benicewicz, B. C.; Schadler, L. S. *Macromolecules* **2013**, *46* (12), 4909.

(13) Rungta, A.; Natarajan, B.; Neely, T.; Dukes, D.; Schadler, L. S.; Benicewicz, B. C. *Macromolecules* **2012**, *45* (23), 9303.

(14) Yan, J.; Kristufek, T.; Schmitt, M.; Wang, Z.; Xie, G.; Dang, A.; Hui, C. M.; Pietrasik, J.; Bockstaller, M. R.; Matyjaszewski, K. *Macromolecules* **2015**, *48* (22), 8208.

(15) Li, Y.; Tao, P.; Viswanath, A.; Benicewicz, B. C.; Schadler, L. S. *Langmuir* **2013**, *29* (4), 1211.

(16) Li, Y.; Wang, L.; Natarajan, B.; Tao, P.; Benicewicz, B. C.; Ullal, C.; Schadler, L. S. *RSC Adv.* **2015**, *5* (19), 14788.

(17) Qiao, Y.; Yin, X.; Wang, L.; Islam, M. S.; Benicewicz, B. C.; Ploehn, H. J.; Tang, C. *Macromolecules* **2015**, *48* (24), 8998.

(18) Sidorenko, A.; Minko, S.; Schenk-Meuser, K.; Duschner, H.; Stamm, M. *Langmuir* **1999**, *15* (24), 8349.

(19) Feng, J.; Haasch, R. T.; Dyer, D. J. *Macromolecules* **2004**, *37* (25), 9525.

(20) Zhao, B.; Zhu, L. *Macromolecules* **2009**, *42* (24), 9369.

(21) Zhao, B. *Polymer (Guildf).* **2003**, *44* (15), 4079.

(22) Zhao, B.; He, T. *Macromolecules* **2003**, *36* (23), 8599.

(23) Li, Y.; Tao, P.; Siegel, R. W.; Schadler, L. S. *MRS Proc.* **2013**, *1547*, 161.

(24) Wang, L.; Benicewicz, B. C. *ACS Macro Lett.* **2013**, *2* (2), 173.

(25) Krentz, T. M.; Huang, Y.; Nelson, J. K.; Schadler, L. S.; Bell, M.; Benicewicz, B. *2014 Annu. Rep. Conf. Electr. Insul. Dielectr. Phenom.* **2014**, 643.

(26) Huang, Y.; Krentz, T. M.; Nelson, J. K.; Schadler, L. S.; Bell, M.; Benicewicz, B. In *2015 IEEE Electrical Insulation Conference (EIC)*; IEEE: Seattle, WA, 2015;

pp 325–328.

(27) Virtanen, S.; Krentz, T.; Nelson, J.; Schadler, L.; Bell, M.; Benicewicz, B.; Hillborg, H.; Zhao, S. *IEEE Trans. Dielectr. Electr. Insul.* **2014**, *21* (2), 563.

(28) Tripp, C. P.; Hair, M. L. *J. Phys. Chem.* **1993**, *97* (21), 5693.

(29) Wang, Y.; Hu, S.; Brittain, W. J. *Macromolecules* **2006**, *39* (17), 5675.

(30) Fadeev, A. Y.; McCarthy, T. J. *Langmuir* **2000**, *16* (18), 7268.

(31) Ranjan, R.; Brittain, W. J. *Macromolecules* **2007**, *40* (17), 6217.

(32) Ata, M. S.; Liu, Y.; Zhitomirsky, I. *RSC Adv.* **2014**, *4* (43), 22716.

(33) Boyer, C.; Bulmus, V.; Priyanto, P.; Teoh, W. Y.; Amal, R.; Davis, T. P. *J. Mater. Chem.* **2009**, *19* (1), 111.

(34) Bulusu, A.; Paniagua, S. A.; Macleod, B. A.; Sigdel, A. K.; Berry, J. J.; Olson, D. C.; Marder, S. R.; Graham, S. *Langmuir* **2013**, *29* (12), 3935.

(35) Dong, H.; Huang, J.; Koepsel, R. R.; Ye, P.; Russell, A. J.; Matyjaszewski, K. *Biomacromolecules* **2011**, *12* (4), 1305.

(36) Hotchkiss, P. J.; Jones, S. C.; Paniagua, S. a; Sharma, A.; Kippelen, B.; Armstrong, N. R.; Marder, S. R. *Acc. Chem. Res.* **2012**, *45* (3), 337.

(37) Koh, S. E.; McDonald, K. D.; Holt, D. H.; Dulcey, C. S.; Chaney, J. a; Pehrsson, P. E. *Langmuir* **2006**, *22* (14), 6249.

(38) Mutin, P. H.; Guerrero, G.; Vioux, A. *J. Mater. Chem.* **2005**, *15* (35-36), 3761.

(39) Neouze, M.-A.; Schubert, U. *Monatshefte für Chemie - Chem. Mon.* **2008**, *139* (3), 183.

(40) Tahir, M. N.; Eberhardt, M.; Theato, P.; Faiß, S.; Janshoff, A.; Gorelik, T.; Kolb, U.; Tremel, W. *Angew. Chemie - Int. Ed.* **2006**, *45* (6), 908.

(41) Thissen, P.; Valtiner, M.; Grundmeier, G. *Langmuir* **2010**, *26* (1), 156.

(42) Ulman, A. *Chem. Rev.* **1996**, *96* (4), 1533.

(43) Silverman, B. M.; Wieghaus, K. A.; Schwartz, J. *Langmuir* **2005**, *21* (1), 225.

(44) Brinker, C. J.; Scherer, G. W. *Sol-Gel Science: The Physics and Chemistry of Sol-Gel Processing*; Academic Press: New York, 3013.

(45) Boyer, C.; Stenzel, M. H.; Davis, T. P. *J. Polym. Sci. Part A Polym. Chem.* **2011**, *49* (3), 551.

(46) Dukes, D.; Li, Y.; Lewis, S.; Benicewicz, B.; Schadler, L.; Kumar, S. K. *Macromolecules* **2010**, *43* (3), 1564.

(47) Barbey, R.; Lavanant, L.; Paripovic, D.; Schuwer, N.; Sugnaux, C.; Tugulu, S.; Klok, H.-A. *Chem. Rev.* **2009**, *109* (Copyright (C) 2012 American Chemical Society (ACS). All Rights Reserved.), 5437.

(48) Solomon, D. H.; Rizzardo, E.; Cacioli, P. Polymerization process and polymers produced thereby. US4581429, April 1986.

(49) Wang, J. S.; Matyjaszewski, K. *J. Am. Chem. Soc.* **1995**, *117* (6), 5614.

(50) Chiefari, J.; Chong, Y. K. B.; Ercole, F.; Krstina, J.; Jeffery, J.; Le, T. P. T.; Mayadunne, R. T. A.; Meijs, G. F.; Moad, C. L.; Moad, G.; Rizzardo, E.; Thang, S. H.; South, C. *Macromolecules* **1998**, *31* (16), 5559.

(51) Odian, G. *Radical Chain Polymerization*, Fourth Ed.; John Wiley & Sons, Inc.: Hoboken, NJ, USA, 2004.

(52) Fukuda, T.; Terauchi, T.; Goto, A.; Tsujii, Y.; Miyamoto, T.; Shimizu, Y. *Macromolecules* **1996**, *29* (8), 3050.

(53) Matyjaszewski, K.; Tsarevsky, N. V. *Nat. Chem.* **2009**, *1* (4), 276.

(54) Greszta, D.; Mardare, D.; Matyjaszewski, K. *Macromolecules* **1994**, *27*, 638.

(55) Catala, J. M.; Bubel, F.; Ouland Hammouch, S. *Macromolecules* **1995**, *28*, 8441.

(56) Georges, M. K.; Veregin, R. P. N.; Kazmaier, P. M.; Hamer, G. K. *Macromolecules* **1993**, *26* (11), 2987.

(57) Moad, G.; Rizzardo, E. *Macromolecules* **1995**, *28,* 8722.

(58) Rizzardo, E.; Serelis, A.; Solomon, D. *Aust. J. Chem.* **1982**, *35* (10), 2013.

(59) Hawker, C. J.; Bosman, A. W.; Harth, E. *Chem. Rev.* **2001**, *101* (12), 3661.

(60) Guillaneuf, Y.; Gigmes, D.; Marque, S. R. A.; Astolfi, P.; Greci, L.; Tordo, P.; Bertin, D. *Macromolecules* **2007**, *40* (9), 3108.

(61) Couvreur, L.; Lefay, C.; Belleney, J.; Charleux, B.; Guerret, O.; Magnet, S. *Macromolecules* **2003**, *36* (22), 8260.

(62) Nicolas, J.; Charleux, B.; Guerret, O.; Magnet, S. *Angew. Chemie* **2004**, *116* (45), 6312.

(63) Chong, Y. K.; Ercole, F.; Moad, G.; Rizzardo, E.; Thang, S. H.; Anderson, A. G. *Macromolecules* **1999**, *32* (21), 6895.

(64) Bartholome, C.; Beyou, E.; Bourgeat-Lami, E.; Chaumont, P.; Lefebvre, F.; Zydowicz, N. *Macromolecules* **2005**, *38* (4), 1099.

(65) Bartholome, C.; Beyou, E.; Bourgeat-Lami, E.; Chaumont, P.; Zydowicz, N. *Polymer (Guildf).* **2005**, *46* (19 SPEC. ISS.), 8502.

(66) Brinks, M. K.; Studer, A. *Macromol. Rapid Commun.* **2009**, *30* (13), 1043.

(67) Chevigny, C.; Gigmes, D.; Bertin, D.; Jestin, J.; Boué, F. *Soft Matter* **2009**, *5* (19), 3741.

(68) Konn, C.; Morel, F.; Beyou, E.; Chaumont, P.; Bourgeat-Lami, E. *Macromol.*

Symp. **2007**, *40*, 7464.

(69) Sill, K.; Emrick, T. *Chem. Mater.* **2004**, *16* (7), 1240.

(70) Husseman, M.; Malmstrom, E. E.; McNamara, M.; Mate, M.; Mecerreyes, D.; Benoit, D. G.; Hedrick, J. L.; Mansky, P.; Huang, E.; Russell, T. P.; Hawker, C. J. *Macromolecules* **1999**, *32* (5), 1424.

(71) Colombani, D. *Prog. Polym. Sci.* **1997**, *22* (8), 1649.

(72) Fristrup, C. J.; Jankova, K.; Hvilsted, S. *Soft Matter* **2009**, *5* (23), 4623.

(73) Singh, N.; Wang, J.; Ulbricht, M.; Wickramasinghe, S. R.; Husson, S. M. *J. Memb. Sci.* **2008**, *309* (1-2), 64.

(74) Marutani, E.; Yamamoto, S.; Ninjbadgar, T.; Tsujii, Y.; Fukuda, T.; Takano, M. *Polymer (Guildf).* **2004**, *45* (7), 2231.

(75) Chen, R.; Feng, W.; Zhu, S.; Botton, G.; Ong, B.; Wu, Y. *J. Polym. Sci. Part A Polym. Chem.* **2006**, *44* (3), 1252.

(76) Yang, W. J.; Neoh, K.-G.; Kang, E.-T.; Lee, S. S. C.; Teo, S. L.-M.; Rittschof, D. *Biofouling* **2012**, *28* (9), 895.

(77) Lee, S. H.; Dreyer, D. R.; An, J.; Velamakanni, A.; Piner, R. D.; Park, S.; Zhu, Y.; Kim, S. O.; Bielawski, C. W.; Ruoff, R. S. *Macromol. Rapid Commun.* **2010**, *31* (3), 281.

(78) Morandi, G.; Heath, L.; Thielemans, W. *Langmuir* **2009**, *25* (14), 8280.

(79) Sun, Y.; Ding, X.; Zheng, Z.; Cheng, X.; Hu, X.; Peng, Y. *Eur. Polym. J.* **2007**, *43* (3), 762.

(80) Keddie, D. J.; Moad, G.; Rizzardo, E.; Thang, S. H. *Macromolecules* **2012**, *45* (13), 5321.

(81) Moad, G.; Rizzardo, E.; Thang, S. H. *Aust. J. Chem.* **2005**, *58* (6), 379.

(82) Moad, G.; Rizzardo, E.; Thang, S. H. *Aust. J. Chem.* **2009**, *62* (11), 1402.

(83) Moad, G.; Rizzardo, E.; Thang, S. H. *Aust. J. Chem.* **2006**, *59* (10), 669.

(84) Zhu, M. Q.; Wang, L. Q.; Exarhos, G. J.; Li, A. D. Q. *J. Am. Chem. Soc.* **2004**, *126* (9), 2656.

(85) Yusa, S. I.; Fukuda, K.; Yamamoto, T.; Iwasaki, Y.; Watanabe, A.; Akiyoshi, K.; Morishima, Y. *Langmuir* **2007**, *23* (26), 12842.

(86) Boyer, C.; Whittaker, M. R.; Luzon, M.; Davis, T. P. *Macromolecules* **2009**, *42* (18), 6917.

(87) Hotchkiss, J. W.; Lowe, A. B.; Boyes, S. G. *Chem. Mater.* **2007**, *19* (1), 6.

(88) Fustin, C.-A.; Colard, C.; Filali, M.; Guillet, P.; Duwez, A.; Meier, M. A. R.; Schubert, U. S.; Gohy, J.-F. *Langmuir* **2006**, *22* (15), 6690.

(89) Aqil, A.; Qiu, H.; Greisch, J.-F.; Jérôme, R.; De Pauw, E.; Jérôme, C. *Polymer (Guildf).* **2008**, *49* (5), 1145.

(90) Kim, S.; Yoo, M.; Kang, N.; Moon, B.; Kim, B. J.; Choi, S. H.; Kim, J. U.; Bang, J. *ACS Appl. Mater. Interfaces* **2013**, *5* (12), 5659.

(91) Jiao, Y.; Chou, T.; Akcora, P. *Macromolecules* **2015**, *48* (14), 4910.

(92) Liang, M.; Lin, I.-C.; Whittaker, M. R.; Minchin, R. F.; Monteiro, M. J.; Toth, I. *ACS Nano* **2010**, *4* (1), 403.

(93) Zhu, L.; Yang, Y.; Farquhar, K.; Wang, J.; Tian, C.; Ranville, J.; Boyes, S. G. *ACS Appl. Mater. Interfaces* **2016**, *8* (7), 5040.

(94) Tao, P.; Viswanath, A.; Schadler, L. S.; Benicewicz, B. C.; Siegel, R. W. *ACS Appl. Mater. Interfaces* **2011**, *3* (9), 3638.

(95) Zhang, Y.; Luo, S.; Liu, S. *Macromolecules* **2005**, *38* (23), 9813.

(96) Li, C.; Benicewicz, B. C. *Macromolecules* **2005**, *38*, 5929.

(97) Li, C.; Han, J.; Ryu, C. Y.; Benicewicz, B. C. *Macromolecules* **2006**, *39* (9), 3175.

(98) Seitz, F. *Phys. Rev.* **1948**, *73* (6), 549.

(99) Seitz, F. *Phys. Rev* **1949**, *76* (9), 1376.

(100) Sparks, M.; Mills, D. L.; Warren, R.; Holstein, T.; Maradudin, A. A.; Sham, L. J.; Loh, E.; King, D. F. *Phys. Rev. B* **1981**, *24* (6), 3519.

(101) Brandstetter, S. S.; Drummy, L. F.; Horwath, J. C.; Schweickart, D. L.; Vaia, R. A. In *2008 IEEE International Power Modulators and High-Voltage Conference*; IEEE, 2008; pp 287–290.

(102) Tomer, V.; Manias, E.; Randall, C. A. *J. Appl. Phys.* **2011**, *110* (4), 0.

(103) Tomer, V.; Polizos, G.; Manias, E.; Randall, C. A. *J. Appl. Phys.* **2010**, *108* (7).

(104) Tomer, V.; Polizos, G.; Randall, C. A.; Manias, E. *J. Appl. Phys.* **2011**, *109* (7).

(105) Imai, T.; Sawa, F.; Nakano, T.; Ozaki, T.; Shimizu, T.; Kozako, M.; Tanaka, T. *IEEE Trans. Dielectr. Electr. Insul.* **2006**, *13* (2), 319.

(106) Tanaka, T.; Kozako, M.; Fuse, N.; Ohki, Y. *IEEE Trans. Dielectr. Electr. Insul.* **2005**, *12* (4), 669.

(107) Ma, D.; Hugener, T. a; Siegel, R. W.; Christerson, A.; Mårtensson, E.; Önneby, C.; Schadler, L. S. *Nanotechnology* **2005**, *16* (6), 724.

(108) Smith, R. C.; Liang, C.; Landry, M.; Nelson, J. K.; Schadler, L. S. *IEEE Trans. Dielectr. Electr. Insul.* **2008**, *15* (1), 187.

(109) Roy, M.; Nelson, J. K.; MacCrone, R. K.; Schadler, L. S.; Reed, C. W.; Keefe, R.; Zenger, W. *IEEE Trans. Dielectr. Electr. Insul.* **2005**, *12* (4), 629.

(110) Roy, M.; Nelson, J. K.; MacCrone, R. K.; Schadler, L. S. *J. Mater. Sci.* **2007**, *42* (11), 3789.

(111) Gao, M.; Zhang, P.; Wang, F.; Li, L.; Li, Z. In *2013 Annual Report Conference on Electrical Insulation and Dielectric Phenomena*; IEEE, 2013; pp 234–237.

(112) Tkalya, E.; Ghislandi, M.; Otten, R.; Lotya, M.; Alekseev, A.; Van Der Schoot, P.; Coleman, J.; De With, G.; Koning, C. *ACS Appl. Mater. Interfaces* **2014**, *6* (17), 15113.

(113) Grabowski, C. a.; Fillery, S. P.; Westing, N. M.; Chi, C.; Meth, J. S.; Durstock, M. F.; Vaia, R. a. *ACS Appl. Mater. Interfaces* **2013**, *5* (12), 5486.

(114) Tan, D.; Cao, Y.; Tuncer, E.; Irwin, P. *Mater. Sci. Appl.* **2013**, *4* (April), 6.

(115) Kim, P.; Jones, S. C.; Hotchkiss, P. J.; Haddock, J. N.; Kippelen, B.; Marder, S. R.; Perry, J. W. *Adv. Mater.* **2007**, *19* (7), 1001.

(116) Lewis, T. J. *IEEE Trans. Dielectr. Electr. Insul.* **1994**, *1* (5), 812.

(117) Rytoluoto, I.; Lahti, K.; Karttunen, M.; Koponen, M.; Virtanen, S.; Pettersson, M. In *2014 IEEE Conference on Electrical Insulation and Dielectric Phenomena (CEIDP)*; IEEE, 2014; pp 655–658.

(118) Tanaka, T. *IEEE Trans. Dielectr. Electr. Insul.* **2005**, *12* (5), 914.

(119) Lu, J.; Wong, C. P. *PORTABLE-POLYTRONIC 2008 - 2nd IEEE Int. Interdiscip. Conf. Portable Inf. Devices 2008 7th IEEE Conf. Polym. Adhes. Microelectron. Photonics* **2008**, 1.

(120) Payne, A. R. *J. Appl. Polym. Sci.* **1965**, *9* (6), 2273.

(121) Schuman, T. P.; Siddabattuni, S.; Cox, O.; Dogan, F. *Compos. Interfaces* **2010**, *17* (8), 719.

(122) Siddabattuni, S.; Schuman, T. P.; Dogan, F. *ACS Appl. Mater. Interfaces* **2013**, *5* (6), 1917.

(123) Ganesh, V.; Sudhir, V. S.; Kundu, T.; Chandrasekaran, S. *Chem. - An Asian J.* **2011**, *6* (10), 2670.

(124) White, M. A.; Maliakal, A.; Turro, N. J.; Koberstein, J. *Macromol. Rapid Commun.* **2008**, *29* (18), 1544.

(125) Li, N.; Binder, W. H. *J. Mater. Chem.* **2011**, *21* (42), 16717.

(126) Mansfeld, U.; Pietsch, C.; Hoogenboom, R.; Becer, C. R.; Schubert, U. S. *Polym. Chem.* **2010**, *1* (10), 1560.

(127) Li, Y.; Benicewicz, B. C. *Macromolecules* **2008**, *41* (21), 7986.

(128) Li, D.; Zhu, J.; Cheng, Z.; Zhang, W.; Zhu, X. *React. Funct. Polym.* **2009**, *69* (4), 240.

(129) Ranjan, R.; Brittain, W. J. *Macromol. Rapid Commun.* **2007**, *28* (21), 2084.

(130) Ebbesen, M. F.; Schaffert, D. H.; Crowley, M. L.; Oupický, D.; Howard, K. A. *J. Polym. Sci. Part A Polym. Chem.* **2013**, *51* (23), 5091.

(131) Quémener, D.; Davis, T. P.; Barner-Kowollik, C.; Stenzel, M. H. *Chem. Commun. (Camb).* **2006**, No. 48, 5051.

(132) Amblard, F.; Cho, J. H.; Schinazi, R. F. *Chem. Rev.* **2009**, *109* (9), 4207.

(133) Li, W.; Yamamoto, Y.; Fukushima, T. *J. Am. Chem. Soc.* **2008**, *130*, 8886.

(134) Ball, I. D. L. *Proc. IEE - Part I Gen.* **1951**, *98* (110), 84.

(135) Fava, R. A. *Proc. Inst. Electr. Eng.* **1965**, *112* (4), 819.

(136) Gao, J.; Li, J.; Benicewicz, B. C.; Zhao, S.; Hillborg, H.; Schadler, L. S. *Polymers (Basel).* **2012**, *4* (1), 187.

(137) Li, Y. Combining raft polymerization and click chemistry to prepare functionalized polymers and nanoparticles, PhD Thesis, Rensselaer Polytechnic Institute, 2008.

(138) Viswanath, A. Surface functionalization of inorganic substrates with polymeric ligands using RAFT polymerization, PhD Thesis, University of South Carolina, 2014.

(139) Lieber, E.; Rao, C. N. R.; Chao, T. S.; Hoffman, C. W. W. *Anal. Chem.* **1957**, *29* (6), 916.

(140) Ligoure, C.; Leibler, L. *J. Phys.* **1990**, *51* (12), 1313.

(141) Mobaraki, N.; Hemmateenejad, B. *Chemom. Intell. Lab. Syst.* **2011**, *109* (2), 171.

(142) Bird, D. W.; Pelzer, H. *Proc. IEE - Part I Gen.* **1949**, *96* (97), 44.

(143) Takala, M.; Ranta, H.; Nevalainen, P.; Pakonen, P.; Pelto, J.; Karttunen, M.; Virtanen, S.; Koivu, V.; Pettersson, M.; Sonerud, B.; Kannus, K. *IEEE Trans. Dielectr. Electr. Insul.* **2010**, *17* (4), 1259.

(144) Kochetov, R.; Tsekmes, I. A.; Chmura, L. A.; Morshuis, P. H. F.; Iizuka, T.; Tatsumi, K.; Tanaka, T. In *2014 IEEE Conference on Electrical Insulation and Dielectric Phenomena (CEIDP)*; IEEE, 2014; pp 715–718.

(145) Johari, G. P. *Chemistry and Technology of Epoxy Resins*; Ellis, B., Ed.; Springer Netherlands: Dordrecht, 1993.

(146) Cheng, L.; Zheng, L.; Li, G.; Zeng, J.; Yin, Q. *Phys. B Condens. Matter* **2008**, *403* (17), 2584.

(147) Barber, P.; Balasubramanian, S.; Anguchamy, Y.; Gong, S.; Wibowo, A.; Gao, H.; Ploehn, H. J.; zur Loye, H.-C. *Materials (Basel).* **2009**, *2* (4), 1697.

(148) Nelson, J. K. *Dielectric Polymer Nanocomposites*; Nelson, J. K., Ed.; Springer Science & Business Media, 2009.

(149) Tanaka, T.; Montanari, G. C.; Mulhaupt, R. *IEEE Trans. Dielectr. Electr. Insul.* **2004**, *11* (5), 763.

(150) Nelson, J. K.; Huang, Y.; Krentz, T. M.; Schadler, L. S.; Benicewicz, B. C.; Bell, M. *2015 IEEE 11th Int. Conf. Prop. Appl. Dielectr. Mater.* **2015**, 40.

(151) Nelson, J. K.; Fothergill, J. C. *Nanotechnology* **2004**, *15* (5), 586.

(152) Chong, B. Y. K.; Krstina, J.; Le, T. P. T.; Moad, G.; Postma, A.; Rizzardo, E.; Thang, S. H. *Macromolecules* **2003**, *36* (7), 2256.

(153) Yamano, Y. *IEEE Trans. Dielectr. Electr. Insul.* **2006**, *13* (4), 773.

(154) Yamano, Y.; Endoh, H. *IEEE Trans. Dielectr. Electr. Insul.* **1998**, *5* (2), 270.

(155) Hanley, T. L.; Burford, R. P.; Fleming, R. J.; Barber, K. W. *IEEE Electr. Insul. Mag.* **2003**, *19* (1), 13.

(156) Sengupta, S. S.; Person, T. J.; Caronia, P. J. In *2010 IEEE International Symposium on Electrical Insulation*; IEEE, 2010; pp 1–6.

(157) Zhang, H.; Shang, Y.; Wang, X.; Zhao, H.; Han, B.; Li, Z. *J. Mol. Model.* **2013**, *19* (12), 5429.

(158) Du, Y.; Lv, Y.; Li, C.; Chen, M.; Zhou, J.; Li, X.; Zhou, Y.; Tu, Y. *J. Appl. Phys.* **2011**, *110* (10), 2.

(159) Champion, J. V; Dodd, S. J.; Stevens, G. C. *J. Phys. D. Appl. Phys.* **1994**, *27* (3), 604.

(160) O'dwyer, J. *J. Phys. Chem. Solids* **1967**, *28* (7), 1137.

(161) Sun, Y.; Boggs, S. A.; Ramprasad, R. In *2014 IEEE Conference on Electrical*

Insulation and Dielectric Phenomena (CEIDP); IEEE, 2014; pp 15–18.

(162) Qiao, Y.; Islam, M. S.; Han, K.; Leonhardt, E.; Zhang, J.; Wang, Q.; Ploehn, H. J.; Tang, C. *Adv. Funct. Mater.* **2013**, *23* (45), 5638.

(163) Qiao, Y.; Islam, M. S.; Wang, L.; Yan, Y.; Zhang, J.; Benicewicz, B. C.; Ploehn, H. J.; Tang, C. *Chem. Mater.* **2014**, *26* (18), 5319.

(164) Kuo, D. H.; Chang, C. C.; Su, T. Y.; Wang, W. K.; Lin, B. Y. *Mater. Chem. Phys.* **2004**, *85* (1), 201.

(165) Dou, X.; Liu, X.; Zhang, Y.; Feng, H.; Chen, J. F.; Du, S. *Appl. Phys. Lett.* **2009**, *95* (13), 132904.

(166) Kim, P.; Doss, N. M.; Tillotson, J. P.; Hotchkiss, P. J.; Pan, M. J.; Marder, S. R.; Li, J.; Calame, J. P.; Perry, J. W. *ACS Nano* **2009**, *3* (9), 2581.

(167) Shah, J. R.; Mosier, P. D.; Roth, B. L.; Kellogg, G. E.; Westkaemper, R. B. *Bioorganic Med. Chem.* **2009**, *17* (18), 6496.

(168) Pyun, J.; Jia, S.; Kowalewski, T.; Patterson, G. D.; Matyjaszewski, K. *Macromolecules* **2003**, *36* (14), 5094.

(169) Bauhofer, W.; Kovacs, J. Z. *Compos. Sci. Technol.* **2009**, *69* (10), 1486.

(170) Corr, S. A. *Nanoscience*; O’Brien, P., Ed.; Nanoscience; Royal Society of Chemistry: Cambridge, 2012; Vol. 1.

(171) Xie, L.; Huang, X.; Wu, C.; Jiang, P. *J. Mater. Chem.* **2011**, *21* (16), 5897.

(172) Yang, K.; Huang, X.; Huang, Y.; Xie, L.; Jiang, P. *Chem. Mater.* **2013**, *25* (11), 2327.

(173) Hanson, E. L.; Guo, J.; Koch, N.; Schwartz, J.; Bernasek, S. L. *J. Am. Chem. Soc.* **2005**, *127* (28), 10058.

(174) Li, J.; Khanchaitit, P.; Han, K.; Wang, Q. *Chem. Mater.* **2010**, *22* (18), 5350.

(175) White, M. a.; Johnson, J. a.; Koberstein, J. T.; Turro, N. J. *J. Am. Chem. Soc.* **2006**, *128* (35), 11356.

(176) Bachmann, W. E.; Kloetzel, M. C. *J. Org. Chem.* **1938**, *03* (1), 55.

(177) Wright, O. L.; Mura, L. E. *J. Chem. Educ.* **1966**, *43* (3), 150.

(178) Sovacool, B. K. *Renew. Sustain. Energy Rev.* **2014**, *37*, 249.

(179) Liang, F.; Sayed, M.; Al-Muntasheri, G. A.; Chang, F. F.; Li, L. *Petroleum* **2016**, *2* (1), 26.

(180) Sharma, M. M.; Gadde, P. B. In *SPE Annual Technical Conference and Exhibition*; Society of Petroleum Engineers, 2005; pp 1–12.

(181) Gu, M.; Dao, E.; Mohanty, K. K. *Fuel* **2015**, *150*, 191.

(182) Zoveidavianpoor, M.; Gharibi, A. *J. Nat. Gas Sci. Eng.* **2015**, *24*, 197.

(183) Kuru, E. A.; Orakdogen, N.; Okay, O. *Eur. Polym. J.* **2007**, *43* (7), 2913.

(184) Tanaka, H. *J. Polym. Sci. Part A Polym. Chem.* **1986**, *24* (1), 29.

(185) Mabire, F.; Audebert, R.; Quivoron, C. *Polymer (Guildf).* **1984**, *25* (9), 1317.

(186) Lin, H. R. *Eur. Polym. J.* **2001**, *37* (7), 1507.

(187) Chen, D.; Liu, X.; Yue, Y.; Zhang, W.; Wang, P. *Eur. Polym. J.* **2006**, *42* (6), 1284.

(188) Xiao, D.; Wirth, M. J. *Macromolecules* **2002**, *35*, 2919.

(189) Dainton, F. S.; Tordoff, M. *Trans. Faraday Soc.* **1956**, *53*, 499.

(190) Thomas, D. B.; Convertine, A. J.; Myrick, L. J.; Scales, C. W.; Smith, A. E.; Lowe, A. B.; Vasilieva, Y. a.; Ayres, N.; McCormick, C. L. *Macromolecules* **2004**, *37*, 8941.

(191) Sharma, B. R.; Dhuldhoya, N. C.; Merchant, U. C. *J. Polym. Environ.* **2006**, *14* (2), 195.

(192) Wisniewska, M. *Appl. Surf. Sci.* **2012**, *258* (7), 3094.

(193) Prucker, O.; Rühe, J. *Macromolecules* **1998**, *31* (3), 592.

(194) Huang, W.; Skanth, G.; Baker, G. L.; Bruening, M. L. *Langmuir* **2001**, *17* (5), 1731.

(195) Kincaid, K. P.; Snider, P. M.; Herring, M.; Mahoney, R. P.; Soane, D. In *SPE Hydraulic Fracturing Technology Conference*; Society of Petroleum Engineers, 2013; pp 1–12.

(196) Vengosh, A.; Jackson, R. B.; Warner, N.; Darrah, T. H.; Kondash, A. *Environ. Sci. Technol.* **2014**, *48* (15), 8334.

(197) Jacquet, J. B. *Environ. Sci. Technol.* **2014**, *48* (15), 8321.

(198) Burton, G. A.; Basu, N.; Ellis, B. R.; Kapo, K. E.; Entrekin, S.; Nadelhoffer, K. *Environ. Toxicol. Chem.* **2014**, *33* (8), 1679.

(199) Jiangtao, T. P. X.; Cyrille, B.; Volga, B.; Davis. *J. Polym. Sci. Part A Polym. Chem.* **2009**, *47*, 4302.

(200) Hruby, M.; Subr, V.; Kucka, J.; Kozempel, J.; Lebeda, O.; Sikora, A. *Appl. Radiat. Isot.* **2005**, *63* (4), 423.

(201) Karir, T.; Sarma, H. D.; Samuel, G.; Hassan, P. A.; Padmanabhan, D.; Venkatesh, M. *J. Appl. Polym. Sci.* **2013**, *130* (2), 860.

(202) Šubr, V.; Koňák, Č.; Laga, R.; Ulbrich, K. *Biomacromolecules* **2006**, *7* (1), 122.

(203) *Polymer Handbook*, 4th ed.; Brandrup, J., Immergut, E. H., Grulke, E. A., Eds.; Wiley, 2003.

(204) Sivy, G. T.; Coleman, M. M. *Carbon N. Y.* **1981**, *19* (2), 137.